COSMOLOGICAL PERTURBATIONS AND THEIR EFFECTS ON THE UNIVERSE:
FROM INFLATION TO ACCELERATION

By

ETHAN R. SIEGEL

A DISSERTATION PRESENTED TO THE GRADUATE SCHOOL
OF THE UNIVERSITY OF FLORIDA IN PARTIAL FULFILLMENT
OF THE REQUIREMENTS FOR THE DEGREE OF
DOCTOR OF PHILOSOPHY

UNIVERSITY OF FLORIDA

2006

I dedicate this work to everybody who stood by me in my darkest hours.

ACKNOWLEDGMENTS

TABLE OF CONTENTS

6

LIST OF TABLES

LIST OF FIGURES

Abstract of Dissertation Presented to the Graduate School
of the University of Florida in Partial Fulfillment of the
Requirements for the Degree of Doctor of Philosophy

COSMOLOGICAL PERTURBATIONS AND THEIR EFFECTS ON THE UNIVERSE:
FROM INFLATION TO ACCELERATION

By

Ethan R. Siegel

December 2006

Chair: James N. Fry
Major Department: Physics

The universe is, on the largest scales, nearly perfectly isotropic and homogeneous. This degree of smoothness was accentuated in the past, when density inhomogeneities departed from perfect uniformity by only thirty parts per million. These tiny imperfections in the early universe, however, have had enormous impact in causing the universe to evolve into its present state. This dissertation examines the role of these cosmological perturbations throughout various important events during the history of the universe, including inflation, linear and nonlinear structure formation, and the current phase of accelerated expansion. The spectrum of perturbations is calculated in the context of extra dimensions, and shown under which conditions it can be thermal. The effects of gravitational collapse are shown to generate magnetic fields, but not to significantly alter the expansion rate or cause acceleration. Finally, Lyman-break galaxies are examined as a possible distance indicator, and it is found that they may emerge as a powerful tool to better understand the energy content of the universe.

CHAPTER 1
INTRODUCTION TO COSMOLOGICAL PERTURBATIONS

1.1   Energy Density

The universe, as observed today, is filled with intricate and complex structure. Looking at length scales on the size of an individual planet ($\sim 10^{-10}$ pc), the solar system ($\sim 10^{-3}$ pc), the galaxy ($\sim 10^{-1}$ Mpc), or even clusters of galaxies (~ 10 Mpc), it is evident that there are large departures from the average value of energy density, $\bar{\rho}$. A measure of the departure from homogeneity at any position is given by the quantity δ, where

$$\delta \equiv \frac{\delta\rho}{\bar{\rho}} \equiv \frac{\rho - \bar{\rho}}{\bar{\rho}}. \tag{1--1}$$

On very small (i.e., planetary) scales, density contrasts can be as high as $\delta \sim 10^{30}$. However, as larger and larger scales are examined, the density contrast of a typical point in space is found to be much smaller. When scales of $\mathcal{O}(100 \text{ Mpc})$ or larger are examined, it is found that density contrasts are nearly always small, such that $\delta \ll 1$ [1].

What can be learned from this is that the universe is, on its largest scales, very nearly isotropic (the same in all directions) and homogeneous (the same at all positions in space). In the framework of general relativity, a universe that is both isotropic and homogeneous is described by the Friedmann-Robertson-Walker metric,

$$ds^2 = -dt^2 + a^2(t)(d\vec{x} \cdot d\vec{x}), \tag{1--2}$$

where $a(t)$ is the scale factor of the universe.

Because the universe is expanding and has a finite age, it is manifest that the degree of isotropy and homogeneity which is observed today was greater in the past. This is confirmed by observations of the relic radiation from the big bang, known as the cosmic microwave background (CMB), which shows the universe to have an amplitude of density fluctuations of $\delta \simeq 3 \times 10^{-5}$ [2]. These fluctuations in density, although insignificant when compared to the homogeneous part at early times, play a vital role in the universe's

evolution, bringing it from a state of near-perfect homogeneity to the complex nonlinear structures observed today.

1.2   Theory of Inflation

The theory of inflation [3] provides a mechanism to put these primordial cosmological perturbations in place at the time of the big bang. The big bang, as a cosmological theory, is the only compelling theory in the context of Einstein's general relativity that provides an explanation for the presence of the CMB radiation, the observed Hubble expansion of the universe, and the light element abundances (through big bang nucleosynthesis). It is shown in Peebles 1993 [4] that all reasonable alternatives to the big bang scenario either fail to reproduce one of the above three observations or cannot be compatible with general relativity. The big bang, however, is not an origin of the universe, but is rather a set of initial conditions. It is the above theory of inflation that naturally produces these initial conditions.

For the big bang theory to evolve into a universe which is compatible with observations, the initial conditions must be that the global curvature of the universe is spatially flat to an accuracy of ± 2 per cent [5]. The temperature and density of the universe must be uniform across scales far larger than the horizon, and the density of magnetic monopoles in the universe must be very small. These three problems are known as the flatness, horizon, and monopole problem. The method by which inflation solves this problem is to have a de Sitter-like phase of expansion during the very early universe. de Sitter expansion is characterized by the metric

$$ds^2 = -dt^2 + e^{\sqrt{\Lambda}t}(d\vec{x} \cdot d\vec{x}), \tag{1–3}$$

which is similar to equation (1–2), except that the scale factor $a = e^{\sqrt{\Lambda}t}$, where Λ is a constant. Λ is related to the expansion rate of the universe at that time by the equation $\Lambda = H^2$, where $H \equiv \dot{a}/a$ is the Hubble parameter.

11

From equation (1–3), it is manifest that the universe is expanding at an exponentially fast rate. Given enough time, the universe can expand by an arbitrary number of e-foldings. A universe expanding in this way will have its matter density reduced by a factor of

$$\frac{\rho_i}{\rho_f} = \left(\frac{a(t_i)}{a(t_f)}\right)^3 = e^{3\sqrt{\Lambda}(t_f - t_i)}, \tag{1–4}$$

where ρ_i and t_i are the density and age of the universe at the start of inflation, and ρ_f and t_f are the density and age at the end of inflation. This removes any initial densities or differences in density, solving both the horizon and monopole problems. Additionally, any initial curvature (departure from flatness) will be driven away by a factor of $a^2(t_i)/a^2(t_f)$, providing a solution to the flatness problem as well.

1.3   Cosmological Perturbations from Inflation

In addition to setting up the initial conditions necessary for the big bang, inflation also predicts very slight departures from homogeneity in the universe, producing fluctuations in both energy density [6–9] and in gravitational radiation [10, 11]. It is these predictions for the departures from perfect homogeneity, produced by quantum fluctuations, which are then stretched during inflation across all scales, that are the focus of this work. The perturbations produced by inflation are Gaussian in their statistical properties, and are also scale-invariant.

The perturbations in gravitational radiation are constrained to be a very small fraction of the energy density in the universe [12]. Nevertheless, the detection of such gravitational radiation and measurement of its properties would have the capabilities to tell us much about the early universe, as gravitational radiation is expected to be decoupled from the rest of the universe from the time of its creation. If a scale-invariant spectrum of gravitational waves were observed, it would be a further great confirmation of the inflationary paradigm, and constraints on the model of inflation could be inferred. However, there also exists the possibility that the spectrum of gravitational waves could be thermal. A thermal gravitational radiation spectrum could result from many possibilities,

one of which is as a signature of extra dimensions [13]. This is discussed at length in Chapter 2 of this work.

When inflation comes to an end, the universe reheats. The process of reheating transfers the energy from the vacuum (which was responsible for the rapid expansion) into matter and energy. This universe is described, in the homogeneous approximation, by the Friedmann-Robertson-Walker metric of equation (1–2). However, it is the density inhomogeneities, or primordial cosmological perturbations, that will lead to the formation of all structure in the universe. Therefore, the equation of interest as a starting point for much of the remainder of this work is that for a *perturbed* Friedmann-Robertson-Walker universe,

$$ds^2 = a^2(\tau)[-(1 + 2\psi)d\tau^2 + (1 - 2\phi)d\vec{x} \cdot d\vec{x}], \tag{1–5}$$

where ϕ and ψ are the scalar-mode perturbations to the gravitational potential. Of course, it makes no difference which gauge is chosen [14], as the physics of cosmological perturbations is the same in all gauges. The preference of the author is to work in the conformal Newtonian gauge (also known as the longitudinal gauge), as chosen in equation (1–5).

1.4 Cosmological Evolution in a Perturbed Universe

As the universe cools from its initial, smooth, hot, dense state, many cosmologically interesting phenomena occur (and many others *may* occur, dependent upon the reheat temperature of the universe and the physics involved at very high energy scales). A cosmological baryon asymmetry must be generated at very early times. As the observed baryon-to-photon ratio today is $\eta \simeq 6.1 \times 10^{-10}$, an asymmetry in the number density of baryons over anti-baryons of this magnitude must be produced. The process by which this occurs is generically referred to as baryogenesis, and there are many different times at which it may occur, including at the GUT-scale, at the electroweak scale, through leptogenesis, or through the Affleck-Dine scenario (see Dine and Kusenko 2004 [15] for a review). Also, in the early universe, a substantial amount of dark matter must be

generated. This can occur either through freeze-out of a stable, thermally produced relic, through the misalignment of the vacuum, through the production of a sterile, heavy neutrino, or through a perhaps more exotic mechanism (see Bertone, Hooper and Silk 2004 [16] for a review). These unsolved puzzles, along with the many questions surrounding the early universe physics of electroweak symmetry breaking, the QCD phase transition, and (possibly) supersymmetry breaking, are expected to be unaffected by the presence of cosmological perturbations. As the universe evolves, most of the physics that occurs in the earliest stages is expected to occur exactly as it would in a perfectly homogeneous Friedmann-Robertson-Walker universe.

One possibility in the very early universe, however, for which cosmological perturbations may play a seminal role is if the universe begins with (or obtains at early times) an asymmetry in its net charge. It has been pointed out that a large net charge in the universe would be ruinous at early times for cosmological ^{4}He synthesis [17] and for the cosmic microwave background [18]. Although a conclusive solution is beyond the scope of this dissertation, cosmological perturbations in an expanding universe may have the capability of driving an electrically charged universe to a neutral state. This possibility, and preliminary work on the subject, can be found in Appendix B.

As the universe continues to expand and cool, the building blocks of the universe begin to form. After the QCD phase transition, quarks and gluons become bound into hadrons. Unstable particles decay and/or co-annihilate, leaving the universe devoid of exotic particles. Neutrinos freeze-out, and decouple from the rest of the universe. Electrons and positrons coannihilate, leaving an electron asymmetry that matches up nearly perfectly with the proton asymmetry. When the universe cools substantially so that stable deuterium can form without being destroyed by the thermal photon bath, nucleosynthesis occurs, producing deuterium, ^{3}He, ^{4}He, and ^{7}Li. Nucleosynthesis is complete roughly four minutes after the big bang. Although there has been work in the past suggesting alternative, complex models of nucleosynthesis (such as inhomogeneous

nucleosynthesis) to be slightly favored (see Steigman 2006 [19] for a review of big-bang nucleosynthesis and its alternatives), the standard picture of big bang nucleosynthesis appears to match up perfectly well with observations within the systematic errors [20].

It is generally assumed that no interesting physics occurs until the time of recombination (where electrons and ions combine to form neutral atoms), roughly 380,000 years later. The only things of note which occur over that era are that cosmological perturbations grow according to the Mészáros effect [21], and the universe transitions from a radiation-dominated state to a matter-dominated one. However, there is a very interesting and subtle effect that occurs during this time. As η (the baryon-to-photon) ratio is very small and the universe is still quite hot and dense during this era, every ion and electron is consistently bombarded by these high energy photons. Ions have comparable charges to electrons, but their masses are orders of magnitude greater. The scattering cross sections of charged particles with photons scales (for non-relativistic scattering) as

$$\sigma = \frac{8\pi}{3} \left(\frac{q^2}{mc^2} \right)^2, \tag{1–6}$$

where q is the charge and m is the mass. As a result of the differences in mass and cross section, electrons are affected by interactions with photons in a much more profound way than ions. While the Coulomb forces keeps the electrons and protons tightly coupled, the momentum transfer from photons works to create charge separations and currents during the radiation era. The tightly coupled component is dominant, and behaves as a baryonic component in cosmological perturbation theory (see Ma and Bertschinger 1995 [22] for a very sophisticated treatment). In contrast, the charge separations and currents created by momentum transfer are very small, but nonetheless are of great import for the generation of magnetic fields at early times [23]. The generation of magnetic fields in the young universe by this mechanism is detailed in Chapter 3, which also discusses the possibility that the origins of presently observed cosmic magnetic fields may lie in this mechanism.

As the universe transitions from a radiation-dominated state to a matter-dominated one, gravitational inhomogeneities begin to substantially grow for the first time. The Mészáros effect dictates that an inhomogeneity δ grows as

$$\delta(t) = \left(1 + \frac{3}{2}Y\right)\delta(t_0), \tag{1–7}$$

where Y is given by

$$Y \equiv \frac{\rho_{\mathrm{m}}(t)}{\rho_{\mathrm{r}}(t)}, \tag{1–8}$$

from an initial time t_0 until the time of interest, t, where ρ_{m} is the matter density and ρ_{r} is the radiation density. This approximation is valid throughout the linear regime of gravitational collapse and structure formation, and provides an accurate description for the growth of overdense inhomogeneities.

During this epoch of complete ionization, electrons and ions are constantly interacting with one another, and attempting to form neutral atoms. There are two processes that impede the formation of neutral atoms. The first, which delays the onset of neutral atom formation (known as recombination), is that the baryon-to-photon ratio, η, is so low. Even though the photon temperature is significantly below the ionization energy of a neutral atom ($T_\gamma \ll 13.6$ eV), the number of photons per baryon is very great, and their energy follows a Poisson distribution. As a result, there are still enough photons of sufficient energy to keep the universe 100 per cent ionized even when the average temperature of the universe is significantly below the typical atomic ionization energy. The second process that is responsible for impeding the formation of a neutral, transparent universe is the fact that each Lyman-series photon (transition to the ground state of hydrogen) emitted by a recombining atom will encounter and reionize another neutral atom. If, however, the emitted photon has enough time to redshift sufficiently that it cannot reionize another atom, the universe will net one neutral atom. Also, a rare two-photon emission process will allow an atom to recombine without emitting a Lyman-series photon. This process of recombining the majority of the atoms in the universe takes about $\sim 10^5$ years to complete

[5], and drops the ionization fraction (χ_e) of the universe from $\chi_e \simeq 1$ to $\chi_e \sim 10^{-4}$ [24]. After this point, ions and electrons can no longer efficiently find one another, and the process of recombination freezes out. As the cosmic background of photons is no longer constantly scattering off of electrons, it freely streams from the epoch of recombination until the present day, making the epoch of recombination synonomous with the surface of last scattering.

1.5 Nonlinear Evolution of Perturbations

Once recombination has occurred, the universe is in a matter-dominated, expanding state, full of small density inhomogeneities on all scales. It is in this post-recombination universe that large-scale structure formation begins to occur. The density inhomogeneities, initially, have an amplitude of $\sim 2 \times 10^{-5} \rho_m$, with the fluctuations having a Gaussian distribution. As the fluctuations evolve according to linear perturbation theory (with overdensities growing according to the Mészáros effect) initially, and as gravitational perturbations continue to grow, gravitational collapse goes nonlinear, causing a rapid acceleration in structure formation. The overdense regions on small scales go nonlinear first, as they enter the horizon (and thus become causally connected) first. The perturbations, on the other hand, are across all scales, and have a roughly scale-invariant spectrum (where the power spectrum, $P(k)$, scales as $P(k) \propto k^n$), where the spectral index $n \simeq 1$. The structure which arises from this follows scaling solutions, as described in Fry 1984 [25] and Schaeffer 1984 [26], for example.

The result of all of this is that an initially smooth universe with only very slight perturbations in energy density becomes a complex web of structure, with substantial power on both small (i.e., galactic) and large (i.e., supercluster) scales. (For a very interesting comparison of numerical simulations of structure formation through the nonlinear regime up to the present day, the reader is referred to O'Shea et al. 2005 [27].) While this large-scale structure forms, the universe continues to expand and cool, dropping

17

from a temperature of $T \simeq 3000\,°\text{K}$ at recombination to a temperature of $T \simeq 2.725\,°\text{K}$ at present.

The various epochs of the universe, home to the onset of extremely interesting physics, are tracked most easily by redshift, z, defined by

$$\frac{a_0}{a(t)} \equiv 1 + z, \qquad (1\text{–}9)$$

where $a(t)$ is the scale factor of the universe at a given time, and a_0 is the scale factor at present. When gravitational collapse occurs to a sufficient extent on small scales, the mass collected in a small area of space becomes large enough to ignite nuclear fusion. This is the epoch at which the first stars form.

Exactly at what epoch star formation begins is very important for understanding the evolution of matter and structure in our universe. A signature of the formation of the first stars would be a surefire signature of nonlinear collapse. The transition from a smooth, linear universe (such as the universe at the time of recombination) to a highly complex, nonlinear one (observed today) is not yet well understood. Recently, many have discussed the possibility that the gravitational energy bound in nonlinear inhomogeneities could back-react, and significantly impact the expansion rate [28–30]. It appears that the impact on the expansion rate is insignificant, however [31–34]. This physical process and its effects on the universe are discussed in great detail in Chapter 4.

The densest regions of nonlinear structure become home to the first stars, as illustrated in adaptive mesh refinement simulations [35]. The data from the WMAP satellite indicate that the optical depth of the universe, τ, is quite large [5]. From this information, it appears that the first stars turned on very early, as the presence of a large number of stars will reionize the neutral gas that formed during recombination. From the optical depth, which is measured to be $\tau = 0.17 \pm 0.04$, it appears that reionization occurs at roughly $11 \lesssim z \lesssim 30$. However, the observation of a Gunn-Peterson trough [36] in quasar spectra around $z \simeq 6$ [37] indicates that reionization is not complete until that

epoch. Seemingly bizarre solutions, such as a double epoch of reionization [38], have been proposed to remedy this situation. Future release of data from satellites exploring the cosmic microwave background may yield lower values of τ, which would be consistent with a more simplistic explanation of gradual reionization.

Once the first complex nonlinear structures form, they continue to evolve, with the densest regions attracting the most matter and forming the most massive structures. Galaxies grow through both monolithic collapse and a series of hierarchical mergers, and via further gravitational collapse on larger scales, the first clusters of galaxies will form as well. The types of objects which can be observed at early times are very bright galaxies (in the optical and infrared) and quasars (primarily in the radio), as well as intervening objects along the line of sight (through absorption and the Lyman-α forest). For a flat universe that contained a critical density in matter, the expansion rate would continue to decrease as the matter density diluted, following the Hubble law of equation (1–10),

$$H^2 \equiv \left(\frac{\dot{a}}{a}\right)^2 = \frac{8\pi G}{3}\rho_m, \tag{1–10}$$

where ρ_m is again the matter density (equal to the critical density) and H is the Hubble expansion parameter. However, the universe's expansion rate, as inferred from a combination of many sources of data (see Chapter 5 and references therein) is consistent with about 30 per cent of the energy density in matter and about 70 per cent in some type of vacuum energy. The expansion law, then, appears to obey equation 1–11

$$H^2 \equiv \left(\frac{\dot{a}}{a}\right)^2 = \frac{8\pi G}{3}\left(\rho_m + \rho_\Lambda\right), \tag{1–11}$$

where ρ_Λ is the energy density in vacuum energy, and the sum of matter density and vacuum energy density is equal to the critical density.

The data from type Ia supernovae have been used to illustrate and support the fact that the picture of the universe is inconsistent without a vacuum energy term in the equation for the Hubble law [39]. However, due to systematic errors inherent in any single

observational method, it is vital to collect data from a large number of methods. Chapter 5 investigates the possibility of using a new method (first detailed in Melnick, Terlevich and Terlevich 2000 [40] and first attempted in Siegel et al. 2005 [41]) to measure the cosmological parameters of matter and vacuum energy density in the universe. As with any type of distance indicator, the method of Chapter 5, to use Lyman-break galaxies as a distance indicator, is subject to many sources of error, both random and systematic. These errors are detailed in Appendix A.

The data sets available are now sufficient to paint a coherent picture of the universe and its energy contents very well on the largest scales, and relatively well on even small scales [12]. There are many interesting problems and phenomena in the universe that are hitherto unexplained, yet physics of the answers may lie in something as simple as departures from the ideal model. The remainder of this work details some instances where cosmological inhomogeneities, whether at early times or late times, on large or small scales, may play a vital role in understanding the universe. Finally, Chapter 6 will summarize the major results of Chapters 2 through 5, and will point towards future avenues of investigation, such as determining the fate of the universe.

CHAPTER 2
THE GRAVITATIONAL WAVE BACKGROUND

Inflationary cosmology predicts a low-amplitude graviton background across a wide range of frequencies. This chapter shows that if one or more extra dimensions exist, the graviton background may have a thermal spectrum instead, dependent on the fundamental scale of the extra dimensions. The energy density is shown to be significant enough that it can affect nucleosynthesis in a substantial way. The possibility of direct detection of a thermal graviton background using the 21-cm hydrogen line is discussed. Alternative explanations for the creation of a thermal graviton background are also examined.

2.1 Primordial Gravitational Waves

One of the most powerful windows into the early universe are backgrounds of particles whose interactions have frozen-out. The primordial photon background, the primordial baryon background and the primordial neutrino background are all examples of particles that were once in thermal equilibrium. At various times during the history of the universe, the interaction rate of the species in question dropped below the Hubble expansion rate of the universe, causing the species in question to freeze-out. The primordial photon background is observed as the cosmic microwave background (CMB), the baryon background is observed as stars, galaxies, and other normal matter, and the neutrino background, although not yet observed, is a standard component of big bang cosmology. In addition to these backgrounds, a primordial background of gravitons (or, equivalently, gravitational waves) is expected to exist as well, although it, too, has yet to be detected. The frequency spectrum and amplitude of this background have the potential to convey much information about the early universe. This chapter focuses on using the cosmic gravitational wave background (CGWB) as a probe of extra dimensions.

The success of the inflationary paradigm [3] in resolving many problems associated with the standard big-bang picture [42] has led to its general acceptance. Inflationary big bang cosmology predicts a stochastic background of gravitational waves across all frequencies [10], [11]. The amplitude of this background is dependent upon the specific

model of inflation, but the fractional energy density in a stochastic CGWB is constrained [12] to be

$$\Omega_g \leq \mathcal{O}(10^{-10}). \tag{2–1}$$

In inflationary cosmology, the predicted CGWB, unlike the CMB and the neutrino background, is non-thermal. Gravitational interactions are not strong enough to produce a thermal CGWB at temperatures below the Planck scale ($m_{pl} \approx 1.22 \times 10^{19}$ GeV). As the existing particles in the universe leave the horizon during inflation, the only major contributions to the energy density will be those particles created during or after reheating, following the end of inflation. Unless the reheat temperature (T_{RH}) is greater than m_{pl}, gravitational interactions will be too weak to create a thermal CGWB. The measurement of the magnitude of the primordial anisotropies from missions such as COBE/DMR [43] and WMAP [5] provides an upper limit to the energy scale at which inflation occurs [44]. From this and standard cosmological arguments [45], an upper limit on T_{RH} can be derived to be

$$T_{RH} \simeq 6.7 \times 10^{18} \ (g_*)^{-1/4} \left(\frac{t_{pl}}{t_\phi} \right)^{1/2} \ \text{GeV}, \tag{2–2}$$

where g_* is the number of relativistic degrees of freedom at T_{RH}, t_{pl} is the Planck time, and t_ϕ is the lifetime of the inflaton. A stronger upper limit on T_{RH} ($\sim 10^8 - 10^{10}$ GeV) can be obtained from nucleosynthesis [46] if supersymmetry is assumed. In all reasonable cases, however, $T_{RH} \ll m_{pl}$, indicating that the CGWB is non-thermal in inflationary cosmology.

2.2 Extra Dimensions

If the universe contains extra dimensions, however, predictions about the shape and amplitude of the CGWB may change drastically. Cosmologies involving extra dimensions have been well-motivated since Kaluza [47] and Klein [48] showed that classical electromagnetism and general relativity could be unified in a 5-dimensional framework. More modern scenarios involving extra dimensions are being explored in particle physics,

with most models possessing either a large volume [49, 50] or a large curvature [51, 52]. Any spatial dimensions which exist beyond the standard three must be of a sufficiently small scale that they do not conflict with gravitational experiments. The 3+1 dimensional gravitational force law has been verified down to scales of 0.22 mm [53]. Thus, if extra dimensions do exist, they must be smaller than this length scale. Although there exist many different types of models containing extra dimensions, there are some general features and signals common to all of them.

In the presence of δ extra spatial dimensions, the $3+\delta+1$-dimensional action for gravity can be written as

$$
\begin{aligned}
\mathcal{S} &= \int d^4x \left\{ \int d^\delta y \sqrt{-g'} \frac{\mathcal{R}'}{16\pi G'_N} + \sqrt{-g}\mathcal{L}_m \right\}, \\
G'_N &= G_N \frac{m_{pl}^2}{m_D^{2+\delta}},
\end{aligned}
\tag{2–3}
$$

where g is the 4-dimensional metric, G_N is Newton's constant, g', G'_N, and $\mathcal{R}'$ denote the higher-dimensional counterparts of the metric, Newton's constant, and the Ricci scalar, respectively, and m_D is the fundamental scale of the higher-dimensional theory. In $3+\delta$ spatial dimensions, the strength of the gravitational interactions scale as $\sim (T/m_D)^{(1+\delta/2)}$. If $\delta = 0$, then $m_D = m_{pl}$, and standard 4-dimensional gravity is recovered.

When energies in the universe are higher than the fundamental scale m_D, the gravitational coupling strength increases significantly, as the gravitational field spreads out into the full spatial volume. Instead of freezing out at $\sim \mathcal{O}(m_{pl})$, as in 3+1 dimensions, gravitational interactions freeze-out at $\sim \mathcal{O}(m_D)$ [49]. (m_D can be much smaller than m_{pl}, and may be as small as $\sim$ TeV-scale in some models.) If the gravitational interactions become strong at an energy scale below the reheat temperature ($m_D < T_{RH}$), gravitons will have the opportunity to thermalize, creating a thermal CGWB. Figure 2-1 illustrates the available parameter space for the creation of a thermal CGWB in the case of large extra dimensions, following the formalism in Giudice, Rattazzi and Wells 1999 [54].
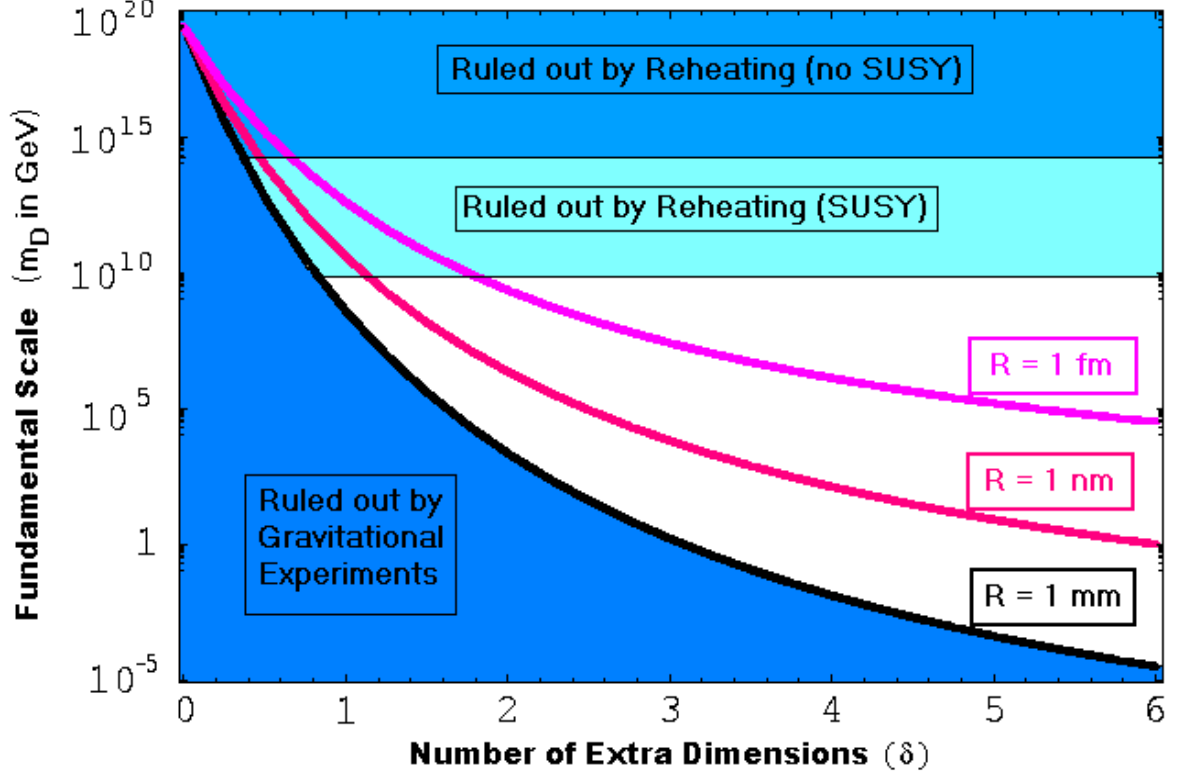
Figure 2-1. Parameter space for the creation of a thermal CGWB in the context of Large
Extra Dimensions. The shaded areas represent areas ruled out by gravitational
experiments and reheating, both with and without the assumption of
supersymmetry. Certain assumptions about gravitino physics, as detailed
in Sarkar 1996 [46], may significantly lower the bound on reheating with
supersymmetry in extra dimensions.

Other types of extra dimensions have minor quantitative differences in the shape of
their parameter spaces. However, the qualitative result, the creation of a thermal CGWB
if $m_D < T_{RH}$, is unchanged by the type of extra dimensions chosen.

2.3   A Thermal Graviton Background

Thus, if extra dimensions do exist, and the fundamental scale of those dimensions is
below the reheat temperature, a relic thermal CGWB ought to exist today. Compared to
the relic thermal photon background (the CMB), a thermal CGWB would have the same
shape, statistics, and high degree of isotropy and homogeneity. The energy density (ρ_g)

and fractional energy density (Ω_g) of a thermal CGWB are

$$\rho_g = \frac{\pi^2}{15} \left(\frac{3.91}{g_*}\right)^{4/3} (T_{CMB})^4, \tag{2–4}$$

$$\Omega_g \equiv \frac{\rho_g}{\rho_c} \simeq 3.1 \times 10^{-4} \, (g_*)^{-4/3}, \tag{2–5}$$

where ρ_c is the critical energy density today, T_{CMB} is the present temperature of the CMB, and g_* is the number of relativistic degrees of freedom at the scale of m_D. g_* is dependent on the particle content of the universe, i.e. whether (and at what scale) the universe is supersymmetric, has a KK tower, etc. Other quantities, such as the temperature (T), peak frequency (ν), number density (n), and entropy density (s) of the thermal CGWB can be derived from the CMB if g_* is known, as

$$
\begin{aligned}
n_g &= n_{CMB} \left(\frac{3.91}{g_*}\right), & s_g &= s_{CMB} \left(\frac{3.91}{g_*}\right), \\
T_g &= T_{CMB} \left(\frac{3.91}{g_*}\right)^{1/3}, & \nu_g &= \nu_{CMB} \left(\frac{3.91}{g_*}\right)^{1/3}.
\end{aligned} \tag{2–6}
$$

These quantities are not dependent on the number of extra dimensions, as the large discrepancy in size between the three large spatial dimensions and the δ extra dimensions suppresses those corrections by at least a factor of $\sim 10^{-29}$. As an example, if m_D is just barely above the scale of the standard model, then $g_* = 106.75$. The thermal CGWB then has a temperature of 0.905 Kelvin, a peak frequency of 19 GHz, and a fractional energy density $\Omega_g \simeq 6.1 \times 10^{-7}$.

2.4   Detection of Extra Dimensions

Although the fractional graviton energy density is expected to be small today, it may be detectable either indirectly or directly. Nucleosynthesis provides an indirect testing ground for a thermal CGWB. Standard big-bang nucleosynthesis predicts a helium-4 abundance of $Y_p = 0.2481 \pm 0.0004$ [55]. With a thermal CGWB included, the expansion rate of the universe is slightly increased, causing neutron-proton interconversion to freeze-out slightly earlier. A thermal CGWB can be effectively parameterized as neutrinos,

as they serve the same function at that epoch in the universe (as non-collisional radiation). The effective number of neutrino species is increased by $N_{\nu-eff} \simeq 27.1 \, (g_*)^{-4/3}$, or $\simeq 0.054$ (for $g_* = 106.75$). This would yield a new prediction of $Y_p = 0.2489 \pm 0.0004$ for helium-4. Although observations are not yet able to discriminate between these two values, the constraints are tightening with the advent of recent data [56]. An increase in the precision of various measurements, along with an improvement in the systematic uncertainties, may allow for the indirect detection of a thermal CGWB.

Direct detection of a thermal CGWB is much more challenging, but would provide quite strong evidence for its existence. Conventional gravitational-wave detectors include cryogenic resonant detectors [57], which have evolved from the bars of Weber [58], doppler spacecraft tracking, and laser interferometers [59]. The maximum frequency that these detectors can probe lies in the kHz regime, whereas a thermal CGWB requires GHz-range detectors. An interesting possibility for detection may lie in the broadening of quantum emission lines due to a thermal CGWB. Individual photons experience a frequency shift due to gravitational waves [60]. For a large sample of radio-frequency photons in a gravitational wave background, the observed line width (W) will broaden by

$$\Delta W \sim h_0 \sim \frac{\sqrt{\Omega_g}}{\nu \, t_0} \sim 10^{-31} \left(\frac{106.75}{g_*} \right)^{1/3}, \qquad (2\text{--}7)$$

where t_0 is the present age of the universe, ν is the peak frequency of the thermal CGWB and h_0 is the metric perturbation today due to the thermal CGWB [61]. As $\mathcal{O}(10^{-31})$ is a very small broadening, a radio line with a narrow natural width is the preferred candidate to observe this effect. One possibility for this type of observation is the 21-cm emission line of atomic hydrogen. So long as the emitting atoms and the detectors are sufficiently cooled, broadening due to thermal noise will be suppressed below ΔW. Because the lifetime ($1/\Gamma$) of the excited state of hydrogen is large ($\sim 10^7$ yr) and the frequency of the

emitted light (ν_γ) is high ($\sim 10^9$ Hz), the natural width (W) is among the smallest known

$$W = \frac{\Gamma}{\nu_\gamma} \simeq \frac{2.869 \times 10^{-15} \ s^{-1}}{1.42040575179 \times 10^9 \ s^{-1}} \simeq 2.02 \times 10^{-24}. \qquad (2\text{--}8)$$

The width of the 21-cm line is regrettably seven orders of magnitude larger than the expected broadening due to a thermal CGWB. Extraordinarily accurate measurements would need to be taken for direct detection of this background. Additionally, temperatures of the atoms and detectors would need to be cryogenically cooled to $\sim 10^{-18}$ Kelvin to suppress thermal noise below ΔW. This last criterion is far beyond the reach of current technology, and either a major advance or experimental innovation would be required to measure the desired effect using this technique.

2.5 Alternative Thermalization Mechanisms

Extra dimensions are not the only possible explanation for the existence of a thermal CGWB. Currently, there are three known alternative explanations that would also create a thermal CGWB. They are as follows: there was no inflation, there was a spectrum of low-mass primordial black holes that have decayed by the present epoch, or the gravitational constant is time-varying (the Dirac hypothesis). Each alternative is shown below to face difficulties that may make extra dimensions an attractive explanation for the creation of a thermal CGWB.

The predictions of inflation are numerous [44], and many have been successfully confirmed by WMAP [5]. The major successes of inflation include providing explanations for the observed homogeneity, isotropy, flatness, absence of magnetic monopoles, and origin of anisotropies in the universe. Additionally, confirmed predictions include a scale-invariant matter power spectrum, an $\Omega = 1$ universe, and the spectrum of CMB anisotropies. To explain a thermal CGWB by eliminating inflation would require alternative explanations for each of the predictions above. Although alternative theories have been proposed, as in Hollands and Wald 2002 [62], they have been shown to face

significant difficulties [63]. The successes of inflation appear to suggest that it may likely provide an accurate description of the early universe.

Primordial black holes with masses less than 10^{15} g would have decayed by today, producing thermal photons, gravitons, and other forms of radiation. Density fluctuations in the early universe, in order to produce a large mass fraction of low-mass primordial black holes, and not to produce too large of a mass fraction of high-mass ones, favor a spectral index n that is less than or equal to $2/3$ [64]. Accepting the observed scale-invariant ($n \simeq 1$) spectrum of density fluctuations [65] may disfavor primordial black holes as a reasonable candidate for creating a thermal CGWB.

The Dirac hypothesis states that the difference in magnitude between the gravitational and electromagnetic coupling strengths arises due to time evolution of the couplings [66]. If true, gravitational coupling would have been stronger in the early universe. At temperatures well below the Planck scale, gravity would have been unified with the other forces, creating a thermal CGWB at that epoch. However, this hypothesis produces consequences for cosmological models that are difficult to reconcile [67], and any time variation is severely constrained by geophysical and astronomical observations [68]. The acceptable limits for variation are small enough that they cannot increase coupling sufficiently to generate a thermal CGWB subsequent to the end of inflation. The difficulties faced by each of these alternative explanations points towards extra dimensions as perhaps the leading candidate for the creation of a thermal CGWB.

2.6   Problems of Extra Dimensions

There exist two major obstacles to the construction of a more complete phenomenological model containing extra dimensions with $m_D < T_{RH}$. The first of these is the moduli problem [69]. String moduli interactions with standard model fields are highly suppressed, leading to a long lifetime of the string moduli. String moduli decay, however, must be consistent with astrophysical constraints [70]. To accomplish this, string moduli need either a small production amplitude or very specific decay channels, which both require

28

fine-tuning. The second problem is the overproduction of long-wavelength tensor modes from inflation [71, 72]. While the short-wavelength modes (the modes inside the horizon when gravitational interactions freeze-out) will thermalize, gravitational waves of longer wavelengths will be unaffected. As the scale of inflation must be above m_D, the amplitude of these waves is expected to be large. This would leave an unacceptable imprint in the CMB. Both problems arise from the fact that at energies above m_D, macroscopic gravity breaks down [73]. Although these problems may not be resolved until a quantum theory of gravity is realized, they do not change the fact that a thermal CGWB would arise from extra dimensions with $m_D < T_{RH}$.

Furthermore, there is a more fundamental question concerning the nature of extra dimensions. The three observed spatial dimensions are quite large, on the order of $\sim 10^{28}$ cm. On the other hand, any extra spatial dimensions must be, at most, of a length scale less than 0.22 mm. It is very difficult to construct a compelling theory that naturally produces three large spatial dimensions and forces the rest to be small. A possible solution to this puzzle may lie in the work of Chodos and Detweiler 1980 [74], where it was shown that a universe with four spatial dimensions of initially comparable size may naturally evolve to a state with three large, expanding dimensions and one small, contracting one.

2.7   Summary

This chapter has attempted to show that extra dimensions may be responsible for the production of a thermal gravitational wave background. A thermal CGWB, as opposed to the stochastic CGWB of standard inflationary cosmology, is a prediction of extra dimensions with a scale below the reheat temperature. The detection of a thermal CGWB, although challenging at present, would provide strong evidence for the existence of extra dimensions. The detected absence of a thermal CGWB would conversely disfavor the existence of extra dimensions up to the energy scale of the reheat temperature.

CHAPTER 3
STRUCTURE FORMATION CREATES MAGNETIC FIELDS

This chapter examines the generation of seed magnetic fields on all scales due to the growth of cosmological perturbations. In the radiation era, local differences in the ion and electron density and velocity fields are induced by momentum transfer from photons. The currents which flow due to the relative motion of these fluids lead to the generation of magnetic fields. Magnetic fields are created on all cosmological scales, peaking at a magnitude of $\mathcal{O}(10^{-23}$ Gauss$)$ at the epoch of recombination. Magnetic fields generated in this manner provide a promising candidate for the seeds of magnetic fields presently observed on galactic and extra-galactic scales.

3.1   Introduction

The presence of magnetic fields on galactic and extragalactic scales is a major unsolved problem in modern astrophysics. Although the observational evidence for magnetic fields in large-scale structures is overwhelming, there is no consensus as to their origins. The standard paradigm for the creation of these fields is the dynamo mechanism, in which an initial, small seed field is amplified by turbulence and/or differential rotation to account for the fields observed today.

In principle, once a seed field is in place, it should be possible to follow its evolution and amplification from the collapse of structure and the effects of any relevant dynamos. In this chapter, a new mechanism for the generation of seed fields is put forward. It is argued that cosmological perturbation theory in the radiation era produces charge separations and currents on all scales, both of which contribute to magnetic fields. These seed fields persist until the onset of gravitational collapse, at which point field amplification and dynamo processes can magnify such seeds, possibly to the $\mathcal{O}(\mu\mathrm{G})$ scales observed today.

This chapter illustrates that the generation of magnetic fields in this manner is a necessary consequence of structure formation. The magnitude of these seed fields is calculated, and it is shown that these seed fields may be sufficiently strong to account for

all of the observed magnetic fields in large-scale structures. The layout of this chapter is as follows: the next section gives an overview of the observational evidence for magnetic fields along with a brief theoretical picture of their generation. After that, there is an explanation of the novel idea that the early stages of structure formation in a perturbed universe generate magnetic fields. Subsequently, a detailed treatment of cosmological perturbations is presented, with a specific view towards the creation and evolution of local charge separations and currents. The magnitudes of the seed magnetic fields which arise via this mechanism as a function of scale and epoch are then calculated. Finally, the results of this mechanism are compared with competing theories. Also included is a discussion of avenues for future investigation of this topic, including possible observational signatures which would arise as predictions of this mechanism.

3.2 Magnetic Fields: Background

In all gravitationally bound or collapsing structures in which the appropriate observations are made, magnetic fields with strength $\sim \mu$G are seen [75]. The four major methods used to study astrophysical magnetic fields are synchrotron radiation, Faraday rotation, Zeeman splitting, and polarization of starlight. These observational techniques are detailed in depth in Ruzmaikin, Sokolov and Shukurov 1988 [76], with Faraday rotation often proving the most fruitful of the above methods.

Magnetic fields have been found in many different types of galaxies, in rich clusters, and in galaxies at high redshifts. Spiral galaxies, including our own, appear to have relatively large magnetic fields of $\mathcal{O}(10 \, \mu\text{G})$ on the scale of the galaxy [77], with some (such as M82) containing anomalously strong fields up to $\simeq 50 \, \mu\text{G}$ [78]. Elliptical and irregular galaxies possess strong evidence for magnetic fields (of order $\sim \mu$G) as well [79], although they are much more difficult to observe due to the paucity of free electrons in these classes of galaxies. Coherence scales for magnetic fields in these galaxies, as opposed to spirals, are much smaller than the scale of the galaxy. Furthermore, galaxies at moderate ($z \simeq 0.4$) and high redshifts ($z \gtrsim 2$) have been observed to require significant

($\sim \mu$G) magnetic fields to explain their observed Faraday rotations [80, 81]. Magnetic fields are also observed in structures larger than individual galaxies. The three main types of galaxy clusters are those with cooling flows, those with radio-halos, and those devoid of both. Galaxy clusters with cooling flows are observed to have fields of $0.2\,\mathrm{to}\,3\,\mu$G [82], the Coma cluster (a prime example of a radio-halo cluster) is observed to have a field strength $\sim\ 2.5\,\mu$G [83], while clusters selected to have neither cooling flows nor radio halos still exhibit indications of strong $(0.1 - 1\,\mu$G) fields [84]. There even exists evidence for magnetic fields on extracluster scales. An excess of Faraday rotation is observed for galaxies lying along the filament between the Coma cluster and the cluster Abell 1367, consistent with an intercluster magnetic field of $0.2 - 0.6\,\mu$G [85]. On the largest cosmological scales, there exist only upper limits on magnetic fields, arising from observations of the cosmic microwave background [86] and from nucleosynthesis [87], setting limits that on scales $\geq 10\,\mathrm{Mpc}$, field strengths are $\leq 10^{-8}\,$G.

Observational evidence for magnetic fields is found in galaxies of all types and in galaxy clusters, both locally and at high redshifts, wherever the appropriate observations can be made. A review of observational results can be found in Valleé 1997 [88]. The theoretical picture of the creation of these fields, however, is incomplete. Fields of strength $\sim \mu$G can be explained by the magnification of an initial, small seed field on galactic (or larger) scales by the dynamo mechanism [89–91]. A protogalaxy (or protocluster) containing a magnetic field can have its field strength increased by many orders of magnitude through gravitational collapse [92, 93], and can then be further amplified via various dynamos. Dynamos which can amplify a small seed field into the large fields observed today involve helical turbulence (α) and/or differential rotation (ω). Various types of these dynamos include the mean-field dynamo [76, 94, 95], the fluctuation dynamo [79, 96], and merger-driven dynamos [97], among others. However, the dynamo mechanism does not explain the origin of such seed fields.

While the initial seeds that grow into magnetic fields are anticipated to be small, they must still come from somewhere [98], and their existence is not explained by the dynamo mechanism alone. There are many mechanisms that can produce small-strength magnetic fields on astrophysically interesting scales, either through astrophysical or exotic processes (see Widrow 2002 [75] for a detailed review). Exotic processes generally rely on new physics in the early universe, such as a first-order QCD phase transition [99, 100], a first order electroweak phase transition [101, 102], broken conformal invariance during inflation [103, 104], specific inflaton potentials [105], or the presence of charged scalars during inflation [106–108]. Astrophysical mechanisms, in contrast, are generally better grounded in known physics, although they have difficulty generating sufficiently strong fields on sufficiently large scales. The difference in mobility between electrons and ions can lead to seed magnetic fields from radiation-era vorticity [109, 110], from vorticity due to gas-dynamics in ionized plasma [111–115], from stars [116], or from active galactic nuclei [117]. Although there are many candidates for producing the seed magnetic fields required by the dynamo mechanism, none has emerged as a definitive solution to the puzzle of explaining their origins.

The novel mechanism proposed in this chapter is that seed magnetic fields are generated by the scattering of photons with charged particles during the radiation era. Unlike the mechanism of [109, 110], which is disfavored [118] due to its requirement of substantial primordial vorticity (although see [119, 120] for an argument that some vorticity is necessary), the fields of interest here are generated by the earliest stages of structure formation, *requiring no new physics*. Ions (henceforth taken to be protons, for simplicity) and electrons are treated as separate fluids, with opposite charges but significantly different masses. The mass-weighted sums of their density and velocity fields will determine the evolution of baryons in the universe, and should agree with previous treatments, such as Ma and Bertschinger 1995 [22]. The difference of the ion and electron density and velocity fields, however, will provide a measure of local charge separation and

of local current density, both of which contribute to magnetic fields. Since cosmological perturbations, which serve as seeds for structure formation, exist on all scales, it is expected that seed magnetic fields will be generated on all scales by this mechanism. The remainder of this chapter focuses on calculating the magnitude of the magnetic fields generated by this process and discussing their cosmological ramifications.

3.3 Cosmological Perturbations

Although the early universe is isotropic and homogeneous to two parts in 10^{-5} [2], it is these small density inhomogeneities, predicted by inflation to occur on all scales [8], which lead to all of the structure observed in the universe today. As it is the early epoch of structure formation that is of interest for the creation of magnetic fields, this chapter calculates the evolution of inhomogeneities in the linear regime of structure formation. The most sophisticated treatment of cosmological perturbations in the linear regime to date is that of Ma and Bertschinger 1995 [22], which provides evolution equations for an inhomogeneous universe containing a cosmological constant, dark matter, baryons, photons, and neutrinos. This section extends their treatment to encompass separate proton and electron components. The mass-weighted sum of protons and electrons will recover the baryon component, whereas the difference of the density fields is representative of a charge separation, and the difference of the velocity fields is that of a net current.

The dynamics of any cosmological fluid can be obtained, in general, from the linear Einstein equations (see Peebles and Yu 1970 [121], Silk and Wilkson 1980 [122], and Wilson and Silk 1981 [123] for earlier treatments). Although the choice of gauge does not impact the results, the Conformal Newtonian gauge leads to the most straightforward calculations. The metric is given by

$$ds^2 = a^2(\tau)[-(1 + 2\psi)d\tau^2 + (1 - 2\phi)dx^i dx_i], \tag{3-1}$$

where $\psi \simeq \phi$ when gravitational fields are weak. The linear Einstein equations are then as follows:

$$
\begin{aligned}
k^2\phi + 3\frac{\dot{a}}{a}(\dot{\phi} + \frac{\dot{a}}{a}\psi) &= 4\pi G a^2 \delta T^0_0, \\
k^2(\dot{\phi} + \frac{\dot{a}}{a}\psi) &= 4\pi G a^2 (\bar{\rho} + \bar{P})\theta, \\
\ddot{\phi} + \frac{\dot{a}}{a}(\dot{\psi} + 2\dot{\phi}) + (2\frac{\ddot{a}}{a} - \frac{\dot{a}^2}{a^2}) + \frac{k^2}{3}(\dot{\phi} - \dot{\psi}) &= \frac{4}{3}\pi G a^2 \delta T^i_i, \\
k^2(\phi - \psi) &= 12\pi G a^2 (\bar{\rho} + \bar{P})\sigma, \quad (3\text{--}2)
\end{aligned}
$$

where σ is the shear term, which is negligible for non-relativistic matter (but important for photons and neutrinos). For a cosmological fluid that is either uncoupled to the other fluids or mass-averaged among uncoupled fluids in the early universe, the following evolution equations hold:

$$
\begin{aligned}
\dot{\delta} &= -(1+w)(\theta - 3\dot{\phi}) - 3\frac{\dot{a}}{a}(c_s^2 - w)\delta, \\
\dot{\theta} &= -\frac{\dot{a}}{a}(1 - 3w)\theta - \frac{\dot{w}}{1+w}\theta + \frac{c_s^2}{1+w}k^2\delta - k^2\sigma + k^2\psi, \quad (3\text{--}3)
\end{aligned}
$$

where δ is defined as the local density relative to the spatial average ($\delta \equiv \delta\rho/\bar{\rho}$), $\theta \equiv ik^j v_j$ where v is the local peculiar velocity, and c_s is the sound speed of the fluid.

For individual components with inter-component interactions, equation (3–3) must be modified to include these interactions. Examples of such interactions include the momentum transfer between photons and charged particles and the Coulomb interaction between protons and electrons. For protons, electrons, and cold dark matter (CDM), an equation of state $w = 0$ is assumed, and for radiation and neutrinos, $w = \frac{1}{3}$. The master equations for each component of interest is computed explicitly in subsections 3.3.1-3.3.5.

3.3.1   Cold Dark Matter

As the cold dark matter component (denoted by the subscript c) is collisionless and pressureless, it can be simply read off from equation (3–3) that the equations which govern

its evolution are

$$\dot{\delta}_c = -\theta_c + 3\dot{\phi},$$
$$\dot{\theta}_c = -\frac{\dot{a}}{a}\theta_c + k^2\psi. \qquad (3\text{--}4)$$

Any cold (i.e., nonrelativistic), collisionless component will behave according to the dynamics given by equation (3–4).

3.3.2 Light Neutrinos

For massless (or nearly massless) particles, pressure is non-negligible. Additionally, the shear term (σ) may be important as well. The only accurate way to compute the evolution of such a component of the universe is by integration of the Boltzmann Equation, which is given for light neutrinos (denoted by subscript ν) by

$$\frac{\partial \mathcal{F}_\nu}{\partial \tau} + ik(\hat{k}\cdot\hat{n})\mathcal{F}_\nu = 4[\dot{\phi} - ik(\hat{k}\cdot\hat{n})\psi], \qquad (3\text{--}5)$$

in Fourier space.

The approximation that neutrinos are massless and uncoupled is very good from an age of the universe of approximately $t \simeq 1$ s until the epoch of recombination. The evolution equations for light neutrinos are then

$$\dot{\delta}_\nu = -\frac{4}{3}\theta_\nu + 4\dot{\phi},$$
$$\dot{\theta}_\nu = k^2(\frac{1}{4}\delta_\nu - \sigma_\nu + \psi),$$
$$\dot{\mathcal{F}}_{\nu l} = \frac{k}{2l+1}[l\mathcal{F}_{\nu(l-1)} - (l+1)\mathcal{F}_{\nu(l+1)}], \qquad (3\text{--}6)$$

where σ_ν is related to $\mathcal{F}_\nu$ by $2\sigma_\nu = \mathcal{F}_{\nu 2}$, and the index l governs the final equation for $l \geq 2$. $\mathcal{F}_{\nu l}$ is defined by the expansion of the perturbations in the distribution function, $\mathcal{F}_\nu$,

$$\mathcal{F}_\nu \equiv \sum_{l=0}^{\infty}(-i)^l(2l+1)\mathcal{F}_{\nu l}(k,\tau)P_l(\hat{k}\cdot\hat{n}), \qquad (3\text{--}7)$$

where $P_l(\hat{k} \cdot \hat{n})$ are the Legendre polynomials. Equations (3–5-3–7) are valid for any non-collisional species behaving as radiation.

3.3.3 Photons

Photons (denoted by subscript γ), although similar to light neutrinos, evolve differently due to their large coupling to charged particles. Thomson scattering describes the interactions of photons with electrons, where the differential cross-section is given by the formula

$$\frac{d\sigma}{d\Omega} = \frac{3\sigma_T}{16\pi}(1 + \cos^2\theta), \tag{3–8}$$

where σ_T is the Thomson cross-section [124]. Photons also scatter with protons, but with a cross-section suppressed by a factor of m_e^2/m_p^2 (the mass-squared ratio of electrons to protons).

$\mathcal{F}_\gamma$, which is the polarization-summed phase-space distribution for photons, is the same as the distribution function for neutrinos (see equation 3–7). Photons also contain a non-zero difference between the two linear polarization components, denoted by $\mathcal{G}_\gamma$. The linearized collision operators for Thomson scattering [22, 125–127] yield the set of master equations for photons,

$$
\begin{aligned}
\dot{\delta}_\gamma &= -\frac{4}{3}\theta_\gamma + 4\dot{\phi}, \\
\dot{\theta}_\gamma &= k^2\left(\frac{1}{4}\delta_\gamma - \sigma_\gamma\right) + k^2\psi + an_e\sigma_T(\theta_b - \theta_\gamma), \\
\dot{\mathcal{F}}_{\gamma 2} &= \frac{8}{15}\theta_\gamma - \frac{3}{5}k\mathcal{F}_{\gamma 3} - \frac{9}{5}an_e\sigma_T\sigma_\gamma \\
&\quad + \frac{1}{10}an_e\sigma_T(\mathcal{G}_{\gamma 0} + \mathcal{G}_{\gamma 2}), \\
\dot{\mathcal{F}}_{\gamma l} &= \frac{k}{2l+1}[l\mathcal{F}_{\gamma(l+1)} - (l+1)\mathcal{F}_{\gamma(l+1)}] - an_e\sigma_T\mathcal{F}_{\gamma l}, \\
\dot{\mathcal{G}}_{\gamma m} &= \frac{k}{2m+1}[m\mathcal{G}_{\gamma(m-1)} - (m+1)\mathcal{G}_{\gamma(m+1)}] \\
&\quad + an_e\sigma_T\left[\frac{1}{10}\mathcal{F}_{\gamma m} - \frac{2}{5}\mathcal{G}_{\gamma m}\right],
\end{aligned}
\tag{3–9}
$$

where $\mathcal{F}_{\gamma 0} = \delta_\gamma$, $\mathcal{F}_{\gamma 1} = 4\theta_\gamma/3k$, $\mathcal{F}_{\gamma 2} = 2\sigma_\gamma$, the indices l and m are valid for $l \geq 3$ and $m \geq 0$, and the subscript b denotes the baryonic component, which is the mass-weighted sum of the electrons and protons. Electron-photon scattering is so dominant over proton-photon scattering as to render the latter negligible, but the electron-proton coupling (via electromagentism) is sufficiently strong that, to leading order, those two fluids move in kinetic equilibrium.

3.3.4 Baryons

The net behavior of the baryonic component can be derived from combining the mass-weighted contributions of the proton fluid and the electron fluid. Both protons and electrons contain all of the terms present in the CDM equations (see section 3.3.1), but additionally contain important sound-speed terms and terms arising from Thomson scattering. Additionally, the Coulomb interaction enters through the contribution of the electric field to the T^0_i components of the stress-energy tensor. The coupling of the Coulomb interaction to density inhomogeneities can be calculated through a combination of the electromagnetic Poisson equation,

$$\nabla^2 \Phi = -\nabla \cdot \vec{E} = -4\pi \rho_C, \tag{3--10}$$

where ρ_C is the electric charge density, and the Euler equation,

$$\frac{1}{a}\frac{\partial(a\vec{v})}{\partial t} + \frac{1}{a}(\vec{v} \cdot \nabla)\vec{v} = -\frac{1}{a}\nabla\phi - \frac{q}{m}\frac{1}{a}\nabla\Phi + \mathcal{C}, \tag{3--11}$$

with q/m as the charge-to-mass ratio of the particle in question and $\mathcal{C}$ the collision operator. The Coulomb contribution appears as $4\pi e(n_p - n_e)q_i/m_i$ in the evolution equation for $\dot{\theta}_i$, where i denotes a species of particle with a mass m_i and charge q_i. The

evolution equations are therefore

$$
\begin{aligned}
\dot{\delta}_e &= -\theta_e + 3\dot{\phi}, \\
\dot{\theta}_e &= -\frac{\dot{a}}{a}\theta_e + c_s^2 k^2 \delta_e + k^2 \psi \\
&\quad + \Gamma_e(\theta_\gamma - \theta_e) - \frac{4\pi e^2}{m_e}(n_p - n_e),
\end{aligned}
\tag{3–12}
$$

for electrons (denoted by subscript e), and

$$
\begin{aligned}
\dot{\delta}_p &= -\theta_p + 3\dot{\phi}, \\
\dot{\theta}_p &= -\frac{\dot{a}}{a}\theta_p + c_s^2 k^2 \delta_p + k^2 \psi \\
&\quad + \Gamma_p(\theta_\gamma - \theta_p) + \frac{4\pi e^2}{m_p}(n_p - n_e),
\end{aligned}
\tag{3–13}
$$

for protons, denoted by subscript p, where the damping coefficients for electrons (Γ_e) and protons (Γ_p) are given by

$$
\begin{aligned}
\Gamma_e &\equiv \frac{4\bar{\rho}_\gamma n_e \sigma_T a}{3\bar{\rho}_e}, \\
\Gamma_p &\equiv \frac{4\bar{\rho}_\gamma n_e \sigma_T a}{3\bar{\rho}_p}\left(\frac{m_e}{m_p}\right)^2 \simeq 1.6 \times 10^{-10}\,\Gamma_e.
\end{aligned}
\tag{3–14}
$$

Note the difference in the sign of the final terms in the equations for $\dot{\theta}_e$ and $\dot{\theta}_p$, which will prove important in the analysis below.

From equations (3–12) and (3–13) for electrons and protons the dominant gravitational and electromagnetic combinations can be constructed separately. The remainder of this subsection details the evolution of baryons in the linear regime of a perturbed universe. Baryonic matter can be treated as the combination of electrons and protons, thus the mass weighted sum of proton and electron overdensities gives rise to the baryonic perturbations,

$$
\delta_b \equiv \frac{m_e}{m_b}\delta_e + \frac{m_p}{m_b}\delta_p, \qquad \theta_b \equiv \frac{m_e}{m_b}\theta_e + \frac{m_p}{m_b}\theta_p.
\tag{3–15}
$$

By substituting the expressions for equations (3–12) and (3–13) into equation (3–15), a set of equations for the evolution of baryonic matter is obtained. So long as approximations

such as $n_p \simeq n_e$ and $m_b \simeq m_p \gg m_e$ hold, quantities which are obviously small compared to the others (such as $n_p - n_e$) can be neglected. The evolution equations are then

$$
\begin{aligned}
\dot{\delta}_b &= -\theta_b + 3\dot{\phi}, \\
\dot{\theta}_b &= -\frac{\dot{a}}{a}\theta_b + c_s^2 k^2 \delta_b + k^2\psi + \Gamma_b(\theta_\gamma - \theta_b),
\end{aligned}
\qquad (3\text{–}16)
$$

where $\Gamma_b \approx \Gamma_e m_e/m_b$. The baryon-photon coupling term in equation (3–16) is driven by the electron-photon interaction. To the extent that electrons and protons move together (the tight-coupling approximation), the baryonic fluid is dragged by the electron-photon interactions, as has been shown by Harrison 1970 [109] and subsequent authors. Equation (3–16) is identical to the equations for baryon evolution derived in Ma and Bertschinger 1995 [22].

3.3.5 Charge Separations

From equations (3–12) and (3–13), a *difference* component as well as a sum component can be obtained. As the limits on a net electric charge asymmetry in the universe are very strict [17, 18, 128], any component arising from the differences in densities and/or velocities of protons and electrons will not be strong enough to significantly impact the evolution of the other species of particles in the universe, including the baryon component.

The charge difference component (denoted by subscript q) is the difference between the proton and electron components, such that $\delta_q = \delta_p - \delta_e$ and $\theta_q = \theta_p - \theta_e$. The gravitational potential ought not to enter into these equations, due to the fact that gravity acts equivalently on electrons and protons. However, velocities and number densities may differ, $n_p - n_e \simeq n_e\delta_q$. The master equations for the charge-asymmetric component are as

follows:

$$\dot{\delta}_q = -\theta_q$$

$$\dot{\theta}_q = -\frac{\dot{a}}{a}\theta_q + c_s^2 k^2 \delta_q + \frac{4\pi n_e e^2}{m_e}\delta_q$$
$$- \Gamma_e(\theta_\gamma - \theta_b + \theta_q), \tag{3-17}$$

where the approximations $\Gamma_p \ll \Gamma_e$ and $m_b \simeq m_p$ have been utilized where applicable. The term $4\pi n_e e^2 \delta_q / m_e$ in equation (3–17) arises from the Coulomb force acting on charged particles, while the final term, $\Gamma_e(\theta_\gamma - \theta_b + \theta_q)$, arises from the difference in Thomson scattering between protons and electrons. This final term is a source of charge separation independent of and in addition to any initial charge asymmetry, and will create a local charge asymmetry *even when there is none initially.* In the evaluation of equation (3–17), the electromagnetic terms dominate the cosmological terms, such that an excellent approximation in the pre-recombination universe is

$$\dot{\delta}_q = -\theta_q, \qquad \dot{\theta}_q = \frac{4\pi n_e e^2}{m_e}\delta_q - \Gamma_e(\theta_\gamma - \theta_b + \theta_q). \tag{3-18}$$

For some purposes, it is useful to express the set of equations found in equation (3–17) as a single ordinary differential equation. This can be accomplished by setting $\dot{\theta}_q = -\ddot{\delta}$, and again by neglecting the unimportant cosmological terms $\theta_q \dot{a}/a$ and $c_s^2 k^2 \delta_q$. Many of the coefficients in equation (3–17) are functions of a, but the derivatives in equation (3–17) are with respect to conformal time, τ. A change of variables can be performed, using the relation that

$$t = \left[\frac{45\hbar^3 c^5}{32\pi^3 G(kT)^4}\right]^{1/2}$$
$$= Na^2 t_0,$$

$$N \simeq 72.2, \tag{3-19}$$

in the radiation era, where t_0 is the age of the universe today, to express all derivatives as derivatives with respect to a, denoted by primes (instead of dots).

The evolution of δ_q can be tracked by evolving equation (3–20) below,

$$
\begin{aligned}
\delta_q'' + 2N\,\Gamma_{e,0}\frac{1}{a^2}\delta_q' \;+\;& \frac{16N^2\,\pi\,n_{e,0}\,e^2}{m_e}\frac{1}{a}\delta_q \\
=\;& 4N^2\,\Gamma_{e,0}\frac{1}{a}(\theta_\gamma - \theta_b),
\end{aligned}
\tag{3–20}
$$

where the subscript 0 denotes the present value of a quantity. This is simply the equation of a damped harmonic oscillator, with coefficients that change slowly with time compared to damping or oscillation times. The behavior can be characterized as overdamped at the earliest times, critically damped when $a \approx 3.9 \times 10^{-15}$, and free at late times.

Of all the terms in equation (3–20), only θ_γ, θ_b, and δ_q (and derivatives) are functions of a; all other quantities are constant coefficents. Although there does not exist a simple analytic form for $(\theta_\gamma - \theta_b)$ in general, at sufficiently early times there exists the simple approximation

$$
\theta_\gamma - \theta_b \simeq 6.0 \times 10^{19}\,k^4\,a^5,
\tag{3–21}
$$

valid when the following condition is met:

$$
\begin{aligned}
a &\lesssim 10^{-5} &&\text{for}&& k \leq 0.1\,\mathrm{Mpc}^{-1}, \\
a &\lesssim 10^{-6}\left(\frac{1\,\mathrm{Mpc}^{-1}}{k}\right) &&\text{for}&& k \geq 0.1\,\mathrm{Mpc}^{-1}.
\end{aligned}
$$

Equation (3–21) is an approximation for a flat ΛCDM cosmology with cosmological parameters $H_0 = 71$ km s^{-1} Mpc^{-1}, $\Omega_m = 0.27$, $\Omega_b = 0.044$, and a Helium-4 mass fraction of $Y = 0.248$. These parameters are used in all subsequent analyses for the calculation of cosmological quantities.

The approximation in equation (3–21) breaks down at sufficiently late times. When this occurs, numerical methods must be used to obtain the quantity $(\theta_\gamma - \theta_b)$. The software package COSMICS [129] is ideal for performing this computation, as it performs numerical evolution of equations (3–4,3–6,3–9, and 3–16) concurrently. Computational results for the quantities θ_γ and θ_b are given by COSMICS, which are valid at all times in the linear

regime of structure formation. It is found that when the approximation in equation (3–21) breaks down, the quantity $(\theta_\gamma - \theta_b)$ grows more slowly initially, and proceeds to oscillate at a roughly constant amplitude at later times. These oscillations in the quantity $(\theta_\gamma - \theta_b)$ are closely related to the acoustic oscillations between baryons and photons observed in the cosmic microwave background [5].

Numerical integration of equation (3–20) can be accomplished in various ways, as illustrated in Press et al. 1992 [130]. At sufficiently late times (when $a \gg 3.9 \times 10^{-15}$), numerical results indicate that the quasi-equlibrium solution

$$\delta_q = \frac{\sigma_T\, m_b}{3\,\pi\, e^2} \left(\frac{\bar{\rho}_{\gamma,0}}{\bar{\rho}_{\mathrm{b},0}} \right) (\theta_\gamma - \theta_b), \tag{3–22}$$

obtained by neglecting the first two terms in equation (3–20), is an excellent approximation. With θ_γ and θ_b given by COSMICS in units of Mpc^{-1}, the prefactor in equation (3–22) can be written as

$$\frac{\sigma_T\, m_b}{3\,\pi\, e^2} \left(\frac{\bar{\rho}_{\gamma,0}}{\bar{\rho}_{\mathrm{b},0}} \right) \approx 1.64 \times 10^{-37}\, \mathrm{Mpc}. \tag{3–23}$$

The quantity θ_q then follows directly from equation (3–17) to be

$$\theta_q = -\frac{\sigma_T\, m_b}{3\,\pi\, e^2} \left(\frac{\bar{\rho}_{\gamma,0}}{\bar{\rho}_{\mathrm{b},0}} \right) (\dot{\theta}_\gamma - \dot{\theta}_b). \tag{3–24}$$

The solutions in equations (3–22) and (3–24) are valid until gravitational collapse becomes nonlinear, which means that they are still valid at the epoch of recombination ($z \simeq 1089$). The results of numerically integrating the equations for δ_q and θ_q on various length scales up through recombination are presented in Figure 3-1.

It is worth pointing out that the results obtained in this section can be applied to a situation where a net electric charge is present. In appendix B, the possibility of using the evolution equations derived for θ_q and δ_q is applied to a universe with a broken $U(1)$ symmetry. The possibility exists that, under the proper circumstances, an initially charged universe may become neutral simply due to the expansion dynamics.
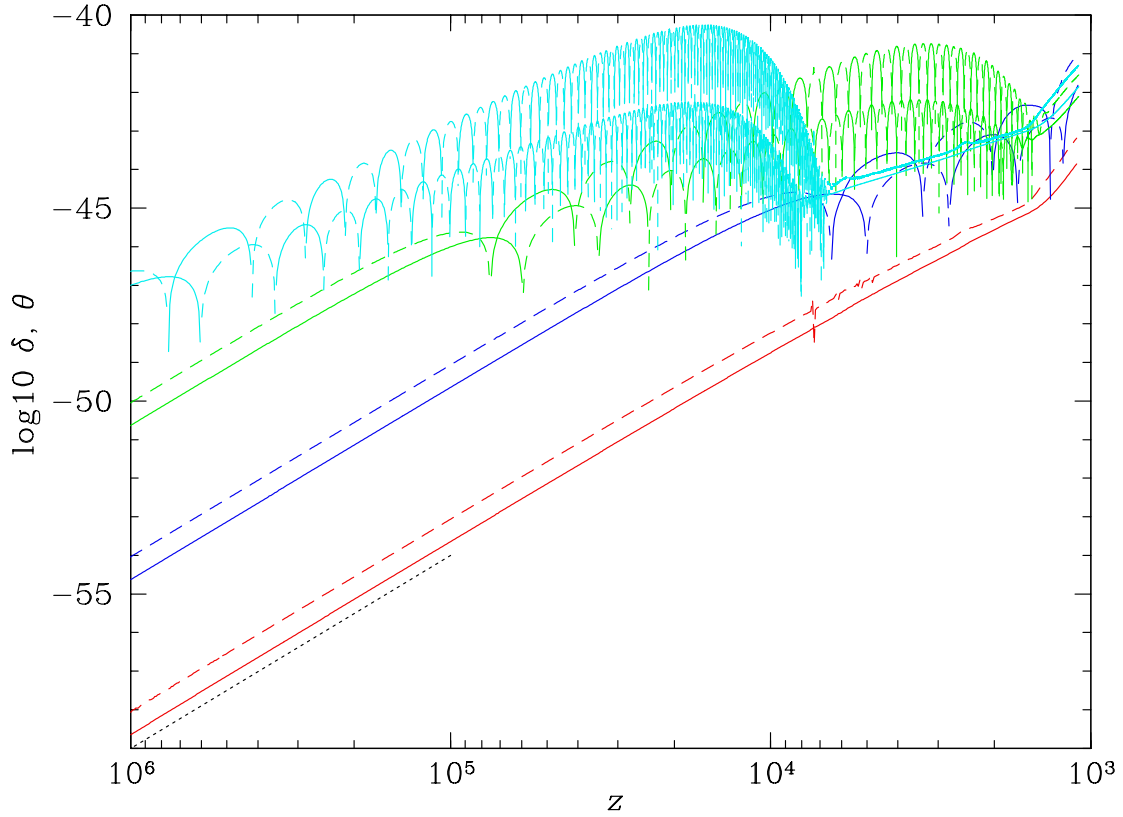
Figure 3-1. δ_q (solid lines) and θ_q/H, where H is the Hubble parameter (dashed lines) as a function of redshift (z). The lines shown are for comoving scales of (from top to bottom) 10, 1, 0.1, and 0.01 Mpc^{-1}. δ_q rises as $\sim a^5$ initially, then ceases to grow when the scale of interest enters the horizon, and oscillates at an amplitude which first continues to rise slowly, then falls, eventually matching on to the equilibrium solution that $\delta_q \propto \theta_b$. θ_q can be obtained from δ_q through equation (3–17). This graph uses output from COSMICS, and as such needs to be multiplied by the COBE normalization of Bunn and White [2].

3.4   Magnetic Fields

With the results derived in Section 3 for θ_q and δ_q, values for the local current

densities and local charge separations can be obtained at any time in the pre-recombination

universe on all scales. Both δ_q and θ_q will contribute to magnetic fields, as currents create

magnetic fields directly, and the bulk motion of a region of net charge will also produce

a magnetic field. For each comoving distance scale (given by the value of k) and each

timeslice (determined by the scale factor a) of the universe, there will be a unique

magnetic field amplitude associated with that scale. This field may serve as the seed

for the large-scale magnetic fields observed today.

An expression for magnetic fields can be derived from the currents arising from

the relative motion of the protons and electrons in the universe. Magnetic fields can be

derived from Maxwell's equations

$$\nabla \cdot \vec{B} = 0, \qquad \nabla \times \vec{B} = 4\pi \vec{J} + \frac{\partial \vec{E}}{\partial t}, \tag{3–25}$$

with the current density $\vec{J}$ given by

$$\vec{J} = n_p\, e\, \vec{v}_p - n_e\, e\, \vec{v}_e \simeq n_e e [\delta_q \vec{v}_b + (1 + \delta_b)\vec{v}_q], \tag{3–26}$$

where $\vec{v}_q \equiv \vec{v}_p - \vec{v}_e$, and the displacement current is neglected.

By taking the curl, a direct expression for magnetic fields as a function of a and k is

obtained as a convolution

$$\vec{B}(\vec{k}) \;=\; \frac{4\pi\, n_{e,0}\, e}{a^2 |\vec{k}|^2} \int \frac{d^3 k'}{(2\pi)^3} \frac{\vec{k} \times \vec{k}'}{|\vec{k}'|^2} [\theta_b(\vec{k}')\, \delta_q(\vec{k} - \vec{k}') \\ + \theta_q(\vec{k}')\, \delta_b(\vec{k} - \vec{k}')]. \tag{3–27}$$

While the magnetic field strength can, in principle, be obtained by solving equation

(3–27), it is more favorable to obtain the power spectrum of the magnetic field. The power

spectrum is obtained by examining the second moment of the magnetic field $\vec{B}(\vec{k})$, which

is

$$\langle B_i(\vec{k}_1)B_j(\vec{k}_2)\rangle \;=\; (2\pi)^3\delta_D(\vec{k}_1+\vec{k}_2)\,P_{ij}^{\perp}\,P_B(k),$$

$$P_{ij}^{\perp} \;\equiv\; \frac{1}{2}(\delta_{ij}-\hat{k}_i\hat{k}_j), \tag{3--28}$$

where δ_D is the Dirac delta function and $P_B(k)$ is the magnetic field power spectrum. Note that the direction parallel to $\vec{k}$ does not contribute to magnetic fields, and therefore the direction perpendicular to $\vec{k}$ is projected out in equation (3–28). The power spectrum, $P_B(k)$, is then given by the expression

$$
\begin{aligned}
P_B(k) \;=\;& \left(\frac{4\pi\,n_{e,0}\,e}{a^2|\vec{k}|^2}\right)^2 \int \frac{d^3k'}{(2\pi)^3}\,|\vec{k}|^2\,\sin^2\lambda \\[4pt]
&\times \Bigg[\frac{1}{|\vec{k}'|^2}\,P_{\theta_q\theta_q}(|\vec{k}'|)P_{\delta_b\delta_b}(|\vec{k}-\vec{k}'|) \\[4pt]
&\quad -\frac{1}{|\vec{k}-\vec{k}'|^2}\,P_{\theta_q\delta_b}(|\vec{k}'|)P_{\theta_q\delta_b}(|\vec{k}-\vec{k}'|) \\[4pt]
&\quad +\frac{1}{|\vec{k}'|^2}\,P_{\theta_b\theta_b}(|\vec{k}'|)P_{\delta_q\delta_q}(|\vec{k}-\vec{k}'|) \\[4pt]
&\quad -\frac{1}{|\vec{k}-\vec{k}'|^2}\,P_{\theta_b\delta_q}(|\vec{k}'|)P_{\theta_b\delta_q}(|\vec{k}-\vec{k}'|) \\[4pt]
&\quad +\frac{2}{|\vec{k}'|^2}\,P_{\theta_q\theta_b}(|\vec{k}'|)P_{\delta_q\delta_b}(|\vec{k}-\vec{k}'|) \\[4pt]
&\quad -\frac{2}{|\vec{k}-\vec{k}'|^2}\,P_{\theta_q\delta_q}(|\vec{k}'|)P_{\theta_b\delta_b}(|\vec{k}-\vec{k}'|)\Bigg],
\end{aligned}
\tag{3--29}
$$

where the angle λ is the angle between the vectors $\vec{k}$ and $\vec{k}'$. The expression for power in any two quantities, ϕ and ψ, $P_{\phi\psi}(k)$, is generically defined by

$$\langle\tilde{\phi}(\vec{k}_1)\tilde{\psi}(\vec{k}_2)\rangle = (2\pi)^3\delta_D(\vec{k}_1+\vec{k}_2)P_{\phi\psi}(k). \tag{3--30}$$

The solutions obtained for θ_q and δ_q in equations (3–22) and (3–24) can be substituted into the equation for the power spectrum, equation (3–29). By numerically integrating the resulting expression, the spectral density can be obtained. The spectral density is

$4\pi k^3 P_B(k)/(2\pi)^3$, and provides both a measure of the magnetic field strength on a given scale (k) and a measure of the energy stored in magnetic fields.

The results for the spectral density of magnetic field energy on comoving scales ranging from 10^{-3} Mpc^{-1} to 10^2 Mpc^{-1} at the epoch of recombination are shown in Figure 3-2. The peak of the spectral density corresponds to a typical magnetic field strength of 10^{-23} Gauss on comoving scales of 0.1 Mpc^{-1}.

3.5   Discussion

The major result of this paper has been to illustrate that seed magnetic fields of cosmologically interesting strengths and scales are necessarily generated by the same processes that cause structure formation. As overdense regions in the early universe slowly grow during the radiation era, photon interactions with both protons and electrons create charge separations and current densities of small magnitudes, but on *all* scales. These charge separations and currents grow in magnitude as the universe ages, causing magnetic fields to grow as well. Magnetic power peaks at approximately the time of horizon crossing, falling slowly after that. The net result is that, at the epoch of recombination (and hence prior to significant field amplification due to gravitational collapse or dynamo effects), seed magnetic fields of magnitude $\mathcal{O}(10^{-23}\,\text{G})$ are created by the simple dynamics of charged particles.

The results of this paper are very accurate up through the epoch of recombination. At this epoch, however, the universe transitions from a fully ionized state (where the ionization fraction $\chi_e \simeq 1$) to a state where the ionization fraction is very small, $\chi_e \approx 10^{-4}$ [24]. While the photons are generally decoupled from the baryons at this point, the free electrons continue to interact with the photons, due to the extraordinary number of photons per free electron. In the absence of any interactions with photons, a charge separation would evolve as

$$\ddot{\delta}_q = -\frac{4\pi\, n_{e,0}\, e^2}{m_e} \delta_q = -\frac{3}{2}\, \Omega_b\, H^2\, K^2\, \delta_q, \tag{3--31}$$

47
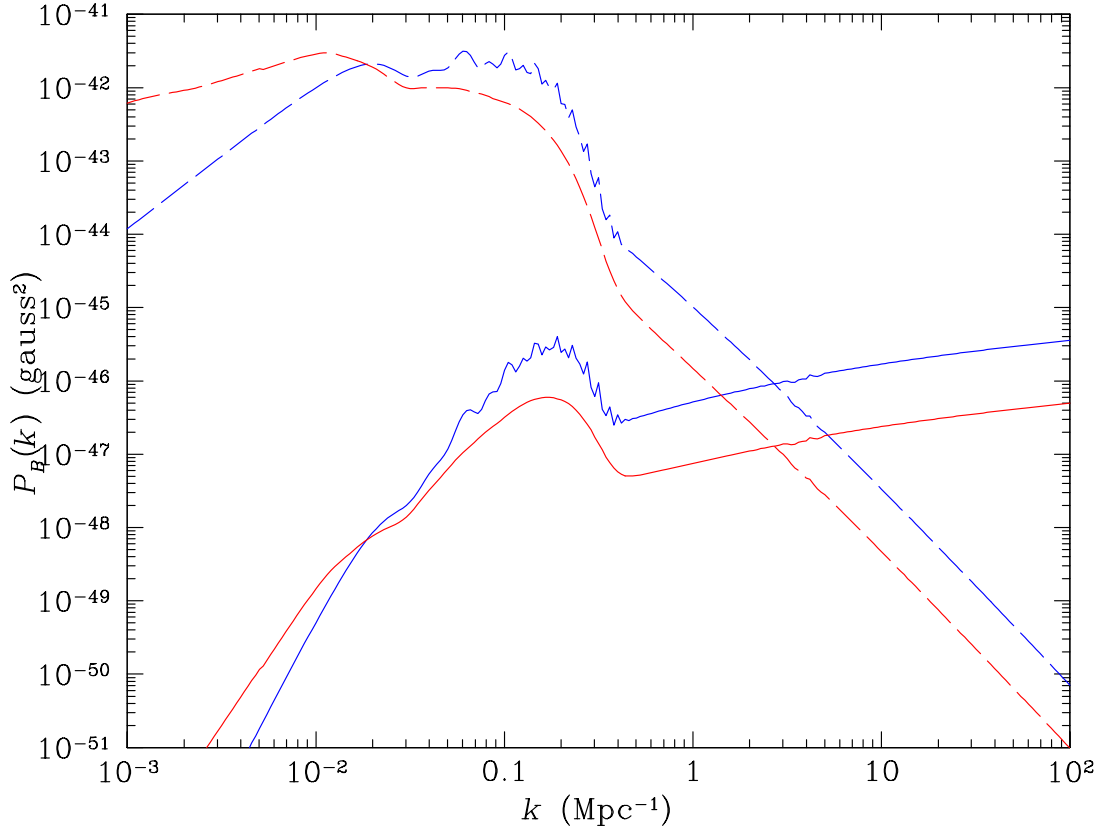
Figure 3-2. Spectral energy density of the magnetic field ($\vec{B}$, in gauss) generated by cosmological perturbations on a given comoving scale (k, in Mpc^{-1}) at the epoch of recombination ($z \simeq 1089$). The line illustrates $4\pi k^3 P_B(k)/(2\pi)^3$, which is the spectral density in units of G^2; the peak value is a magnetic field strength $B \sim 10^{-23}$ G. The upper lines are the simple power spectrum, $P_B(k)$.

where K^2 is the ratio of the electric to gravitational forces,

$$K^2 = \frac{e^2}{Gm_p m_e} \approx (4.77 \times 10^{19})^2.$$

A charge separation free of external interactions would oscillate (via plasma oscillations) with frequency $\omega \approx KH$. However, as there are many complicated effects that begin to become important after recombination, including gravitational collapse, dynamo effects, and continued electron-photon scattering, it is unlikely that the simple equation (3–31) accurately describes the evolution of charge separations in the post-recombination universe.

While field amplification due to gravitational collapse is negligible at the epoch of recombination, this will not be the case at all times. At recombination, the universe has only been matter-dominated for a brief time, and thus density perturbations have only grown by a small amount in that time, leading to an insignificant amplification of the field strength. As magnetic flux gets frozen in, however, nonlinear collapse causes $|\vec{B}|$ to increase by many orders of magnitude [92, 93].

The major source of amplification of an initial seed field, however, comes from dynamo effects, as discussed in Section 2. The key to solving the puzzle of the origin of cosmic magnetic fields lies in determining whether the seed fields produced by a given mechanism can be successfully amplified into the $\mathcal{O}(\mu G)$ fields observed today. A major problem with many of the astrophysical mechanisms that produce seed fields is that they produce low-magnitude fields at insufficiently early times for dynamo amplification to produce fields as large as $\sim \mu G$. The Biermann mechanism, for instance, can produce seed fields of order $\sim 10^{-19}$ G, but only at a redshift of $z \sim 20$. Although those initial fields are larger than the $\sim 10^{-23}$ G fields produced by the growth of cosmic structure, the fact that magnetic fields from structure formation are in place at $z \simeq 1089$ makes them an extremely attractive candidate for the seeds of cosmic magnetic fields. As argued by Davis et al. 1999 [131], a seed field as small as 10^{-30} G at recombination could

possibly be amplified into a μG field today. Clearly, more work on understanding dynamo amplification is necessary before a definitive solution to the puzzle of cosmic magnetic fields can emerge.

One interesting mechanism worth investigating further is for the cosmic seed fields generated by density perturbations to seed supermassive black holes. It is known that the magnetic field energy in active galactic nuclei and quasars is comparable to the magnetic field energy in an entire galaxy. However, these structures cannot generate their own magnetic fields from nothing; they require a pre-existing seed field. It therefore appears to be a reasonable possibility that the seed fields generated by cosmic structure formation could provide the necessary fields to seed supermassive black holes. The resultant amplification via collapse and dynamo effects could explain the origin of large-scale magnetic structures in the universe.

If large-scale magnetic fields exist at the epoch of recombination, they may be detectable by upcoming experiments. The results shown in Figure 3-2 provide a prediction of large-scale magnetic fields at the epoch of the cosmic microwave background. Sufficiently large magnetic fields on large scales at recombination may be detectable by PLANCK [132, 133], although current estimates of their sensitivity indicate that the field strengths predicted in this paper ($\sim 10^{-23}$ G) would be significantly out of range of PLANCK's capabilities ($\sim 10^{-10}$ G). Nonetheless, a knowledge of the field strengths at recombination allow for predictions of CMB photon polarizations and Faraday rotation, both of which may be, at least in principle, observable.

It is also of interest to note that any primordial charge asymmetry or large-scale currents (and therefore magnetic fields) created in the very early universe ($a \lesssim 3.9 \times 10^{-15}$) will be driven away by these dynamics. Equation (3–20) has an approximate solution for δ_q which is critically (exponentially) damped at $a \simeq 3.9 \times 10^{-15}$, capable of reducing an arbitrarily large charge or current by as much as a factor of $e^{-10^{15}}$. Any pre-existing δ_q or θ_q will be driven quickly to the value given by equations (3–22) and (3–24) at the epoch

of critical damping. This ought to be applicable even to a global asymmetry, which can be treated as a charge anisotropy (δ_q) on the scale of the horizon. Therefore, the results in this paper for charge separations, currents, and magnetic fields are independent of the initial conditions on δ_q, θ_q, and $|\vec{B}|$ in the universe.

There has been other recent work that claims to generate a magnetic field from cosmological perturbations via "baryon-photon slip," photon anisotropic stress, and a second order velocity vorticity [134]. The results of this work do not require a velocity vorticity or anisotropic stress, nor do they require second order quantities. This paper derives magnetic fields from cosmological perturbations in a very straightforward manner, simply by calculating the charge separations and currents which necessarily arise from the differing interactions on protons and electrons, and obtaining magnetic fields directly from those quantities. The motivation behind the methods used in Ichiki et al. 2006[134] are obscure and not easily comprehended, while their results are inconsistent with those obtained in this paper, as their results for magnetic field strength and spectral density are suspiciously large. Furthermore, it is unclear how their results for velocity vorticity are obtained, as it is well-known that the vorticity vanishes at second and all orders if there is none initially.

Overall, the dynamics of ions, electrons, and photons during the radiation era necessarily leads to charge separations and currents on all scales, which in turn generate magnetic fields. These fields supersede any pre-existing fields and are in place prior to substantial gravitational collapse. Thus, the dynamics of structure formation from cosmological perturbations emerges as a promising and well-motivated new candidate to explain the origins of cosmic magnetic fields.

CHAPTER 4
EFFECTS ON COSMIC EXPANSION

We evaluate the effect of cosmological inhomogeneities on the expansion rate of the universe. Our method is to expand to Newtonian order in potential and velocity but to take into account fully nonlinear density inhomogeneities. To linear order in density, kinetic and gravitational potential energy contribute to the total energy of the universe with the same scaling with expansion factor as spatial curvature. In the strongly nonlinear regime, growth saturates, and the net effect of the energy in inhomogeneities on the expansion rate remains negligible at all times. In particular, inhomogeneity contributions never mimic the effects of dark energy or induce an accelerated expansion.

4.1   Accelerated Expansion

Recent observations of type-Ia supernovae [135] and the cosmic microwave background [5] in tandem suggest that the cosmological expansion is accelerating. Understanding the source of this accelerated expansion is one of the greatest current unsolved problems in cosmology [136]. Acceleration seems to render inadequate a universe consisting entirely of matter, and appears to require an additional, unknown type of energy (dark energy, perhaps realized as a cosmological constant). An alternative to dark energy is that acceleration arises from a known component of the universe whose effects on the cosmic expansion have not been fully examined. One possibility currently being examined is that inhomogeneities in a matter dominated universe, on either sub-horizon [29, 30] or super-horizon scales [28, 137–139], may influence the expansion rate at late times. The central idea is that the energy induced by inhomogeneities leads to additional source terms in the Friedmann equations, with effects on the dynamics that leave no need for a separate dark energy component. In their entirety, these proposals present conflicting claims and a general state of much confusion: does the energy in inhomogeneities produce an accelerated expansion, acting in effect as dark energy [138], or does it behave as curvature [31]? Is the magnitude of the effect small, large, or even divergent, on either large scales [138], or on small scales at late times [30]?

Part of the confusion arises from the fully relativistic perturbation theory formulation of many of these calculations. Although this is undeniably a valid approach, the number of terms in a perturbation theory calculation can be large and can mask the underlying physics. In this Chapter, taking advantage of phenomenological results that have been derived from a combination of quasilinear perturbation theory, nonlinear theory, and numerical simulations, we compute the potential and kinetic inhomogeneity energies within the horizon to Newtonian order in potential and velocity for fully nonlinear density contrasts. We find these energies to be small at present, and their projected values remain small, even far into the future. The following section considers the effect of inhomogeneities, for weak gravity and slow motions but for arbitrary density perturbations, characterized in terms of the density power spectrum. After that, the results for the kinetic and potential energies in both the linear and the fully nonlinear regimes are presented, as a function of the cosmological expansion factor. Finally, the implications of these results for the present and future expansion history of the universe are discussed.

4.2   Effects of Inhomogeneities

The purpose of this chapter is to investigate whether energy in inhomogeneities can mimic the effects of dark energy for a universe containing only matter. To this end, we work in an $\Omega_m = 1$ Einstein-de Sitter universe, with no curvature or cosmological constant, and compute the effects of inhomogeneities on the cosmic expansion rate. The dynamics of cosmological expansion are governed by the Friedmann equations,

$$\left(\frac{\dot{a}}{a}\right)^2 = \frac{8\pi}{3} G\rho, \qquad \left(\frac{\ddot{a}}{a}\right) = -\frac{4\pi}{3} G(\rho + 3p). \qquad (4\text{--}1)$$

Any mass or energy density that makes up a significant fraction of the total can influence the evolution of the cosmological scale factor $a(t)$. A contribution to the energy density of the universe with equation of state $p_i = w\rho_i$ has $\rho_i \propto a^{-3(1+w)}$, or $\rho_i/\rho_m \propto a^{-3w}$; in

particular, a component with $\rho \propto a^{-2}$ behaves as $w = -\frac{1}{3}$ or curvature, and a component with constant ρ behaves as a cosmological constant or dark energy.

We introduce the effects of inhomogeneities following the formulation of Seljak and Hui 1996 [140]. In the conformal Newtonian gauge, with metric

$$ds^2 = a^2(\tau)[-(1 + 2\psi)d\tau^2 + (1 - 2\phi)dx^2], \qquad (4\text{–}2)$$

the time-time Einstein equation ($G^0_{\ 0}$) yields

$$3\left(\frac{\dot{a}}{a}\right)^2(1 - 2\psi) + (2 \ + \ 6\phi)\frac{1}{a^2}\nabla^2\phi + \frac{1}{a^2}(\nabla\phi)^2$$
$$= \ 8\pi G\bar{\rho}(1 + \delta)(1 + v^2), \qquad (4\text{–}3)$$

Where $\phi \simeq \psi$ from the space-space components of $G^\mu_{\ \nu}$. (Our numerical factors are slightly corrected from those found in Seljak and Hui 2006 [140]; these factors make little difference in the overall results.) The source on the right-hand side includes a density perturbation $\delta = \delta\rho/\bar{\rho}$ in the material rest frame, with the transformation to the cosmological frame expanded to leading order for small v^2. Ignoring $\phi\,\nabla^2\phi$, $(\nabla\phi)^2$, and v^2, the homogeneous part of this equation reproduces the usual Friedmann equation. The inhomogeneous part reveals that ϕ obeys the Poisson equation with source $4\pi G\bar{\rho}a^2\delta$. The volume average of the entire equation then leads to

$$\left(\frac{\dot{a}}{a}\right)^2 = \frac{8\pi}{3}G\bar{\rho}\left(1 - 5\,W + 2K\right), \qquad (4\text{–}4)$$

where W and K are the Newtonian potential and kinetic energy per unit mass,

$$W = \frac{1}{2}\left\langle(1 + \delta)\,\phi\right\rangle, \qquad K = \frac{1}{2}\left\langle(1 + \delta)v^2\right\rangle. \qquad (4\text{–}5)$$

These expressions are correct to first order in ϕ and v^2, but neither an assumption nor an approximation in δ. We assume that $\langle\nabla^2\phi\rangle = 0$; in all other places the Poisson equation is adequate to determine ϕ.

The Newtonian potential and kinetic energies thus can influence cosmological expansion. We can compute both W and also K completely and exactly from knowledge only of the density power spectrum. The potential is related to the density inhomogeneity by the Poisson equation, $\nabla^2 \phi = 4\pi G \bar{\rho} a^2 \delta$, an expression which holds even for nonlinear inhomogeneities. From this, we obtain

$$W = -\frac{1}{2} \, 4\pi G \bar{\rho} a^2 \int \frac{d^3 k}{(2\pi)^3} \, \frac{P(k)}{k^2} = -\int \frac{dk}{k} \, \Delta_W^2(k), \tag{4--6}$$

an expression correct in both linear and nonlinear regimes if $P(k)$ is the appropriate linear or nonlinear power spectrum. The last equality defines the dimensionless spectral density $\Delta_W^2(k)$.

In linear perturbation theory, valid for small inhomogeneities, the density contrast grows as $\delta = \delta_0(x) D(t)$, where in a matter dominated universe $D(t) \propto a(t) \propto t^{2/3}$ [141]. The kinetic energy follows from the linearized equation of continuity, $\dot{\delta} + \nabla \cdot v/a = 0$ [141],

$$K_{\mathrm{lin}} = \frac{1}{2} \dot{a}^2 \int \frac{d^3 k}{(2\pi)^3} \, \frac{P(k)}{k^2} \tag{4--7}$$

(the usual factor $f(\Omega) \simeq \Omega^{0.6} = 1$ for $\Omega_m = 1$). The kinetic energy scales with $a(t)$ as $\dot{a}^2 D^2$, while the potential energy scales as $\bar{\rho} a^2 D^2$; and so both W and K grow as $D^2/a \propto a(t)$, or $\rho_U = \bar{\rho}(W + K) \propto a^{-2}$. As was noted by Geshnizjani, Chung and Afshordi 2005 [31] for super-horizon inhomogeneities, energy in inhomogeneities has the same effect on the expansion rate as spatial curvature in perturbation theory. We note that $K_{\mathrm{lin}}/|W_{\mathrm{lin}}| = H^2/4\pi G \bar{\rho} = \frac{2}{3}$, a fixed ratio in the linear regime. The full kinetic energy in principle involves higher order correlation functions and is not a simple integral over the power spectrum. Nonetheless, the full kinetic energy can be obtained simply from the potential energy through the cosmic energy equation of Irvine 1961 [142] and Layzer 1963 [143],

$$\left(\frac{d}{dt} + \frac{2\dot{a}}{a} \right) K = - \left(\frac{d}{dt} + \frac{\dot{a}}{a} \right) W, \tag{4--8}$$

with initial conditions set in the linear regime, $K_{\text{lin}} = \frac{2}{3}|W_{\text{lin}}|$. Equations (4–6) and (4–8) provide us with expressions sufficient to calculate nonperturbative contributions to the expansion rate for both the gravitational potential perturbation and kinetic energy components. The results of these calculations are given in the next section.

4.3   Effects on the Expansion Rate

Equations (4–6) and (4–8) determine the energy in inhomogeneities of the universe as a function of epoch, which we characterize by the expansion factor a/a_0. For the primordial power spectrum, we use the CDM power spectrum as given by [144], with spectral index $n = 1$, $\Omega_m = 1$, and COBE normalized amplitude $\delta_H = 1.9 \times 10^{-5}$ [2]. To obtain the nonlinear power spectrum we use the linear-nonlinear mapping of Peacock and Dodds 1994 & 1996 [145, 146]. The results of these calculations are shown in Figures 4-1 and 4-2.

Figure 4-1 shows the dimensionless spectral density of gravitational potential energy $\Delta_W^2(k)$ defined in equation (4–6), evaluated at the present, plotted as a function of wavenumber k. The dashed curve shows the density in linear perturbation theory, and the solid curve shows its fully nonlinear form.

Figure 4-2 shows the contributions of potential energy and kinetic energy to the energy density of the universe, for past and future expansion factors in an $\Omega_m = 1$ universe. At early times, perturbation theory gives an accurate result, but at $a/a_0 \approx 0.05$ (redshift $z \approx 20$) the behavior starts to change, for an interval growing faster than a^1 with the fastest growth as $a^{1.2}$, and then saturating and growing significantly more slowly, eventually as $\ln a$.

4.4   Contributions of Nonlinear Inhomogeneities

In this chapter we have evaluated the size and the time evolution of the contribution of inhomogeneities to the expansion dynamics of a matter-dominated universe, including the effects of fully nonlinear density inhomogeneities. When density fluctuations are in the linear regime, the ratio of the inhomogeneity contribution to the matter density
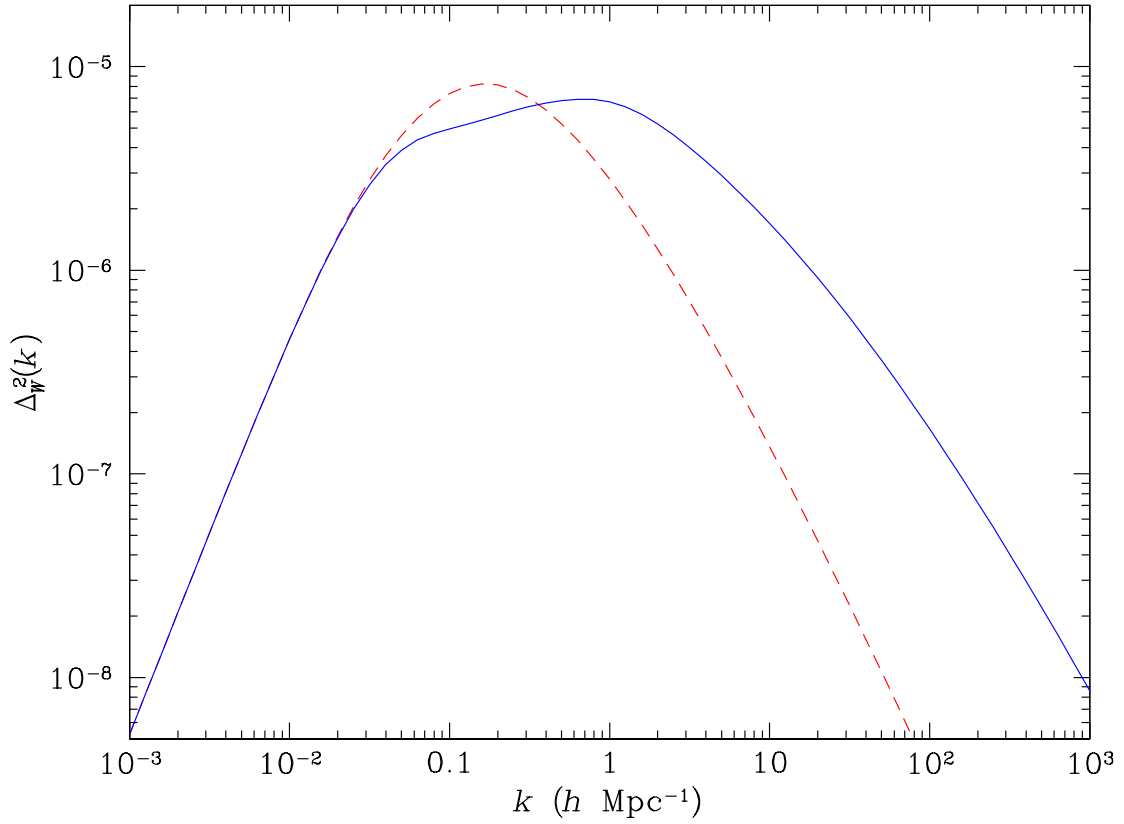
Figure 4-1. Spectral density of gravitational potential energy $\Delta_W^2(k)$ [the integrand of equation (4–6)], evaluated at the present, plotted as a function of wavenumber k. The dashed line shows Δ_W^2 in linear perturbation theory; the solid line shows the fully nonlinear form.

Figure 4-2. Fractional contributions of gravitational potential energy W (long-dashed line) and kinetic energy K (solid line) to the total energy density of the universe, plotted as a function of past and future expansion factor for an $\Omega_m = 1$ universe. The short-dashed line is the sum of contributions from inhomogeneities. The dotted lines show results from linear perturbation theory.

58

grows linearly with expansion factor, as does curvature in an open universe, making only a very small contribution to the expansion rate. As density fluctuations begin to go nonlinear, the energy in inhomogeneities grows at a slightly faster rate, at most as $a^{1.2} \propto a^{-3w}$, or $w = -0.4$. This by itself, even if the dominant energy component, would be only temporarily and only very slightly accelerating, with deceleration parameter $q_0 = \frac{1}{2}(1 + 3w) = -0.1$. Since, at this time, the total fraction of energy in inhomogeneities is $\Omega_U \approx 10^{-5} \ll 1$, this has a negligible effect on cosmological expansion dynamics.

As the universe further evolves, so that the main contributions to W and K come from deeply nonlinear scales, we compute the potential energy from integration of the nonlinear power spectrum, and obtain kinetic energy from the cosmic energy equation, as detailed in equation (4–8). In a scale-invariant model with power spectrum $P \sim k^n$ as $k \to 0$, the kinetic and potential energies K and W scale with the expansion factor as $a^{(1-n)/(3+n)}$ [147] (logarithmically in a as $n \to 1$), with ratio

$$\frac{K}{|W|} = \frac{4}{7 + n}. \tag{4–9}$$

Numerical simulations show that this continues to hold for the CDM spectrum with effective index $n = d \log P / d \log k$ at an appropriate scale, the basis of the linear-nonlinear mapping [145, 146]. For the CDM spectrum, with $n \to 1$ on large scales, this means that growth stops, and the ratio tends to the virial value $K/|W| \to \frac{1}{2}$ at late times. We note that aside from the integration of the Layzer-Irvine equation, many of these results were obtained by [140].

Our results show that the contributions of the potential and kinetic energies of inhomogeneities has never been strong enough to dominate the expansion dynamics of the universe. For a universe with $\Omega_m = 1$ today, normalized to the large scale fluctuations in the microwave background, the net effect of inhomogeneities today is that of a slightly open universe, with $\Omega_k \approx 10^{-4}$ in curvature. The maximum contribution comes from scales of order 1 Mpc, falling off rapidly for smaller and larger k, as illustrated in Figure

4-1. The behavior on asymptotically small scales ($k \gg 10^6 \, h \, \mathrm{Mpc}^{-1}$) depends on an extrapolation that ignores such details as star formation, but Fukugita and Peebles 2004 [12] estimate that the net contribution of dissipative gravitational settling from baryon-dominated parts of galaxies, including main sequence stars and substellar objects, white dwarfs, neutron stars, stellar mass black holes, and galactic nuclei, is in total $10^{-4.9}$ of the critical energy density.

The suggestion that nonlinear effects for large inhomogeneities may mimic the effect of dark energy is not the case for the fully nonlinear theory. It is true that higher order terms in perturbation theory grow faster; the general n-th order term grows as $D^n(t)$. There indeed comes a scale in space or an evolution in time where the behavior of higher order terms appears to diverge. This is illustrated in Figure 4-3, where it can clearly be seen that, to second order in density contrast, the contributions from potential and kinetic terms appear to diverge. Nevertheless, the fully nonlinear result is well behaved. It is only the perturbation expansion that breaks down, and the actual energy saturates and grows more and more slowly at late times. As illustrated in Figure 4-2, the nonlinear potential and kinetic energies remain small compared to the total matter density at all times, even an expansion factor of 10^3 into the future. Inhomogeneity effects do not substantially affect the expansion rate at any epoch.

4.5   Variance of the Energy in Inhomogeneities

It has been pointed out that although the average inhomogeneity energy is small, its variance has a logarithmically divergent contribution from the variance of the potential on super-horizon scales [28],

$$
\begin{aligned}
\left\langle (\Delta W)^2 \right\rangle &= \frac{1}{V^2} \int d^3x \, d^3x' \, \frac{1}{4} \, \bar{\rho} \left\langle \phi(x) \, \phi(x') \right\rangle \\
&= (2\pi G \bar{\rho} a^2)^2 \int \frac{d^3k}{(2\pi)^3} \, \frac{P(k)}{k^4} \, W^2(kR),
\end{aligned}
\tag{4–10}
$$

windowed over the horizon volume (for calculational convenience we use a Gaussian rolloff rather than a sharp radial edge). For $n \to 1$ as $k \to 0$, this is indeed logarithmically
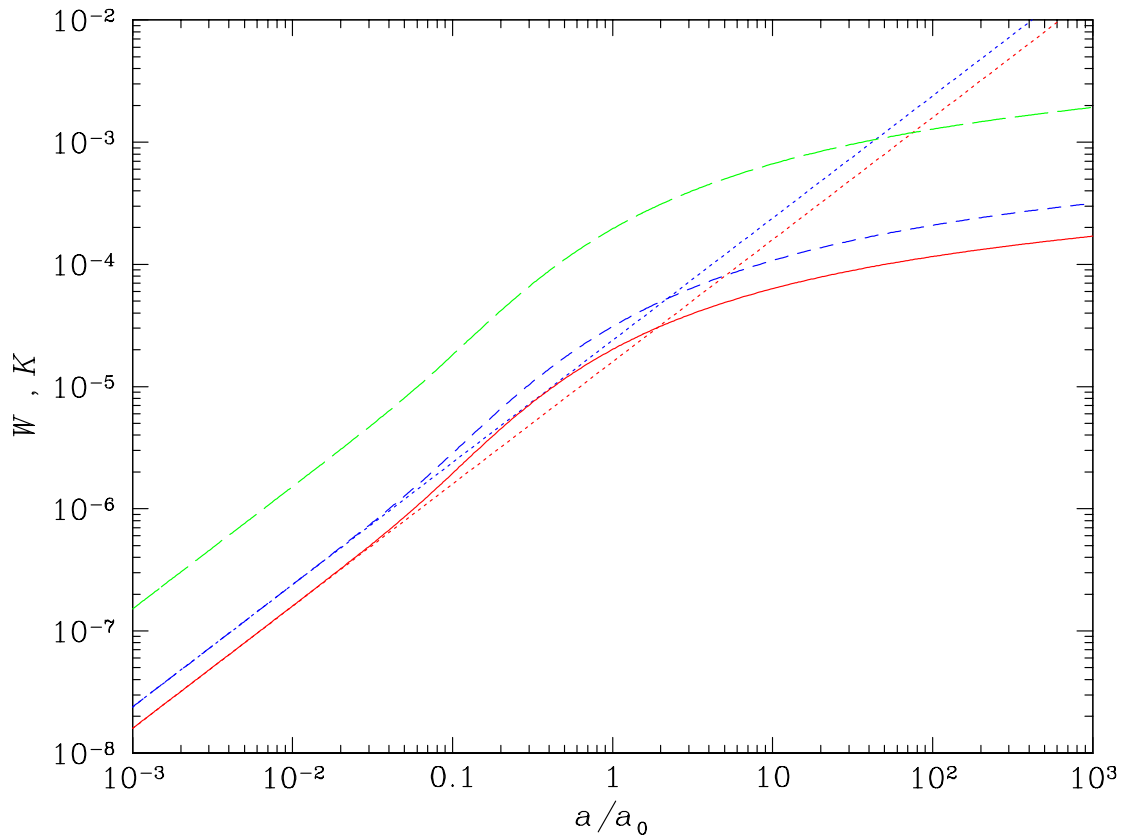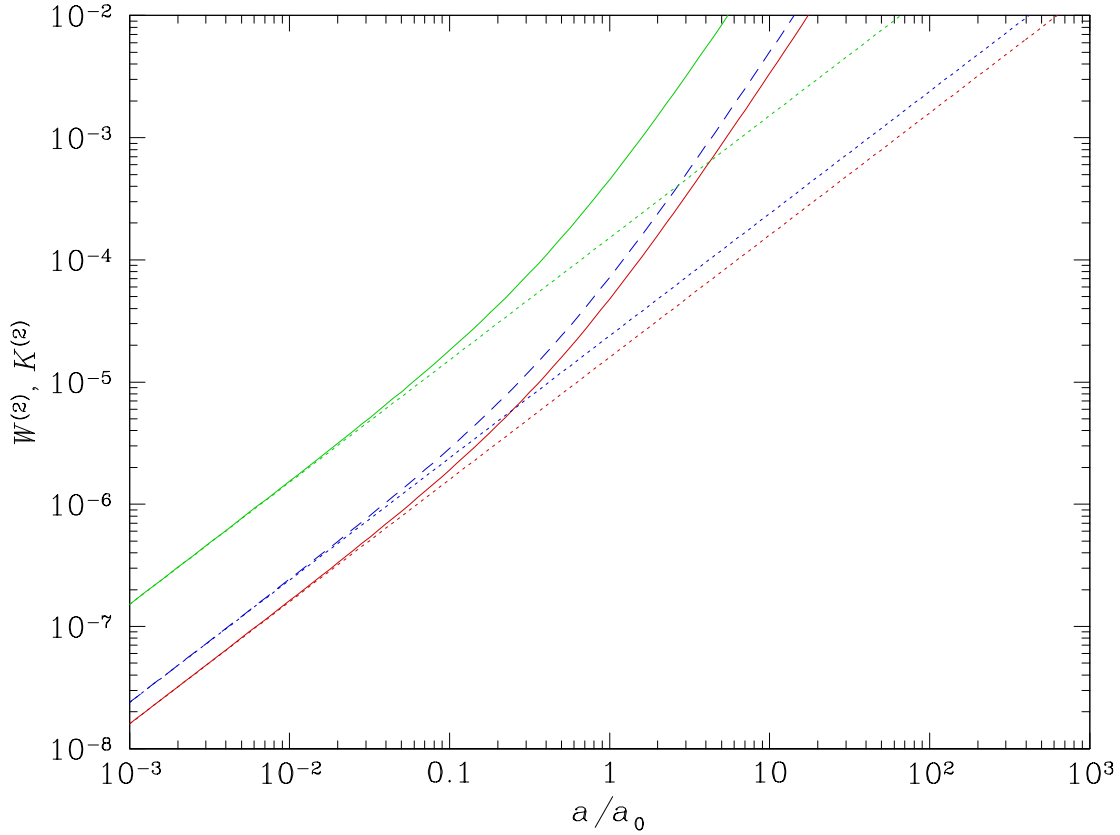
Figure 4-3. Fractional contributions of gravitational potential energy W (long-dashed line) and kinetic energy K (solid line) to the total energy density of the universe, plotted as a function of past and future expansion factor for an $\Omega_m = 1$ universe. The short-dashed line is the sum of contributions from inhomogeneities. This graph shows the contributions to second order in density contrast, δ. Note the apparent divergence is a result of perturbation theory breaking down, as the fully nonlinear result in Figure 4-2 is well behaved.

61

dependent on the low-k cutoff (and if $n < 1$ the divergence is worse), but the rest of the integral is finite for the CDM spectrum. The fluctuation in potential energy, $\langle(\Delta W)^2\rangle^{1/2}$, is shown in Figure 4-4 as a function of the infrared cutoff $k_{\min}$.

The integral is dominated by the smallest values of k, where perturbations are deep in the linear regime. For $n = 1$ the result is very accurately $\Delta W = 1.45 \times 10^{-5} |\ln k_{\min} R_H|^{1/2}$. (We note that for $n \to 1$ the units of $k_{\min}$ are unimportant.) The fluctuation is comparable to the mean $\langle W \rangle = 3.1 \times 10^{-5}$ when the cutoff is near the scale of the horizon $k = H_0/c$, and does not become of order 1 until $k_{\min} \sim 10^{-170}$ (for $n = 0.95$), or $k_{\min} \sim 10^{-10^9}$ (for $n \to 1$), or ever (for $n > 1$). While such an exponentially vast range of scales may not be beyond the range of possibility in an inflationary universe, it requires a fearless extrapolation well beyond what is known directly from observation. The fluctuation ΔW is dominated by contributions from modes that are deep in the linear perturbation regime, and scales with expansion factor as $\Delta W \propto \bar{\rho} a^2 D$, constant in time. This contribution to the energy will appear dynamically in the Friedmann equation as another matter component. Furthermore, in the presence of a true dark energy component, any effects on cosmological expansion arising from inhomogeneities quickly becomes unimportant once dark energy becomes dominant [140].

The fact that fluctuations in the potential diverge remains troublesome. It has been recognized for some time that potential fluctuations in the standard model with $n \to 1$ are logarithmically divergent, but since for most purposes the value of the potential is unimportant, this has not been perceived as a significant problem. The effect of potential on the expansion dynamics is real, but the weak logarithmic divergence and the fact that it is a feedback of a gravitational energy on gravitational dynamics may lead one to hope that this divergence is alleviated in a renormalized quantum theory of gravity.

4.6   Summary

We have found that, to leading order in ϕ and v^2 but with fully nonlinear density fluctuations, inhomogeneities on sub-horizon scales have only a minimal effect on the
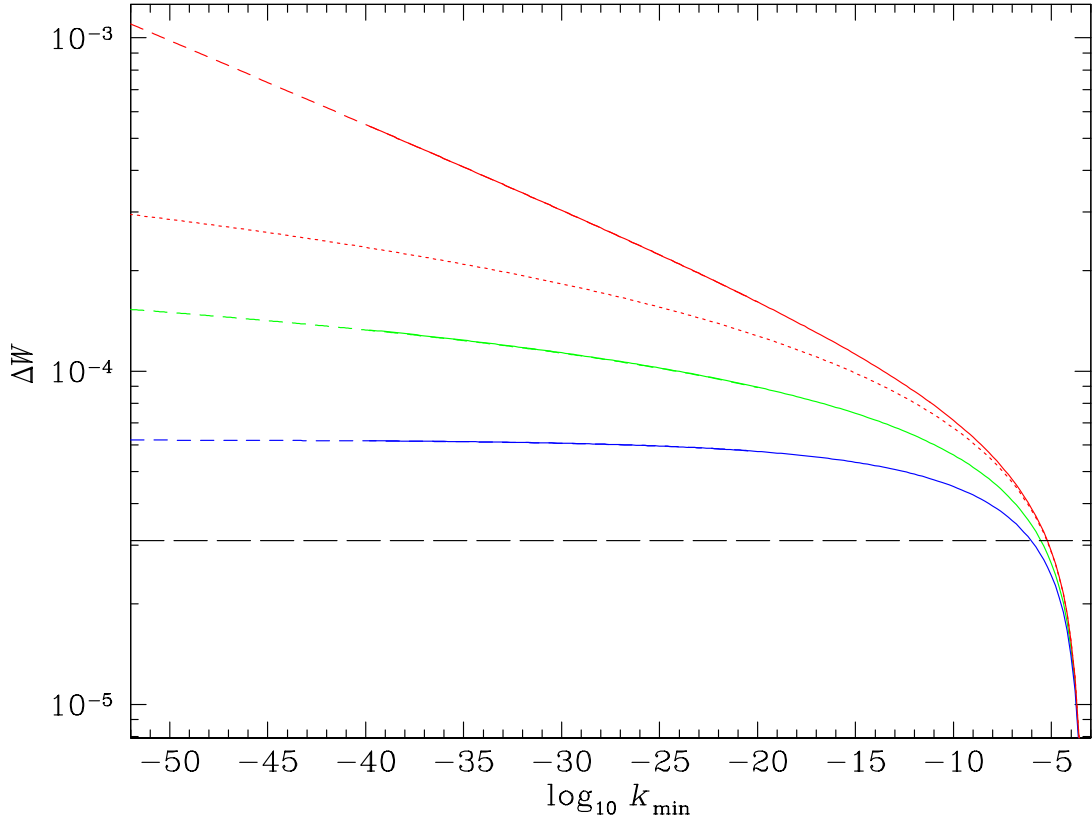
Figure 4-4. The expected fluctuation in the potential energy per unit mass $\langle (\Delta W)^2 \rangle^{1/2}$ evaluated at the present as a function of infrared cutoff $k_{\min}$ for $n = 0.95$, $n = 1$, and $n = 1.05$ (solid lines, top to bottom). Dashed lines are analytic approximations that asymptotically become $k^{-0.025}$, $(\log k)^{1/2}$, or constant, respectively. The dotted line shows the result for a rolling spectral index that has $n = 0.95$ on the horizon today but approaches $n = 1$ as $k \to 0$, as predicted by most models of slow-roll inflation. The mean value $\langle W \rangle = 3.1 \times 10^{-5}$ is shown as the horizontal dashed line.

cosmological expansion dynamics, even far into the future, and in particular never result in an accelerated expansion. Other authors have also shown that recent attempts to explain an accelerated expansion through super-horizon perturbations face significant difficulties [31–33]. The possibility that a known component of the universe may be responsible for the accelerated expansion remains intriguing. However, we conclude that sub-horizon perturbations are not a viable candidate for explaining the accelerated expansion of the universe.

CHAPTER 5
FULLY EVOLVED COSMOLOGICAL PERTURBATIONS

This chapter investigates the use of a well-known empirical correlation between the velocity dispersion, metallicity, and luminosity in $H\beta$ of nearby H II galaxies to measure the distances to H II-like starburst galaxies at high redshifts. This correlation is applied to a sample of 15 starburst galaxies with redshifts between $z = 2.17$ and $z = 3.39$ to constrain Ω_m, using data available from the literature. A best-fit value of $\Omega_m = 0.21^{+0.30}_{-0.12}$ in a Λ-dominated universe and of $\Omega_m = 0.11^{+0.37}_{-0.19}$ in an open universe is obtained. A detailed analysis of systematic errors, their causes, and their effects on the values derived for the distance moduli and Ω_m is carried out. A discussion of how future work will improve constraints on Ω_m by reducing the errors is also presented.

5.1   Precision Cosmology

Precision cosmology, or accurately constraining the parameters describing the universe, has recently become an active field of research due to the precision of available data sets. Stringent contraints have recently been placed on cosmological parameters from measurements of the microwave background [5], type Ia supernovae [135], and galaxy surveys [1, 148]. Although these sources of data are sufficient for generating consistent values for the mass density (Ω_m), vacuum energy density (Ω_Λ), the dark energy equation of state parameter (w), and the value of spatial curvature in the universe (Ω_k), these values must be checked via as many independent methods as possible for consistency, accuracy, and avoiding systematic biases. Furthermore, without the data from supernovae, there would be weak evidence at best for stating that $w \approx -1$, thus it is important to seek another, independent observation supporting the existence of dark energy.

The cosmological parameter with the greatest number of observable cross-checks is Ω_m. It has been derived using many techniques, including the Sunyaev-Zel'dovich effect [149], weak gravitational lensing [150], X-ray luminosities [151], large scale clustering [152], peculiar velocities of galaxy pairs [153], and supernovae data [39]. These methods yield results ranging from $\Omega_m = 0.13$ to $\Omega_m = 0.35$, and are all consistent with one another at

the 2-σ level. However, they all face difficulties when attempting to differentiate between cosmological models, as they are only weakly dependent on Ω_Λ, Ω_k, and w. If a reliable standard candle were found at high redshifts, cosmological models could be discriminated between by precise and accurate observations, as the distance modulus becomes sensitive to Ω_Λ, Ω_k, and w at higher redshifts. It is known that local H II galaxies and giant H II regions in local galaxies are physically similar systems [154]. This chapter extrapolates a link between nearby H II galaxies and H II-like starburst galaxies at high redshifts to use such objects as standard candles. This is accomplished through the application of the known correlation between the luminosity in the $H\beta$ line ($L_{H\beta}$), the velocity dispersion (σ), and metallicity (O/H) of nearby H II galaxies discovered in Melnick, Terlevich and Moles 1988 [155] to the H II-like starburst galaxies found at high redshifts. This correlation, when applied to starburst galaxies at $z > 2$, allows for discrimination between different values of Ω_m as first suggested in Melnick, Terlevich and Terlevich 2000 [40], and can discern which cosmological model is most favored by the data.

H II galaxies (and H II regions of galaxies) are characterized by a large star-forming region surrounded by singly ionized hydrogen. The presence of O- and B-type stars in an H II region causes strong Balmer emission lines in $H\alpha$ and $H\beta$. The size of a giant H II region was shown to be correlated with its emission line widths inMelnick 1978 [156]. This correlation was improved upon in Terlevich and Melnick 1981 [157], who showed that $L_{H\beta}$ of giant H II regions is strongly correlated with their σ. This basic correlation, its extension to H II galaxies, and its usefulness as a distance indicator have been explored in the past [154, 155, 158]. The empirical correlation for H II galaxies [155] relates their $L_{H\beta}$, σ, and O/H. The relationship is

$$\log L_{H\beta} = \log M_z + 29.60, \qquad M_z \equiv \frac{\sigma^5}{O/H}, \tag{5–1}$$

where the constant 29.60 is determined by a zero-point calibration of nearby giant H II regions [40] and from a choice of the Hubble parameter, $H_0 = 71\,\mathrm{km\,s^{-1}\,Mpc^{-1}}$ [159, 160].

The 1-σ rms scatter about this correlation is ± 0.33 dex on $\log L_{H\beta}$ from the local sample of H II galaxies found in Melnick, Terlevich and Terlevich 1988 [155]. Starburst galaxies observed at high redshifts exhibit the same strong Balmer emission lines and intense star formation properties [161, 162] as nearby H II galaxies. This chapter follows the suggestion of Melnick, Terlevich and Terlevich 2000 [40] that equation 5–1 applies to the H II-like starburst galaxies found at high redshifts, and provides evidence to validate that assumption.

The remainder of this chapter discusses the constraints that can be placed on Ω_m and the restrictions that can be placed on the choice of cosmology using starburst galaxies. Section 5.2 details how the data set was selected and analyzed. Section 5.3 states the results obtained from the selected data. The random and systematic errors associated with any distance indicator is a fundamental (and often overlooked) problem inherent to observational cosmology. Appendix A discusses the errors specific to the observational method used in this chapter, including a detailed discourse on the assumption of universality between local H II galaxies and high redshift starburst galaxies. Finally, section 5.4 presents the conclusions drawn from this chapter, and points towards useful directions for future work on this topic.

5.2   Selection of the Data Sample

The goal of the analysis presented here is to obtain distances for each H II-like starburst galaxy at high redshift. H II galaxies must first be detected at high redshift. A sample is then selected on the basis of the correlation in equation (5–1) holding and for which the distance modulus (DM) can be computed from the observed quantities. The quantities required for analysis of these galaxies are σ, the flux in $H\beta$ ($F_{H\beta}$), O/H, the extinction in $H\beta$ ($A_{H\beta}$), and the equivalent width in the $H\beta$ line (EW).

Following the analysis in Melnick, Terlevich and Terlevich 2000 [40], the distance modulus of H II galaxies can be derived from:

$$DM = 2.5 \log(\frac{\sigma^5}{F_{H\beta}}) - 2.5 \log(O/H) - A_{H\beta} - 26.18, \qquad (5\text{–}2)$$

where the constant 26.18 is determined by H_0 and equation (5–1). This chapter makes extensive use of equation (5–2) because it expresses DM purely in terms of observables. DM is insensitive to Ω_m, Ω_Λ, Ω_k, and w at low redshifts ($z \leq 0.1$), differing by 0.1 magnitudes or fewer for drastic changes in the choice of parameters above. At high redshifts ($z > 2$), however, DM can vary by up to 3 magnitudes depending on the choice of parameters. Of the four parameters above available for variation, DM is most sensitive to changes in Ω_m, as has been noted previously [40]. However, for values of $\Omega_m \leq 0.3$, DM is sensitive to variations in the other parameters by 0.2 to 0.5 magnitudes. Since other measurements indicate that indeed $\Omega_m \lesssim 0.3$, this chapter also considers variations in Ω_Λ and Ω_k.

Data for starburst galaxies at $z > 2$ are found in Pettini et al. 2001 [161] and Erb et al. 2003 [162], which contain measurements for many of the desired observables (and related quantities), along with redshift data. Partial measurements exist for 36 starburst galaxies. According to Melnick, Terlevich and Terlevich 2000 [40], the correlation in equation (5–1) holds true for young H II galaxies whose dynamics are dominated by O- and B-type stars and the ionized hydrogen surrounding them. As H II galaxies evolve in time, short-lived O- and B-stars burn out quickly. Although some new O- and B-stars are formed, eventually the death rate of O- and B-stars exceeds their birth rate, causing a galaxy to be under-luminous in $H\alpha$ and $H\beta$ for its mass. This effect can be subtracted out by examining the EW of these galaxies, and cutting out the older, more evolved galaxies (those with smaller equivalent widths). For this chapter, a cutoff of $EW > 20\,\text{Å}$ is adopted, and galaxies with $EW \leq 20\,\text{Å}$ are not included, similar to the cutoff of $25\,\text{Å}$ used previously [40]. There are also galaxies with large EW that do not follow the correlation

Table 5-1. High-redshift galaxies selected to be used as standard candles on the basis of their equivalent widths and velocity dispersions.

z	σ [1]	$F_{H\beta}$ [2]	$12+\log{(O/H)}$	$A_{H\beta}$ [3]	EW [4]	DM [5]
2.17	62 ± 29	0.9 ± 0.2	8.55	0.013	23	$47.49^{+2.10}_{-3.43}$
2.18	51 ± 22	1.9 ± 0.5	8.55	0.157	72	$45.45^{+1.97}_{-3.07}$
2.54	≤ 42	1.3 ± 0.3	8.55	0.141	21	$44.82^{+0.31}_{-1.58}$
2.44	≤ 60	1.3 ± 0.3	8.55	0.285	25	$46.64^{+0.31}_{-1.58}$
2.32	75 ± 21	2.4 ± 0.6	8.55	0.735	47	$46.72^{+1.38}_{-1.80}$
2.17	107 ± 15	2.6 ± 0.7	8.55	0.214	31	$48.96^{+0.78}_{-0.85}$
3.11	≤ 63	3.4 ± 1.0	8.55	0.505	28	$45.77^{+0.31}_{-1.58}$
3.23	69 ± 4	≤ 1.7	8.55	0.237	≤ 27	$47.12^{+0.44}_{-0.32}$
3.39	87 ± 12	2.7 ± 0.3	8.70 ± 0.08	0.773	37	$46.96^{+0.71}_{-0.81}$
3.10	116 ± 8	4.1 ± 0.4	8.62 ± 0.07	0.237	43	$48.81^{+0.38}_{-0.40}$
3.09	67 ± 6	≤ 2.3	8.55	0.110	≤ 31	$46.76^{+0.56}_{-0.51}$
3.07	113 ± 7	1.3 ± 0.3	8.39 ± 0.16	1.01	25	$49.71^{+0.43}_{-0.41}$
3.32	100 ± 4	3.5 ± 0.4	8.55	0.852	25	$47.73^{+0.25}_{-0.25}$
3.09	55 ± 15	3.0 ± 1.0	8.55	0.284	40	$45.22^{+1.38}_{-1.76}$
2.73	81	1.35 ± 0.2	8.49 ± 0.10	1.14	26	$47.49^{+1.22}_{-1.57}$

of equation (5–1) within a reasonable scatter. It is well-known that a large fraction of local H II galaxies contain multiple bursts of star formation [158]. If multiple unresolved star-forming regions are present, the observed σ will be very large due to the relative motion of the various regions. Such galaxies are not expected to follow the correlation of equation (5–1) [158]. The simplest way to remove this effect is to test for non-gaussianity in the emission lines from this effect, but signal-to-noise and resolution are insufficient to observe this effect. Since σ for a system of multiple star-forming regions will be much higher than for a single H II galaxy, a cut can be placed on σ to remove this effect. Monte Carlo simulations (detailed in Appendix A) indicate that if σ is observed to be greater than 130 km s^{-1}, it is likely due to the presence of multiple star-forming regions. To account for this presence, all galaxies with $\sigma > 130$ km s^{-1} are discarded. Imposing the above cuts on σ and EW selects 15 of the 36 original galaxies, creating the data sample used for the analysis presented here. The properties of those selected galaxies are detailed in Table 5-1, with further information about the galaxies available in the source papers [41, 161, 162].

Once the sample has been selected, the quantities required to calculate DM using equation (5–2) must be tabulated for each selected galaxy. Not all of the necessary data elements are available in the literature for these galaxies, so assumptions have been made to account for the missing information. z was measured for all galaxies by the vacuum heliocentric redshifts of the nebular emission lines. σ was obtained for all galaxies from the broadening of the Balmer emission lines, $H\alpha$ for the galaxies from Erb et al. 2003 [162] and $H\beta$ for the galaxies from Pettini et al. 2001 [161]. $F_{H\beta}$ is measured directly for the galaxies in Pettini et al. 2001 [161], but Erb et al. 2003 [162] measures $F_{H\alpha}$ instead, thus $F_{H\alpha}$ must be converted to $F_{H\beta}$. The conversion for emitted flux is given in Osterbrock 1989 [163] as $F_{H\alpha} = 2.75\,F_{H\beta}$, but observed fluxes must correct for extinction. Thus, the complete conversion from $F_{H\alpha}$ to $F_{H\beta}$ will be given by equation (5–3) below,

$$F_{H\beta} = \frac{1}{2.75}\, F_{H\alpha}\, 10^{(\frac{A_{H\alpha} - A_{H\beta}}{2.5})}, \qquad (5\text{–}3)$$

where $A_{H\alpha}$ and $A_{H\beta}$ are the extinctions in $H\alpha$ and $H\beta$, respectively. Obtaining O/H is more difficult, as measurements of metallicity only exist for 5 of the 36 original starburst galaxies. An average value of O/H is used for the galaxies where O/H measurements are unavailable.

Values of O/H are obtained through measurement of the [O II] emission line at $3727\,\mathring{A}$ and the [O III] lines at $4959\,\mathring{A}$ and $5007\,\mathring{A}$ for five of the galaxies in Pettini et al. 2001 [161]. The strong line index R_{23} [164] is assumed to have its temperature-metallicity degeneracy broken towards the higher value of O/H, as is shown to be the case for luminous starburst galaxies at intermediate redshifts in Kobulnicky and Koo 2000 [165]. The combination of the oxygen line measurements with this assumption yields values for O/H for these galaxies. The mean value of O/H is then taken to be the average metallicity for each of the other galaxies where such line measurements are unavailable. Recently, measurements of metallicity in high redshift starburst galaxies have been made [166], using the [N II]/$H\alpha$ ratio as their metallicity indicator. The authors in Shapley et

al. 2004 [166] obtain an average O/H of 8.33 for the galaxies previously found in Erb et al. 2003 [162]. This value is noted as a possible improvement to the one chosen here, and is further discussed as a source of error in this analysis in appendix A of this work.

$A_{H\beta}$ is derived from the $E(B - V)$ color of the galaxy in question. Extinction laws are known and established for the Milky Way, the Large and Small Magellanic Clouds (LMC and SMC, respectively), and the H II regions of the LMC and SMC [167], but have not been established for starburst galaxies in general (although see Calzetti et al. 1994 & 2000 [168, 169] for an argument to the contrary). This chapter assumes dust in H II galaxies to be comparable to that in giant H II regions, thus $A_{H\beta}$ for starburst galaxies is taken to be the $A_{H\beta}$ derived in Gordon et al. 2003 [167] for the H II regions of the LMC and SMC. A best fit applied to the data in Gordon et al. 2003 [167] yields

$$A_{H\beta} = (3.28 \pm 0.24)\, E(B - V),$$
$$A_{H\alpha} = (2.14 \pm 0.17)\, E(B - V), \tag{5–4}$$

for starburst galaxies. These results are also applicable to the flux conversion in equation 5–3. $E(B - V)$ is unavailable for the galaxies from Pettini et al. 2001 [161], but can be derived by noticing the correlation between $E(B - V)$ and corrected $(G - R)$ colors for starburst galaxies in Erb et al. 2003 [162]. The conversion adopted is $E(B - V) \approx 0.481\,(G - R)$. Finally, EW is measured for all galaxies in Pettini et al. 2001 [161], but Erb et al. 2003 [162] gives only the spectra for the $H\alpha$ line. EW is estimated for the Erb et al. 2003 [162] galaxies by estimating the continuum height from each spectra and the area under each $H\alpha$ peak, calculating the equivalent width in $H\alpha$, and converting to $H\beta$ using the Balmer decrements of Osterbrock 1989 [163]. The complete data set is listed in Table 5-1, and is illustrated alongside various cosmologies in Figure 5-1.

5.3   Constraints on Cosmological Parameters

In the previous section, the distance modulus was calculated for each galaxy in the selected sample. The comparison of these values of DM and the predicted values of
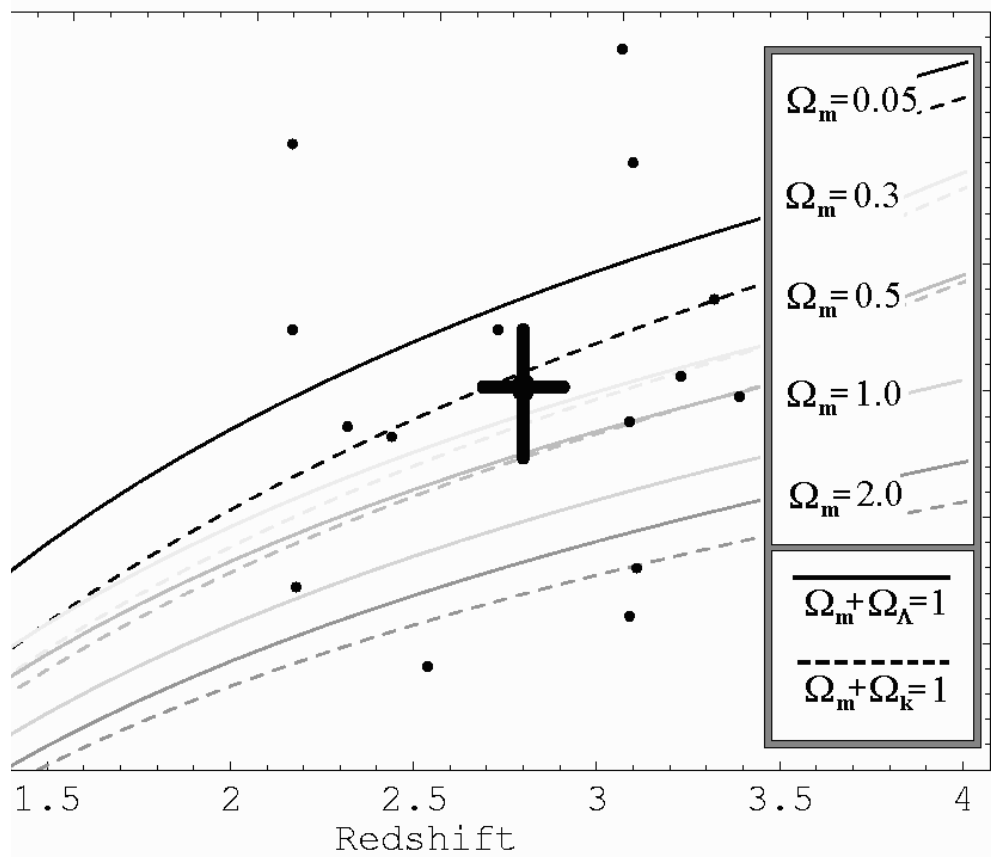
Figure 5-1. The distance modulus plotted as a function of redshifts for various cosmological models, along with data from the selected galaxies. Open-CDM universes and Λ-CDM universes with Ω_m of 0.05, 0.30, 0.5, 1.0, and 2.0 are shown. The crosshairs represents the 1-σ constraints on the DM vs. z parameter space from the selected data sample. The best fits to the data are for a ΛCDM universe with $\Omega_m = 0.21$ and $\Omega_\Lambda = 0.79$, or for an open-CDM universe with $\Omega_m = 0.11$.

DM at a given redshift for different cosmological models provides a constraint on the cosmological parameters. DM is most sensitive at high redshifts to the variation of the cosmological parameter Ω_m, as pointed out by Melnick, Terlevich and Terlevich 2000 [40]. Ω_m is therefore the parameter which is constrained most tightly by observations of starburst galaxies. Each galaxy yields a measurement for DM and for z. Although there are multiple models consistent with each individual measurement, observations of many galaxies at different redshifts will allow the construction of a best-fit curve, which is unique to the choice of cosmological parameters Ω_m, Ω_Λ, Ω_k, and w. The data sample of 15 galaxies in this chapter is insufficient to distinguish between models in this fashion, as the uncertainties in each individual measurement of DM are too large. The method by which the uncertainties can be reduced is to bin the data according to redshift and find a best-fit value of DM at that point. Due to the size of the sample in this chapter, all 15 points are averaged into one point of maximum likelihood to constrain the cosmology, with errors arising from the random errors of the individual points and from the distribution of points. The average value obtained is $DM = 47.03^{+0.46}_{-0.56}$ at a redshift $z = 2.80 \pm 0.11$. The different cosmological models, along with the most likely point and the raw data points, are displayed in figure 5-1, with $H_0 = 71$ km s^{-1} Mpc^{-1}.

The constraints placed on Ω_m from this analysis are $\Omega_m = 0.21^{+0.30}_{-0.12}$ in a Λ-dominated universe ($\Omega_m + \Omega_\Lambda = 1$; $\Omega_k = 0$) and $\Omega_m = 0.11^{+0.37}_{-0.19}$ in an open universe ($\Omega_m + \Omega_k = 1$; $\Omega_\Lambda = 0$). Figure 5-2 shows the comparison in Ω_m vs Ω_Λ parameter space between the preliminary constraints of this chapter and early constraints arising from CMB data and SNIa data, available in de Bernardis et al. 2000 [170].

CMB and SNIa constraints led to the first reliable estimates of Ω_m and Ω_Λ. The preliminary constraints presented here are comparable to early constraints from CMB and SNIa data, as illustrated in figure 5-2. The accuracy in Ω_m and Ω_Λ, as determined from the most recent CMB and SNIa data [5] is now ± 0.04 in each parameter. A similar, and perhaps even superior accuracy can be achieved using starburst galaxies at high redshifts.
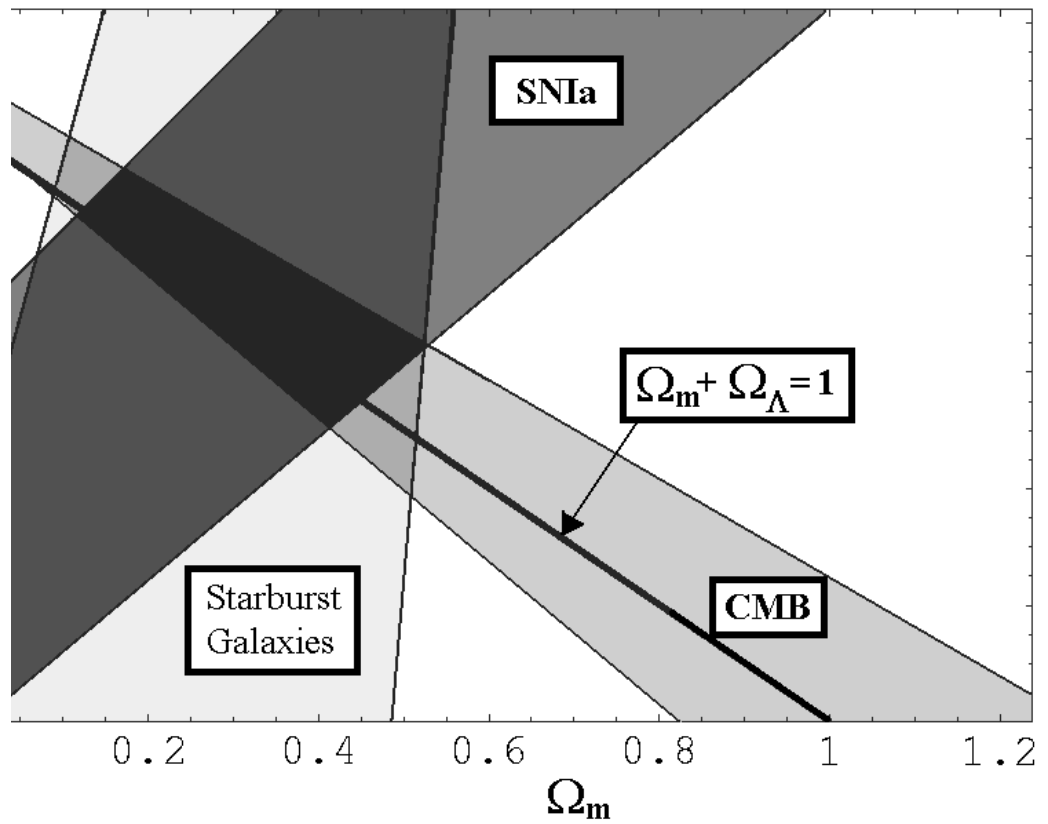
Figure 5-2. 1-σ constraints in Ω_m vs. Ω_Λ parameter space from starburst galaxies, along with older constraints from CMB and SNIa data, found in de Bernardis et al. 2000 [170].

The final section below discusses this possibility, and the systematic and statistical errors which must be overcome are discussed in Appendix A.

5.4   Conclusions and Future Prospects

This chapter has demonstrated that using H II-like starburst galaxies at high redshifts as a standard candle is a promising and well-motivated avenue to explore for precision cosmology. A future survey of high redshift starburst galaxies with measurements of z, σ, $A_{H\beta}$, $F_{H\beta}$, O/H, and EW will reduce both random and systematic errors dramatically. Since the inherent scatter of the method is large (as can be seen in figure 5-1), a large sample size is required to obtain meaningful constraints. This chapter contains a sample size of only 15 galaxies, but future surveys should be able to obtain hundreds of starburst galaxies that survive the selection cuts. For a sample of 500 galaxies, this will improve constraints on Ω_m to a restriction of ± 0.03 due to random errors. Additionally, all of the systematics specific to this sample due to incomplete data will disappear. Appendix A discusses how these errors may be reduced, and how, with such a sample, the concordance cosmological model can be tested at a redshift of $z \sim 3$, something that has not been done to date.

If the assumption of universality between local H II galaxies and high redshift starburst galaxies is correct, this method of measuring Ω_m is capable of providing very tight constraints, independent of any constraints arising from other sources, including CMB and SNIa data. Additionally, if galaxies are obtained at a variety of redshifts between $2 \lesssim z \lesssim 4$, different cosmological models (including vacuum-energy dominated models with different values of w) can be tested for consistency with the future data set. If $\Omega_m \leq 0.3$, the differences in DM at various redshifts become quite pronounced, and meaningful results as to the composition of the non-matter components of the universe can be obtained as well. Future work on this topic has the potential to provide strong independent evidence either supporting or contradicting the concordance cosmological

model of $\Omega_m + \Omega_\Lambda = 1$, $w = -1$, in addition to providing a very stringent constraint on the $\Omega_m + \Omega_\Lambda$ parameter space.

CHAPTER 6
CONCLUDING REMARKS

This dissertation has illustrated the invaluable role of cosmological perturbations throughout the evolution of the universe. These perturbations are departures from perfect homogeneity in density and in gravitational radiation. They are created during the epoch of inflation by quantum fluctuations, which are in turn stretched across all length scales by the exponential expansion of the universe. When inflation ends, the cosmological perturbations become overdense and underdense regions in a radiation-dominated universe. The universe then expands and cools, and these cosmological perturbations evolve under the influence of gravity, radiation pressure, and all the other forces of the universe. Cosmological perturbations grow linearly at first, and when the overdense regions have reached a sufficient density, they collapse nonlinearly. This nonlinear collapse leads to the rapid growth of complex structure, forming stars, galaxies, clusters, and filaments, among other structures. The structure exhibited on cosmological scales at the present is a direct result of the evolution of primordial cosmological perturbations. The remainder of this chapter summarizes the major findings of this paper, and points towards future directions for research on the topic of cosmological perturbations and their effects on the universe. Also included is a section on how cosmological perturbations are expected to impact the eventual fate of the universe.

6.1   Creation of Perturbations

The perturbations produced by inflation are capable of imprinting both primordial scalar modes (density perturbations) and tensor modes (gravitational radiation). Vector modes may also be produced, but these decay over time, and are unimportant for cosmology. The tensor modes that are produced can either be of a comparable amplitude to the scalar modes (as in chaotic inflation [171]), or can be of practically zero amplitude compared to the scalar modes (as in new inflation [172, 173]). In either case, the spectrum of both density perturbations and gravitational radiation are predicted to be nearly scale invariant, with a possible slight tilt preferring either small scales or large scales.

77

If there is a preference towards larger scales, it is possible that, on vastly superhorizon scales, the increased power can affect either the expansion rate or the global spatial curvature of the universe. Differing opinions and many discussions can be found in the literature [31–34, 137] as well as in chapter 4. The work presented in this dissertation indicates that although the *variance* of the potential energy (ΔW) in these superhorizon perturbations can become very large, it is the potential energy itself (W), not ΔW, that couples to the expansion rate of the universe. Therefore, it appears at this juncture that cosmological perturbations on superhorizon scales cannot affect the expansion rate of the universe.

On the other hand, there could be a preference towards smaller scales, which would lead to early nonlinearity (and faster structure formation) of the smallest structures. The power spectrum is fairly accurately known [1] for values of k up to ~ 100 Mpc^{-1}, and matches very well with simulations of a scale-invariant spectrum [174]. Although there is no reason to believe the density perturbations on scales smaller than this depart significantly from an $n \simeq 1$ spectrum, the perturbations in gravitational radiation may. As shown in Siegel and Fry 2005a [13] and in chapter 2, in the presence of extra dimensions at a fundamental scale m_D, primordial gravitational radiation will acquire a thermal spectrum and an energy density given by equation (2–4) if the reheat temperature, T_{RH}, is sufficiently high. The possibilities for detecting a thermal background of gravitational radiation (and thus indirectly detecting extra dimensions) could be accomplished through a precision measurement of the primordial ^{4}He abundance or through the broadening of the $21-$cm H I line.

6.2   Early Evolution of Perturbations

Once the initial cosmological perturbations of the universe are in place amidst the other initial conditions of the big bang (expanding, dense, radiation-dominated universe), their densities evolve in accordance with all of the physical effects acting on them. These include the gravitational force, which provides a gradient towards the overdense

perturbations and away from underdense ones, radiation pressure, the Coulomb force, the nuclear (strong and weak) forces, and scattering from particle-particle interactions.

The net result of all the interactions is that overdense regions in the universe grow according to the Mészáros effect at sufficiently early (linear) times, as given in equation (1-7). While the Mészáros effect does a good job describing the overall evolution of the energy density in a region of space, it cannot give any information about the evolution of the different types of components which compose the universe. As an example, at various epochs in the universe, each of baryons, dark matter, photons, neutrinos, and vacuum energy compose at least 10 per cent of the energy density of the universe. While the universe is radiation-dominated, photons and neutrinos are most important, while when it is matter-dominated, baryons and dark matter are the most important components.

In order to understand how cosmological perturbations have evolved into the large-scale structures observed today, it is vital to understand the evolution of the matter components of the universe from very early times until the present day. Chapter 3, based heavily on the works of Ma and Bertschinger 1995 [22] and Siegel and Fry 2006 [23], details the evolution of the matter components of the universe.

One novel idea of this work is that the evolving cosmological perturbations give rise to seed magnetic fields on all scales. This can also be found in chapter 3 and in Siegel and Fry 2006 [23], but note that there is a competing group that obtains quite different results through a significantly different calculation [120, 134, 175]. The essential idea is that photons have a much larger interaction cross section with electrons than with protons, inducing charge separations and currents. The Coulomb force also plays a major role, acting as a restoring force. The net result obtained in chapter 3 is that magnetic fields on all scales are created, following the spectrum in figure 3-2. On the most interesting scales (from $\sim 1 - 100$ Mpc), fields of $\mathcal{O}(10^{-23}\,\text{Gauss})$ are produced at the epoch of recombination. These seed fields may provide the seeds for the magnetic fields observed on large scales today. This may be accomplished either directly, by having these seed fields

directly grow into the fields observed today, or by these fields seeding the supermassive black holes/AGNs which then amplify the field, and populate the universe with the resultant magnetic field energy.

The sets of equations for a difference component between ions and electrons derived in chapter 3 are the first of their kind. Problems which hitherto could not be solved for lack of having equations that describe a charge difference can now be tackled using these new tools. Appendix B presents the possibility that a net electric charge was present at some point in the universe's past. Prior treatments (see Lyttleton and Bondi 1959 [176] and articles which cite it) have found that many of these scenarios would present unacceptable consequences for cosmology. However, Appendix B points towards the possibility that a net charge in the universe, which could arise (for instance) from a broken $U(1)$ symmetry, would be driven away by the simple dynamics of cosmological perturbations. If this proves to be the case, many possibilities for physics in the early universe, where are presently considered to have unacceptable cosmological consequences, may turn out to be quite valid after all.

6.3   Final State of Perturbations

Cosmological perturbations continue to grow linearly, with the most substantial growth occurring once the universe has become matter-dominated, until a critical density is reached. Once this occurs, density perturbations enter the *nonlinear* regime, and grow very rapidly. The nonlinear structure formed in this manner collapses to often very large density contrasts (see chapter 1), but the structure formed is eventually stable to further collapse due to the virial theorem.

Were the universe completely devoid of angular momentum, or rather, were the Zel'dovich approximation exact, the universe might look vastly different from its present state. If gravitational collapse were to occur *exactly* along field gradients, then nuclear reactions would be the only interactions in the universe that prevented all structure from collapsing to singularities. Yet, angular momentum is a fact of life in the universe, as

evidenced by the rotations of many astronomical systems. As a result, when structure formation goes nonlinear and gravitational collapse becomes a major effect, angular momentum conservation also becomes a major factor in forming a stable, final-state structure.

Complex physics, such as shocks and heating (which can create magnetic fields via the mechanism in Biermann 1950 [111]), star formation, baryonic collisions, and collapse on multiple scales all play a role in the formation of the present-day structure of the universe. One question that has been answered in Chapter 4 of this work is the question of whether this nonlinear structure will backreact sufficiently, and impact the global expansion rate of the universe. While many authors [28–30] contend that the effects of nonlinear collapse could substantially impact the expansion rate, it has been calculated (both in chapter 4 and in Siegel and Fry 2005b [34]) what the effect is explicity. The conclusion is that the effect is negligibly small (of $\mathcal{O} \sim 10^{-5}$ the normal expansion rate) at all times.

Cosmological perturbations, in an Einstein-de Sitter universe ($\Omega_m = 1$, no curvature or vacuum energy), will grow nonlinearly only once the scale of interest is inside the horizon. In this scenario, structure in the universe is self-similar, with smaller scales at earlier times behaving identically to larger scales at later times. However, observations of structure formation, among other observables [177, 178], do not support this picture of an Einstein-de Sitter universe. The picture which is most consistent with all the observations is known today as the concordance cosmology, which indicates that the universe has roughly 30 per cent of the critical energy density in matter and roughly 70 per cent in a cosmological constant. The consequences of this for large-scale structure in the universe are examined in section 6.4 of this Chapter.

Once galaxies form (at a redshift of around $z \sim 10$ in a ΛCDM universe), they can be used as deep cosmological probes. In order for something to be a useful distance indicator, there must be a relation between observable quantities and a cosmological distance [179]. Many of these techniques involve individual stars or stellar remnants, or other

low-luminosity objects. To be used at the largest distance scales, a distance indicator must first be visible at such large distances. There are only a few classes of objects which are visible out at redshifts $z \gtrsim 2$, such as the most luminous galaxies, supernovae, gamma-ray bursts, and quasars. It is only at $z \gtrsim 2$ that it becomes reasonable to constrain the various cosmological parameters (such as Ω_m, Ω_Λ, and the dark energy equation of state, w).

Thus far, only the supernovae (and only the type Ia supernovae, at that) have successfully been used as a distance indicator out at this high of a redshift. Although there has recently been an attempt to use gamma-ray bursts as a distance indicator [180], the systematic errors inherent to the method are far larger than the uncertaintly between different cosmological models. Systematic errors, as illustrated in Appendix A, are a constant source of difficulty for any observational cosmologist. Uncertainties in the universality of a distance indicator (i.e. that it behaves the same at all redshifts), as well as uncertainties in the environment where the distance indicator lies, can all bias results obtained with any one indicator. It is for these reasons that many differing distance indicators at high redshift are desired for probing cosmological parameters. Chapter 5 (and Siegel et al. 2005 [41]) builds upon the work of Melnick, Terlevich and Terlevich 2000 [40], and uses star-forming galaxies at $z > 2$ to constrain the cosmological parameters. Although systematic errors for this method are both numerous and worrisome, they are quantified and given a detailed treatment in both Appendix A and Siegel et al. 2005 [41]. The result obtained is that, despite systematic errors, in a Λ-dominated universe, it can be concluded that $0.09 < \Omega_m < 0.51$, with a best-fit value of $\Omega_m = 0.21$. This is the only known independent estimate for cosmological parameters from distance indicators at such high redshifts other than supernovae or the cosmic microwave background.

6.4 Fate of the Universe

One of the most puzzling cosmological discoveries of the last decade has been the discovery that the expansion rate of the universe is accelerating (discovered by Riess et al. 1998 [181] and Perlmutter et al. 1999 [182], independently). These observations have

been confirmed and appear very convincing, yet a compelling theoretical mechanism for explaining the existance of this so-called dark energy has not yet been discovered. Understanding the nature of this accelerated expansion and the physics behind it is one of the great challenges for modern cosmology. An interesting avenue for future research would be to predict the future history and evolution of structure in the universe based on the presence of this accelerated expansion.

The accelerated expansion is most easily and simply parametrized by a cosmological constant of energy density $\rho_\Lambda \simeq 6.9 \times 10^{-30}$ g cm^{-3}. The presence of a non-zero cosmological constant (Λ) incorporates a built-in scale to the physics of structure formation. The main consequence of this new type of energy density for structure formation is that scales which are not gravitationally bound to one another at the time of matter-Λ equality never become bound to one another.

The Hubble expansion parameter, H, in a universe containing matter, radiation, and a cosmological constant, evolves as

$$H^2 = H_0^2 \left(\frac{\rho_r}{\rho_c} a^{-4} + \frac{\rho_m}{\rho_c} a^{-3} + \frac{\rho_\Lambda}{\rho_c} \right), \tag{6--1}$$

where ρ_r, ρ_m, and ρ_Λ are the energy densities in radiation, matter, and Λ, respectively. (ρ_c is the critical density.) From equation 6–1, it is facile to deduce that at late times (when a becomes large), the Hubble expansion parameter, H, is given by the constant

$$H = H_0 \sqrt{\Omega_\Lambda}, \qquad \Omega_\Lambda \equiv \frac{\rho_\Lambda}{\rho_c}. \tag{6--2}$$

Therefore, the final expansion state of the universe will be much like the initial inflationary state, in that there will be an asymptotically exponential expansion. The scale factor of the universe, a, will evolve in the far future as

$$a \sim e^{H_0 \sqrt{\Omega_\Lambda}\, t}. \tag{6--3}$$

The net result is that the structure that is bound at the time of matter-Λ equality remains bound, whereas structure that is not yet bound never becomes bound, and will exponentially recede from one another. The local group contains the Andromeda galaxy, the large and small Magellanic clouds, and a few other, small structures. At a time $\simeq 5 \times 10^{10}$ years in the future, the local group, gravitationally bound to our galaxy, will be the only matter in our universe within 500 Mpc of the Milky Way! In fact, in twice that time ($\sim 10^{11}$ years), everything outside of our local group will "red out," meaning that objects in our local group will be the only objects causally in contact with our galaxy in the universe.

The current behavior of the universe points towards this exact scenario for the energy content of the universe, with ~ 70 per cent in dark energy and ~ 30 per cent in matter. If this is the case, and the universe continues to evolve according to the known laws of physics, then galaxies and the objects bound to them, the children of cosmological perturbations, will be the last remaining objects in the universe. The univese will consist of a few isolated clumps of matter exponentially expanding away from one another, with nothing but empty space in between. In the end, these lonely clumps of matter, having arisen from the growth and collapse of slightly overdense cosmological perturbations, may be the only substantial things in a cold, empty universe.

APPENDIX A
ERRORS IN HIGH-Z GALAXIES AS DISTANCE INDICATORS

There have been many assumptions made along the path to obtaining Ω_m via the use of starburst galaxies as a distace indicator, as detailed in chapter 5. The major danger in every observational method is that every assumption made carries along with it an associated error. Some of the assumptions made are inherent to the method used, while others affect only the data sample specific to the one selected in chapter 5. Both will lead to systematic errors, although the sample-specific errors will largely be eliminated by improved measurements, to be taken in future observing runs. Additionally, random errors result from both uncertainties in the measurements and from the intrinsic scatter in the distribution of points. An analysis of all three types of errors ensues below.

A.1   Universality among H II Galaxies

The most important assumption made was the assumption of universality of the distance indicator used for both local H II galaxies and H II-like starburst galaxies. Support for this assumption is provided by the fact that both galaxy types follow the empirical correlation of equation (5–1), as shown in figure A-1. Although the physics underlying starburst galaxies has been an open question for over thirty years [183], it is fortunately not necessary to uncover the complete answer to establish universality. It is likely (although unproven) that the physics underlying the correlation for H II galaxies is similar to the physics underlying the Tully-Fisher relation [184] for spiral galaxies. Specifically, it is thought that line widths (a measure of velocity dispersion) and the luminosity in the Hβ line are both intimately tied to the amount of mass in the star-forming region. A theoretical investigation of exactly what this link is could prove quite fruitful in understanding the underlying physics of the correlation presented in Melnick, Terlevich and Moles 1988 [155].

The validity of the correlation between $L_{H\beta}$ and M_z can be tested directly to determine its range of applicability. By assuming a cosmology, $\log L_{H\beta}$ can be written purely in terms of luminosity distance (d_L), $F_{H\beta}$, and $A_{H\beta}$, which are either measurable

or computable from observables for each galaxy, as shown in equations (5–1) and (5–2). $\log M_z$ can be determined through measured values for σ and O/H. Comparing the quantities $\log L_{H\beta}$ and $\log M_z$ then allows a test of the correlation in equation 5–1 for all galaxies of interest. All available H II and H II-like starburst galaxies with appropriately measured quantities are included to test the correlation. Local galaxies are taken from Melnick, Terlevich and Moles 1988 [155] and from the Universidad Complutense de Madrid (UCM) survey [185, 186], intermediate redshift starburst galaxies are taken from Guzman et al. 1997 [187], and high redshift starburst galaxies are from Pettini et al. 2001 [161] and Erb et al. 2003 [162]. The cosmology assumed to test universality is $\Omega_m = 0.3$, $\Omega_\Lambda = 0.7$, and cuts are applied to all samples so that $EW > 20\,\mathring{A}$ and $\sigma < 130$ km s^{-1}. The results are shown in figure A-1.

The major reasons to conclude that the assumption of universality is valid lie in figure A-1. There exists an overlap between all four samples in both $L_{H\beta}$ and M_z, from the sample where the correlation is well established (nearby samples, such as Melnick, Terlevich and Moles 1988 [155] and the UCM survey [185, 186]), to intermediate redshift H II-like starburst galaxies Guzman et al. 1997 [187], to the high redshift sample used in chapter 5, from Erb et al. 2003 [162] and Pettini et al. 2001 [161]. These four samples all follow the same correlation between $L_{H\beta}$ and M_z within the same intrinsic scatter. (However, it is worth noting that the observed scatter broadens at high redshifts due to measurement uncertainties). By performing a statistical analysis of the data points in figure A-1, it can be shown that the data selected from all samples are consistent with the same choice of slope and zero-point for the empirical correlation. For these reasons, equation (5–1) appears to hold not just for local H II regions and galaxies, but for all starburst galaxies regardless of redshift.

It is important to note that there is an uncertainty in the zero-point calibration of figure A-1 of ± 0.08 dex, which has not improved since the correlation was first discovered [155]. This corresponds to an uncertainty in DM of ± 0.20, which is an unacceptably

large error for the accuracy desired. If starburst galaxies are to be taken seriously as a distance indicator for precision cosmology, it is essential that the zero-point be determined to significantly greater accuracy. This can be accomplished via a twofold approach: a comprehensive survey of the nearby ($z < 0.1$) H II galaxy population, and a survey of the nearby, very low-luminosity, low velocity-dispersion H II regions. Accomplishing both of these goals will allow a marked reduction in the zero-point error by significantly increasing the sample size from the sample used in Melnick, Terlevich and Moles 1988 [155], and will also probe the very low end of the relation between M_z and $L_{H\beta}$, where data are sparse.

A.2   Systematic Errors

The other assumptions which are inherent to this method are the choices of where to cut on EW and on σ, and the assumption that $A_{H\beta}$ is the same for starburst galaxies as it is for local H II regions. These two sources of uncertainty (how to select the sample and what the correct extinction law is for high redshift starburst galaxies) are systematics that cannot be removed by improved observations. Each assumption that is made has an associated error. The assumed extinction laws of equations (5–4), the cut on EW of $20\,\mathring{A}$, and the cut on σ of 130 km s^{-1} all induce inherent systematic errors. Moving the EW cut from $EW > 20\,\mathring{A}$ up to $EW \geq 25\,\mathring{A}$, as suggested in Melnick, Terlevich and Terlevich 2000 [40], would systematically raise the DM by 0.14 mag for all galaxies present in this sample. The EW threshold for the onset of major evolutionary effects is not yet well-established, and necessitates further research. The cut on σ comes about in order to remove contamination from objects containing multiple unresolved star-forming regions. Since the correlation between $L_{H\beta}$ and M_z is only valid for single H II galaxies and H II regions [158], a cut must be made to remove objects containing multiple star-forming regions. Single H II galaxies are observed to have a gaussian distribution in σ peaked at ~ 70 km s^{-1}, but objects with multiple unresolved regions are expected to have an entirely different distribution. On the basis of Monte Carlo simulations performed to simulate both single and multiple H II galaxies, a cut on σ at 130 km s^{-1} retains 95 per cent of the
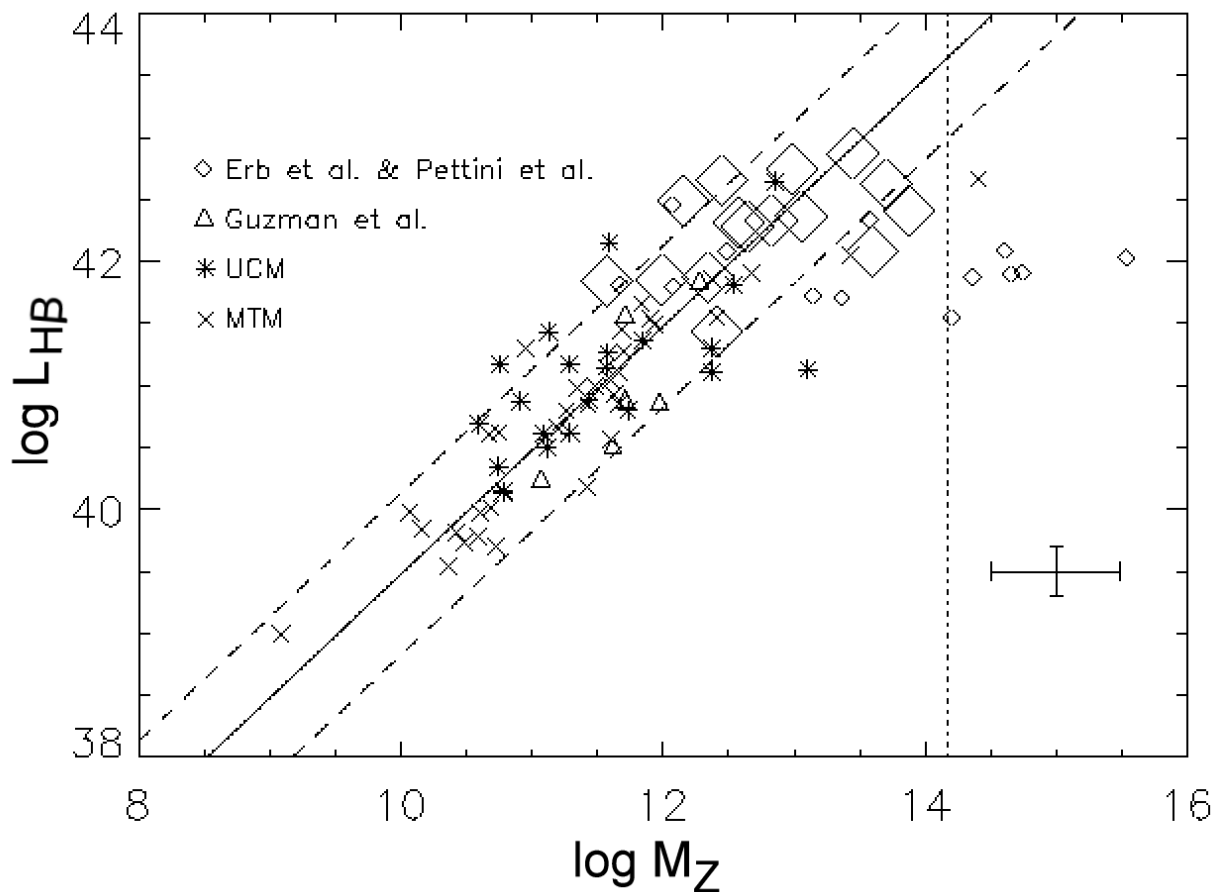
Figure A-1. $\log M_z$ vs. $\log L_{H\beta}$ for local H II galaxies and starburst galaxies at intermediate and high redshifts. The solid line is the best fit of the correlation to the local data set, flanked by the dashed lines, which give the 2-σ rms scatter. The large diamonds represent the selected high redshift data sample; the small diamonds are the data not selected on the basis of either EW or σ. The vertical dotted line is the derived cut on σ of 130 km s^{-1}. The crosshairs represents the typical uncertainty in each selected data point.

valid, single H II galaxies, while eliminating 75 per cent of the contaminating objects. The results of the Monte Carlo simulations can be seen in figure A-2 below. Additionally, it can be shown that the contaminating objects which are not eliminated depart only slightly from the empirical correlation of equation (5–1).

It is therefore essential, for any future survey, that the proper cuts be determined and applied to EW and σ, otherwise substantial uncertainties will arise from the selection of the data sample. Finally, the derived extinction law in $A_{H\beta}$ itself, from equation (5–4), has an uncertainty of ± 38 per cent, due to the fact that there are competing extinction laws that give different results [167–169]. Both laws are comparably grey, but have different normalizations. The difference between the two laws leads to a systematic uncertainty in the DM of the high-redshift galaxies of ± 0.17 mag.

A.3 Measurement Uncertainties

There have also been assumptions made specifically to compensate for incomplete data in the data sets of Pettini et al. 2001 [161] and Erb et al. 2003 [162]. The systematic uncertainties that these assumptions induce can be eliminated in future surveys through measurements of all required quantities. The assumption that the temperature-metallicity degeneracy is most likely broken towards the upper branch of the R_{23} vs. O/H curve for luminous starburst galaxies at high redshift is based on sound analysis [165], but is still a dangerous one to make. Measurement of the $4363\,\mathring{A}$ oxygen line would break the R_{23} vs. O/H degeneracy, and yield a definite value for metallicity for each galaxy. Furthermore, O/H had to be assumed for 11 of the 15 galaxies in the sample, inducing a possible systematic which could affect DM if the assumed average O/H differs from the true value. If the value for O/H from Shapley et al. 2004 [166] is used for the galaxies selected from Erb et al. 2003 [162], the average DM is raised by 0.22 mag. This systematic can be removed in future surveys by a measurement of the [O II] line at $3727\,\mathring{A}$ and the [O III] lines at $4959\,\mathring{A}$ and $5007\,\mathring{A}$ for each galaxy. There are also other metallicity indicators (see Kewley and Dopita 2002 [188]) which may prove to be more reliable at
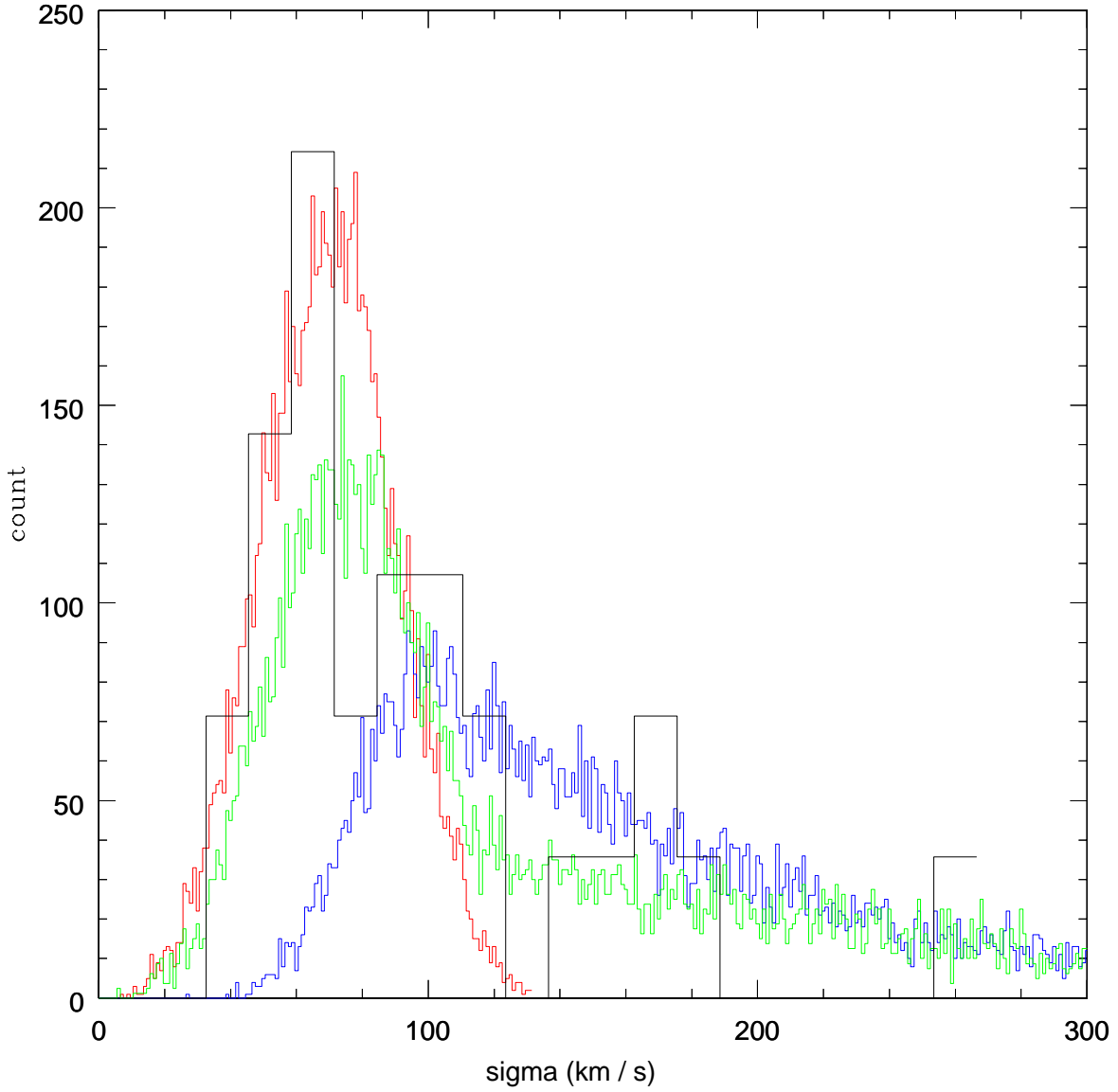
Figure A-2. Simulation of the distributions of velocity dispersions, as would be measured for a single, isolated star-forming region (red curve), for multiple, interacting star-forming regions (blue curve, a simulation of multiple unresolved regions), and for a mixture of both types (green curve). The observed data is plotted in black. Note that the actual data appears to be a superposition of the single region data and the multiple unresolved region data. Multiple unresolved regions at high redshifts appear in the form of enclosed galaxy mergers, and must be removed, as they do not follow the correlation of equation (5–1). From the simulations, removal of most of the enclosed mergers can be accomplished through a derived cut on σ of 130 km s^{-1}.

high redshifts. Measurement of the [N II] line at $6584\,\mathring{A}$, along with $H\alpha$, can provide another measurement of metallicity [166]. In theory, many abundance indicators are available and may even be practically accessible [188], and future surveys should allow multiple, independent techniques to be used, significantly reducing errors. Note also that it is unsettling that different metallicity indicators appear to give different values of the metallicity for the same galaxy samples; this may be yet another source of inherent error.

There is a large uncertainty on the order of ± 30 per cent in the measurement of EW for the Erb et al. 2003 [162] sample due to the difficulty of establishing the height of the continuum. Some galaxies may have been included which should not have been, and others may have been excluded which should have been present. The effect on the distance modulus is estimated to be ± 0.16 mag, but this will be removed by measuring equivalent width in $H\beta$ with a higher signal-to-noise spectra for all galaxies in future surveys. Finally, $E(B-V)$ colors, a substitute for $A_{H\beta}$ measurements, are unavailable for galaxies from Pettini et al. 2001 [161], and were derived from an approximate correlation noticed between $E(B-V)$ and the corrected $(G-R)$ colors in Erb et al. 2003 [162]. There is an overall uncertainty in the extinction due to the fact that the average derived extinction for the Erb et al. 2003 [162] and the Pettini et al. 2001 [161] samples differ by 0.34 dex. Thus, there is an induced systematic in DM of 0.17 mag, which will be eliminated when $A_{H\beta}$ measurements are explicity taken for all galaxies.

A.4   Statistical Errors

Random errors, due to both uncertainties in measurement and to the large scatter in the distribution of points, are perhaps the best understood of the sources of error. Measurements of $A_{H\beta}$ are uncertain by 0.04 to 0.11 dex, depending on the galaxy's brightness. Improved measurements, which rely on the $H\alpha/H\beta$ ratio instead of solely on $E(B-V)$ colors, may reduce the uncertainty significantly. Measurements of $F_{H\beta}$ are uncertain by roughly 20 to 25 per cent on average, and random uncertainties in O/H are of order 0.10 dex. The largest measurement uncertainty comes from measurements of σ,

which is obtained by the broadening of the Balmer emission lines. Even relatively small uncertainties in σ of order 15 per cent can induce uncertainties in DM of 0.8 mag per galaxy. The induced uncertainty is so large because, as seen in equation (5–2), DM is dependent on σ^5, whereas it depends only linearly on the other quantities. It is therefore vital to obtain excellent measurements of the velocity dispersion of these galaxies (which is certainly possible, as some of the high-redshift galaxies in Pettini et al. 2001 [161] have uncertainties of only ± 4 km s^{-1}). Future work will be able to measure the $H\alpha$ and $H\beta$ lines, as well as three oxygen lines, as these are where the three windows in the infrared are in the atmosphere. For galaxies between $2 \lesssim z \lesssim 4$, the $H\alpha$, $H\beta$, and multiple oxygen lines will appear at the appropriate wavelengths. These observations should improve the measurements of σ, further reducing the random uncertainties. The distribution of points may not improve as statistics improve due to the intrinsic scatter on the M_z vs. $L_{H\beta}$ relation, but random errors all fall off as the sample size increases. The errors decrease as $N^{-1/2}$, where N is the number of galaxies in the sample. Even if random errors associated with intrinsic properties (such as $F_{H\beta}$, σ, or O/H) remain large for individual galaxies, increasing the sample size will drive down the overall random errors. Hence, a sample of 500 galaxies, as opposed to 15, will have its random uncertainties reduced by a factor of 6 or better. The new generation of Near-IR Multi-Object Spectrographs (such as FLAMINGOS and EMIR) in 10 meter class telescopes will be ideal for obtaining all necessary measurements for such a sample.

APPENDIX B
ON AN ELECTRICALLY CHARGED UNIVERSE

The possibility that the universe could have a net electric charge has been investigated off-and-on by many scientists for the past half-century. A net electric charge could arise as a consequence of many different types of early-universe physics, but there are strict limits on a net charge in the universe today from various cosmological constraints. This appendix examines the possibility that the mathematical formalism and equations developed in chapter 3 could remove an initial net charge from the universe through cosmological dynamics. If this successfully occurs, many interesting physical mechanisms, previously thought to be tightly constrained through present-day measurements, may have operated in the early universe.

B.1 Introduction

This appendix explores the consequences of a cosmological charge asymmetry in cosmology. One interesting effect of this was first presented in Lyttleton and Bondi 1959 [176], where it was pointed out that a sufficiently large electric charge asymmetry, on the order of $\sim 1\,e$ per 10^{18} baryons, would enable the repulsive Coulomb force to exceed gravitational attraction on large scales. The original motivation for this proposal was to explain the origin of cosmic expansion. It was explained that if the magnitude of the respective charges on electrons and protons differed by $\sim 2 \times 10^{-18}\,e$, large scale repulsion would follow.

With the advent of the big bang theory, which proved to be a necessity to explain the observed cosmic microwave background radiation (CMB, discovered in Penzias and Wilson 1965 [189]), Hubble expansion was explained as a necessary consequence of that theory. It further appears that, to a much higher degree of accuracy than $2 \times 10^{-18}\,e$, the proton and electron charges are equal. From the anisotropies of cosmic rays, which can act as a probe of the net charge in the universe at the present day, it is determined that the overall charge-per-baryon (Δ) is constrained to be $|\Delta| < 10^{-29}\,e$ [128]. Furthermore, the degree of isotropy in the CMB provides constraints on the net electric charge in the universe at

93

a redshift of $z \simeq 1089$ [18], where again the restriction is that the net charge-per-baryon is very small, $|\Delta| < 10^{-29} \, e$. A net charge-per-baryon would also impact primordial nucleosynthesis. Cosmological helium synthesis provides a probe of the net charge at very high redshifts ($z \sim 4 \times 10^8$). Constraints from nucleosynthesis [17] indicate that, in the early universe, $|\Delta| \lesssim 10^{-32} \, e$, the most stringent constraints available on the net charge in the universe.

If a net charge-per-baryon does exist, there are two straightforward ways to obtain it, both of which were identified in Lyttleton and Bondi [176]. Either, as stated above, the proton charge (q_p) differs slightly from the electron charge (q_e) in magnitude, or the number density of protons (n_p) differs from that of electrons (n_e). The former possibility is highly disfavored, as terrestrial experiments indicate that the electric field is zero at the Earth's surface. Assuming equal numbers of protons and electrons on Earth ($\sim 10^{51}$ of each species) places strict constraints on $|q_p| \neq |q_e|$, as do refined versions of the Millikan experiment. It is observed that charge is quantized in units of $\pm e$ for physically observable particles (although quarks are predicted to have fractional charges), as predicted by the standard model of particle physics [53]. Barring exotic scenarios, such as electrically charged neutrinos, photons, or dark matter [190], it is only reasonable to consider unequal number densities of protons and electrons as giving rise to an electric charge in the universe. The creation of an electric charge asymmetry in this fashion is analogous to the creation of a baryon asymmetry in grand unified theories (see Dine and Kusenko 2003 [15] for a review of baryogenesis). An electric charge asymmetry can be generated by a similar mechanism to the baryon asymmetry, and both are expected to have the same types of inhomogeneities [191].

B.2 Generating a Net Electric Charge

A global charge asymmetry can be generated via many channels. The most intuitive method is to temporarily break the $U(1)$ electromagnetic gauge symmetry [191–193]. If this $U(1)$ symmetry is broken at some point, an electric charge asymmetry must be

produced [191]. When the $U(1)$ symmetry is later restored, the charge asymmetry may remain [192]. Care must be taken to ensure that electric charge remains quantized in units of $\pm e$ [193]. The production of a net charge is analogous to baryogenesis in grand unification models, which have a decay process at high energies that is asymmetric, preferring (slightly) to produce baryons over antibaryons. Similar mechanisms could easily prefer the production of one sign of charge over the other, so long as that production symmetry is restored today. Other mechanisms also exist which admit the production of a net electric charge. Examples include Kaluza-Klein models with extra dimensions [128, 194], cosmologies with a varying speed of light [195, 196], and effective interactions allowing electric charge non-conservation by units of $2e$ at a time [197].

Once a net charge has been established in the form of unequal proton and electron densities, previous treatments assume for simplicity that the total charge within a spatial volume is constant [128, 191, 198]. The major purpose of the work in this appendix is to show that this assumption is not true in general. Electromagnetic forces will induce relative motion between oppositely charged species. Charge will be conserved locally (in that there are no charge non-conserving interactions), but the expansion rates of positive and negative charges are found to differ. This allows currents to flow and the net electric charge density to change with time. This appendix examines how charge asymmetries, both local and global, evolve in an expanding universe.

As a result of the dynamics of cosmological expansion, an initial net charge can be either removed completely or reduced significantly. So long as the cosmological bounds on a charge asymmetry due to cosmic rays [128], the CMB [18], and nucleosynthesis [17] are satisfied, there is no limit on any initial electric charge. The remainder of this appendix focuses on how cosmological dynamics affect the overall charge density in an expanding universe. Section B.3 presents an intuitive Newtonian formulation of a universe with an initial charge asymmetry, based upon the gravitational and electromagnetic force laws alone. While section B.3 may be useful for gathering an intuitive picture of the

cosmological dynamics, it does not capture all of the correct physical behavior. A fully relativistic formulation, based upon the evolution equations derived in chapter 3, is found in section B.4. This section takes into account not only the Coulomb and gravitational forces, but also interactions between photons and charged particles, as well as all of the other interactions associated with structure formation. Although the physics of section B.4 is less intuitive, it is far more rigorous, and captures a much greater degree of the essential physical behavior. A discussion of the preliminary results discovered here and their implications for the early universe is presented in section B.5.

B.3   Newtonian Formulation

The simplest scenario that can be written down to explore a universe with a global charge asymmetry is a Newtonian cosmology containing an additional Coulomb term. The standard Newtonian cosmology is derivable from the Newtonian force law

$$F_i = m_i \, a_i, \tag{B--1}$$

where i denotes a test particle of either a proton (p) or an electron (e). The Newtonian gravitational law,

$$F_i = -\frac{G_N \, m_i \, M}{r^2}, \tag{B--2}$$

where G_N is Newton's constant, and M is the total mass enclosed by a sphere with radius equal to the universe's expansion factor, r. As acceleration is defined as $a \equiv \ddot{r}$, the resultant equation for the evolution of the expansion factor becomes

$$\frac{\ddot{r}}{r} = -\frac{4\pi}{3} G\rho, \tag{B--3}$$

where ρ is the energy density of the universe. Using Einstein's equations instead of Newton's in an isotropic, homogeneous universe would modify equation (B--3) by replacing ρ with $(\rho + 3p/c^2)$, where p is the general relativistic pressure of the universe.

A toy model of interest is an Einstein-de Sitter universe composed solely of protons and electrons. In this model,

$$\rho \equiv m_p n_p + m_e n_e \tag{B–4}$$

for the energy density, where n_p and n_e are the proton and electron number densities, respectively. The Coulomb force is given by

$$F_C = \frac{1}{4\pi\epsilon_0} \frac{q_i Q}{r^2}, \tag{B–5}$$

where q_i is the charge of a proton (q_p) or electron (q_e), and Q is the total charge enclosed by a sphere of radius r. The physics acting on protons and electrons is different, due to their opposite charges. Therefore, when the expansion factors are derived from the combined force laws for electrons and protons, it is found that they evolve differently than in equation (B–3). The proton and electron expansion factors (r_p and r_e, respectively) are found to be

$$\frac{\ddot{r_p}}{r_p} = -\frac{4\pi}{3}G(m_p n_p + m_e n_e) + \frac{e^2}{3\epsilon_0 m_p}(n_p - n_e) \tag{B–6}$$

and

$$\frac{\ddot{r_e}}{r_e} = -\frac{4\pi}{3}G(m_p n_p + m_e n_e) - \frac{e^2}{3\epsilon_0 m_e}(n_p - n_e). \tag{B–7}$$

To rewrite these two equations in terms of r_p, r_e, and their time derivatives alone (i.e. to remove n_p and n_e from the equations), N is defined to be the total number of protons or electrons contained within a sphere of radius r_p or r_e, respectively.

$$N \equiv \frac{4\pi}{3}n_p r_p^{\;3} \equiv \frac{4\pi}{3}n_e r_e^{\;3}. \tag{B–8}$$

Let $r_{p,0} = r_{e,0} = r_0 \equiv 1$, where the subscript 0 indicates the value of a given quantity at present. r_p and r_e are henceforth written as fractions of their value today. The ratio of the Coulomb to the gravitational forces appears in the cosmological evolution equations, defined as the dimensionless parameter K, where

$$K \equiv \frac{e^2}{4\pi\epsilon_0\, G(m_p + m_e)^2} \approx 1.235 \times 10^{36}. \tag{B–9}$$

Finally, define quantities f_p, f_e, and H_0 by

$$f_p \equiv \frac{m_p}{m_p + m_e}, \qquad f_e \equiv \frac{m_e}{m_p + m_e}, \qquad H_0^2 \equiv \frac{8\pi}{3} G \rho_0, \tag{B–10}$$

where H_0 is the Hubble parameter (H) evaluated today. The evolution equations now take the form

$$\frac{\ddot{r}_p}{r_p} = -\frac{1}{2} H_0^2 \left[\left(\frac{f_p}{r_p^3} + \frac{f_e}{r_e^3} \right) - \frac{K}{f_p} \left(\frac{1}{r_p^3} - \frac{1}{r_e^3} \right) \right], \tag{B–11}$$

$$\frac{\ddot{r}_e}{r_e} = -\frac{1}{2} H_0^2 \left[\left(\frac{f_p}{r_p^3} + \frac{f_e}{r_e^3} \right) + \frac{K}{f_e} \left(\frac{1}{r_p^3} - \frac{1}{r_e^3} \right) \right]. \tag{B–12}$$

K is large, but r_p is almost equal to r_e, therefore the final terms in equations (B–11) and (B–12) will only be important if there is a significant charge asymmetry. In fact, if $r_p = r_e$ exactly, then both equations reduce to equation (B–3). The case of an exaggerated net charge in the universe is illustrated in figure B-1.

The expansion factor exhibits the standard behavior for an Einstein-de Sitter Universe, which is $r/r_0 = (t/t_0)^{2/3}$. Protons and electrons are found not to flow smoothly together, but rather to oscillate about an equilibrium which they never reach. The charge asymmetry is not a constant over proper volume, but itself oscillates with a decreasing frequency and decreasing amplitude. The oscillation frequency is rapid compared to the rate of decrease of both frequency and amplitude.

Changing variables to a center-of-mass expansion factor (r_{cm}) and an asymmetry parameter (δr) assists the exploration of equations (B–11) and (B–12) in the limit of a small charge asymmetry. The mass-weighted sum of protons and electrons (r_{cm}) and the difference between protons and electrons (δr) are given by

$$r_{cm} \equiv f_p r_p + f_e r_e, \qquad \delta r \equiv r_p - r_e, \tag{B–13}$$

where δr is experimentally and theoretically motivated to be much less than r_{cm}. The evolution equations are then

$$\frac{\ddot{r}_{cm}}{r_{cm}} = -\frac{1}{2} H_0^2 \frac{1}{r_{cm}^3} - \frac{3}{2} H_0^2 (K + 2 f_p f_e) \frac{\delta r^2}{r_{cm}^5}, \tag{B–14}$$
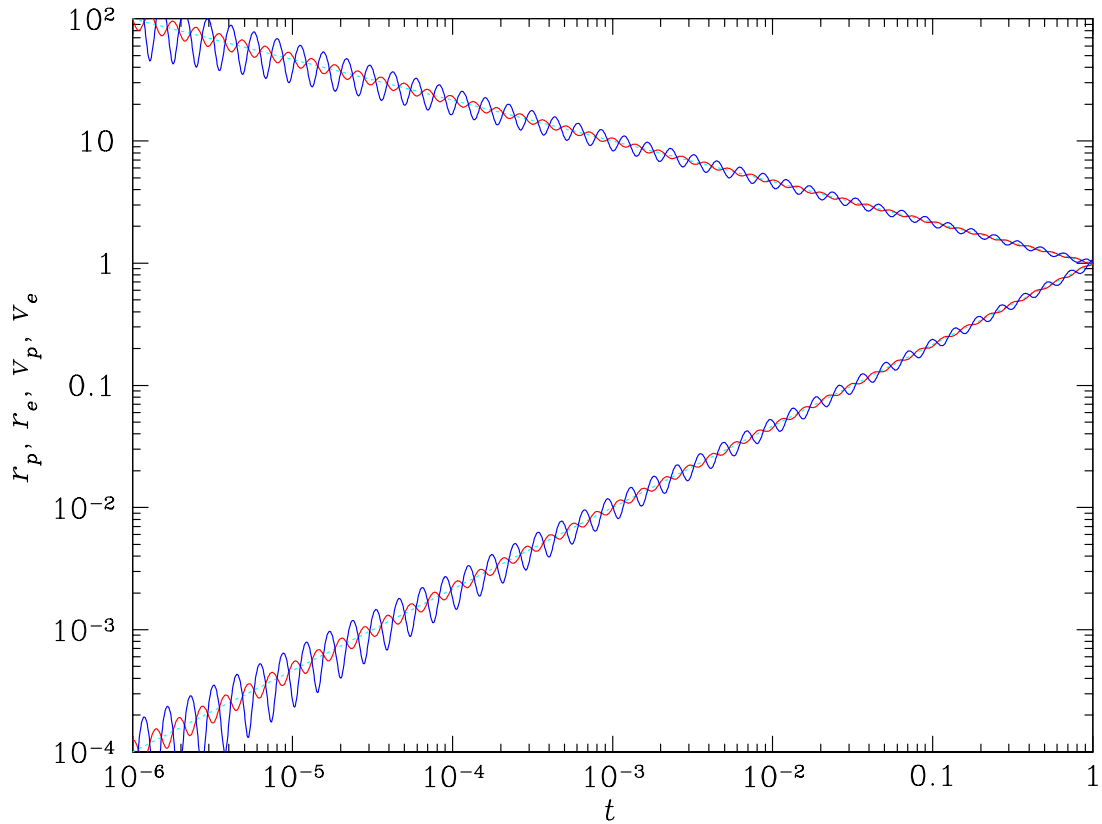
Figure B-1. Expansion factors r_p (red) and r_e (blue), for positive and negative charge distributions (rising) and their time derivatives, v_p and v_e (falling). The amplitude of the asymmetry is enhanced by a factor of 10^4 for visibility.

$$\frac{\ddot{\delta r}}{\delta r} = -\frac{3KH_0^2}{2f_p f_e}\frac{1}{r_{cm}^3}, \tag{B–15}$$

to leading order in δr. In the limit as $\delta r \to 0$, the standard Newtonian cosmological expansion is recovered.

Since K is large ($K \gg 1$), the asymmetry (δr) behaves as a slowly decaying harmonic oscillator over short timescales. It is useful to parametrize $\delta r = A \cos\phi$. Calculation of $\ddot{\delta r}$ shows, in conjunction with equation B–15, that

$$\dot{\phi}^2 \simeq \frac{3KH_0^2}{2f_p f_e}\frac{1}{r_{cm}^3}, \qquad A^2 \dot{\phi} \simeq \text{constant}. \tag{B–16}$$

Equation (B–16) illustrates that $\ddot{A} \ll \dot{\phi}^2 A$, since $\dot{\phi}^2 \sim KH^2$, whereas $\ddot{A}/A \sim H^2$. (Recall that $K \simeq 1.235 \times 10^{36}$.) Because $K \gg 1$, the amplitude of the asymmetry, the change in the amplitude of the asymmetry, and the expansion rate of the universe all vary slowly with respect to the oscillation frequency.

From equation (B–16) and the definition that $\phi \equiv \omega t$, the oscillation frequency at any epoch is

$$\omega = \sqrt{\frac{3e^2 n_0}{8\pi\epsilon_0 G m_p m_e}} H_0 (1+z)^{3/2}, \tag{B–17}$$

where n_0 is the number density today ($n_0 \equiv 1$), and z is the redshift of interest. This corresponds to a frequency today ($z = 0$) of 134 rad s^{-1}, or approximately 21 Hz. The oscillation frequency at any epoch in an Einstein-de Sitter universe is therefore $21(1+z)^{3/2}$ Hz.

A slightly more sophisticated treatment includes radiation in the universe. For radiation, the pressure (p_{rad}) is given by $p_{rad}/c^2 = \frac{1}{3}\rho_{rad}$. The overall energy density of the universe is modified by the additional term

$$(\rho_{rad} + 3p_{rad}) = \frac{2\langle E_\gamma \rangle n_B}{\eta}, \tag{B–18}$$

where $\langle E_\gamma \rangle$ is the average energy of a photon, n_B is the number density of baryons, and $\eta \simeq 6.1 \times 10^{-10}$ is the baryon-to-photon ratio today. With radiation included, the equations

for evolution of protons and electron components become

$$\frac{\ddot{r}_p}{r_p} = -\frac{1}{2}H_0^2 \left[\left(\frac{f_p}{r_p^3} + \frac{f_e}{r_e^3} + \frac{2\langle E_0 \rangle}{r_{cm}^4 \eta} \right) - \frac{K}{f_p} \left(\frac{1}{r_p^3} - \frac{1}{r_e^3} \right) \right],$$
(B–19)

$$\frac{\ddot{r}_e}{r_e} = -\frac{1}{2}H_0^2 \left[\left(\frac{f_p}{r_p^3} + \frac{f_e}{r_e^3} + \frac{2\langle E_0 \rangle}{r_{cm}^4 \eta} \right) + \frac{K}{f_e} \left(\frac{1}{r_p^3} - \frac{1}{r_e^3} \right) \right],$$
(B–20)

assuming photons follow the same expansion rate as r_{cm} (which they do), and $\langle E_0 \rangle$ is the average photon energy today.

Equations (B–19) and (B–20) can be solved numerically, yielding results for r_{cm} and δr. Those results are displayed in figure B-2. Although the asymmetry (δr) itself increases slowly, the relative amplitude of the asymmetry to the expansion factor, $\delta r / r_{cm}$, decreases. Adiabatic damping causes the relative amplitude to evolve as

$$\frac{\delta r}{r_{cm}} \propto r_{cm}^{-1/4}.$$
(B–21)

The frequency of oscillation in a universe containing both matter and radiation is

$$\omega = \sqrt{\frac{3e^2 n_0}{8\pi\epsilon_0 G m_p m_e}} H,$$
(B–22)

which reduces to equation B–17 in the limit of no radiation ($\eta \to \infty$). The universe evolves as matter dominated ($r_{cm} \propto t^{2/3}$) at late times, and as radiation dominated ($r_{cm} \propto t^{1/2}$) at early times.

To summarize the results of this section, which provided a Newtonian treatment of a charge asymmetry, an expanding universe with an initial charge asymmetry has that charge asymmetry evolve with time. The asymmetry oscillates with frequency ω, as given in equation (B–22), with its amplitude falling as $|\delta r|/r_{cm} \propto r_{cm}^{-1/4}$.

B.4 Relativistic Formulation

The previous section treats an adiabatically expanding universe with a global charge asymmetry in the context of a Newtonian cosmology. A more realistic approach is to include scattering (between radiation and charged particles) and local inhomogeneities

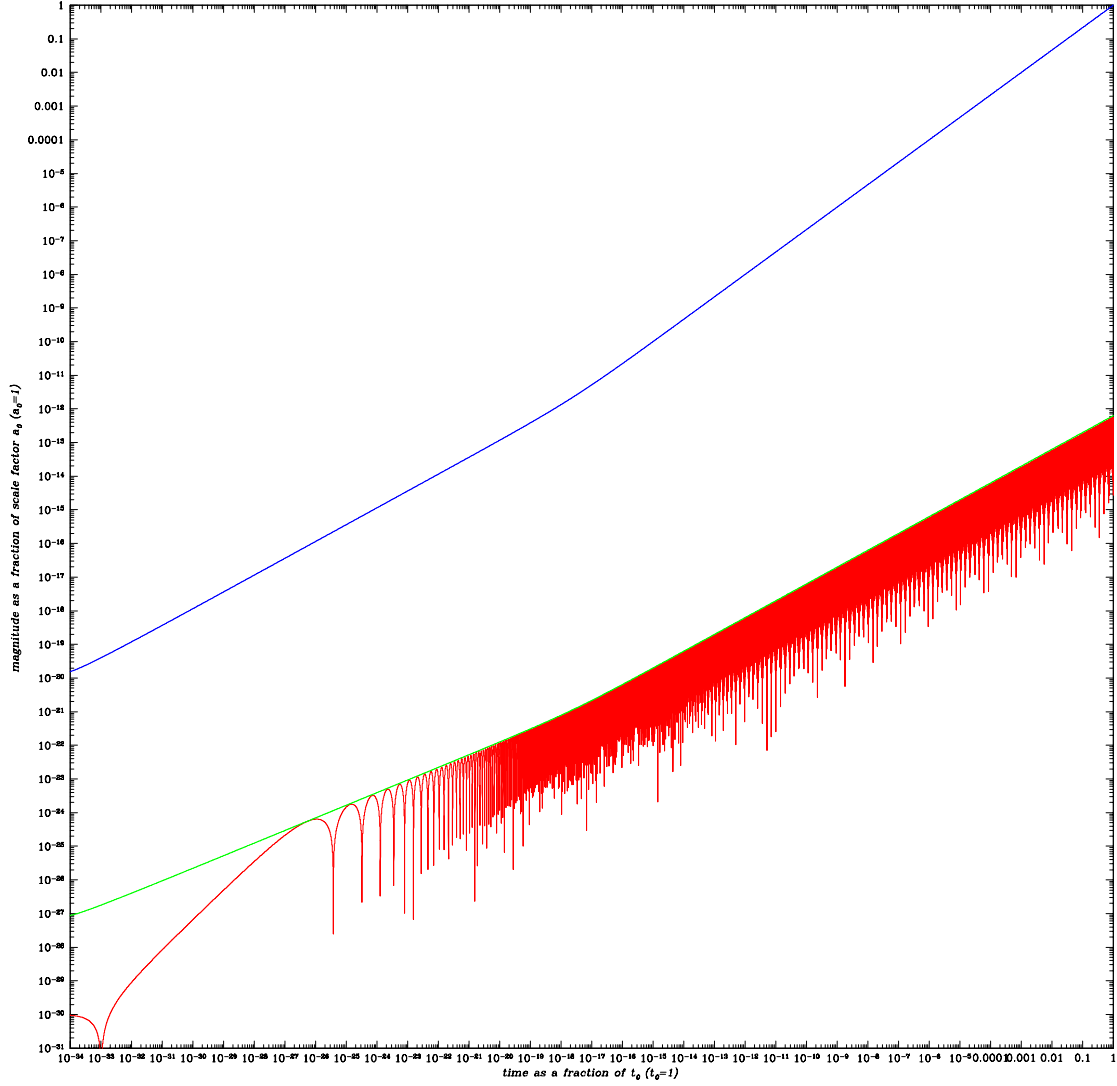Figure B-2. The evolution of a net charge asymmetry in a universe containing both matter and radiation. The blue curve plots the evolution of the expansion factor, r_{cm}, against time. The red curve is the rapidly oscillating asymmetry, δr, plotted against time. The green curve is an analytic fit to the amplitude of the asymmetry, showing that it evolves as $|\delta r| \propto r_{cm}^{3/4}$.

(both gravitational and electromagnetic). This section provides a fully relativistic treatment of this scenario, considering a universe containing protons, electrons, and photons, in addition to all other components of the universe that contribute a significant energy density (such as neutrinos, dark matter, and dark energy).

In chapter 3, with the assistance of Ma and Bertschinger 1995 [22] and Siegel and Fry 2006 [23], the formalism was developed to deal with the evolution of cosmological perturbations of all types in an expanding universe. The presence of a net charge in the universe, or a charge asymmetry, can be treated identically to a universe containing a charge separation on an arbitrary scale. The equations for the evolution of density perturbations (overdensities and underdensities) in electrons and protons, as derived in section 3.3.4, are

$$
\begin{aligned}
\dot{\delta}_e &= -\theta_e + 3\dot{\phi}, \\
\dot{\theta}_e &= -\frac{\dot{a}}{a}\theta_e + c_s^2 k^2 \delta_e + k^2\psi + \frac{4\bar{\rho}_\gamma}{3\bar{\rho}_e}an_e\sigma_T(\theta_\gamma - \theta_e) \\
&\quad -\frac{4\pi e^2}{m_e}[n_p - n_e], \\
\dot{\delta}_p &= -\theta_p + 3\dot{\phi}, \\
\dot{\theta}_p &= -\frac{\dot{a}}{a}\theta_p + c_s^2 k^2 \delta_p + k^2\psi + \frac{4\bar{\rho}_\gamma}{3\bar{\rho}_p}an_p\sigma_T\left(\frac{m_e^2}{m_p^2}\right)(\theta_\gamma - \theta_p) \\
&\quad +\frac{4\pi e^2}{m_p}[n_p - n_e], \quad\quad\quad\quad\quad\quad (\text{B--23})
\end{aligned}
$$

where δ_e and δ_p are the density perturbations in electrons and protons, and θ_e and θ_p are the fourier-transformed velocity perturbations in the electron and proton fields.

As stated previously, a universe with a net charge will most likely achieve that state through different numbers of protons and electrons in the universe. Therefore, the formalism developed for a local charge separation in section 3.3.5 can be applied to a net charge asymmetry in the universe. By taking the difference between the density and velocity fields in electrons and protons, a set of evolution equations for the evolution of a net charge within a given volume is obtained, identically to equation (3--17). The

equations for δ_q and θ_q, where $\delta_q \equiv \delta_p - \delta_e$ and $\theta_q \equiv \theta_p - \theta_e$, are

$$
\begin{aligned}
\dot{\delta}_q &= -\theta_q \\
\dot{\theta}_q &= -\frac{\dot{a}}{a}\theta_q + c_s^2 k^2 \delta_q + \frac{4\pi e^2}{m_e} n_e \delta_q \\
&\quad -\frac{4\bar{\rho}_\gamma}{3\bar{\rho}_b} a n_e \sigma_T \left(\frac{m_b}{m_e}\right)(\theta_\gamma - \theta_b + \theta_q),
\end{aligned}
\tag{B–24}
$$

where all other quantities have the same definitions as in chapter 3.

An initial net charge will appear in equation (B–24) as an initial value of δ_q that is non-zero, and presumably large enough to be of interest. Rewriting this equation as a single second-ordinary ordinary differential equation, the following expression is obtained:

$$
\begin{aligned}
\ddot{\delta}_q &= -\left[\frac{\dot{a}}{a} + \frac{4\bar{\rho}_\gamma}{3\bar{\rho}_b} a n_e \sigma_T \left(\frac{m_b}{m_e}\right)\right]\dot{\delta}_q - \left(c_s^2 k^2 + \frac{4\pi e^2}{m_e}n_e\right)\delta_q \\
&\quad +\frac{4\bar{\rho}_\gamma}{3\bar{\rho}_b}a n_e \sigma_T \left(\frac{m_b}{m_e}\right)(\theta_\gamma - \theta_b).
\end{aligned}
\tag{B–25}
$$

If δ_q is initially either 0 or very small, the final term in equation (B–25) will be important, and the behavior will scale as it did in chapter 3. However, if δ_q is initially large, the final term of equation (B–25) ought to be unimportant.

By transforming equation (B–25) so that derivatives are taken with respect to scale factor (a) instead of conformal time (τ), equation (B–25) becomes

$$
\begin{aligned}
\delta_q'' &+ \left[\frac{8N\bar{\rho}_\gamma}{3\bar{\rho}_b}a^2 n_e \sigma_T \left(\frac{m_b}{m_e}\right) + 2N\dot{a} - a^{-1}\right]\delta_q' \\
&+ \left[\frac{16N^2\pi e^2}{m_e}n_e a^2 + 4N^2 c_s^2 k^2 a^2\right]\delta_q \\
&= \frac{16N^2\bar{\rho}_\gamma}{3\bar{\rho}_b}a^3 n_e \sigma_T \left(\frac{m_b}{m_e}\right)(\theta_\gamma - \theta_b),
\end{aligned}
\tag{B–26}
$$

where N is the numerical factor from equation (3–19). By neglecting the subdominant terms in equation (B–26), and by defining the constants Γ and ω^2 to be

$$
\Gamma \equiv \frac{4N\bar{\rho}_{\gamma,0}}{3\bar{\rho}_{b,0}}n_{e,0}\sigma_T \left(\frac{m_b}{m_e}\right),
\tag{B–27}
$$

$$\omega^2 \equiv \frac{16N^2\pi e^2}{m_e} n_{e,0}, \tag{B–28}$$

where the subscript 0 denotes the present day, a simple differential equation can be written down. Equation (B–26), with the definitions in equations (B–27) and (B–28) substituted, and the subdominant terms neglected, becomes

$$\delta_q'' + 2\Gamma a^{-2}\delta_q' + \omega^2 a^{-1}\delta_q = 0, \tag{B–29}$$

for an initial, large charge asymmetry, δ_q.

The above equation, (B–29), will be solved in the future, most probably involving the use of integrating factors, following the well-known technique illustrated in Turner and Fry 1981 [199]. However, a very good approximation for when critical (i.e., exponential) damping occurs for equation (B–29) is given by setting $\Gamma \simeq \omega$. Solving the subsequent equation for a yields that critical damping occurs when

$$a \simeq \left(\frac{8}{243\pi}\right)^{1/6} \left(\frac{\bar{\rho}_{\gamma,0}}{\bar{\rho}_{b,0}} \frac{m_b}{m_e}\right)^{2/3} n_{e,0}^{1/3} \, \sigma_T^{1/2} = 3.9 \times 10^{-15}. \tag{B–30}$$

This corresponds to a temperature of the universe of $T \simeq 60$ GeV, which is slightly lower than the electroweak scale.

Therefore, any charge asymmetry created prior to $a \simeq 3.9 \times 10^{-15}$ will be eliminated by the expansion dynamics of the universe coupled with scattering and Coulomb interactions.

B.5   Discussion

There are many conservation laws which appear to be obeyed in every experiment performable today. Conserved quantities include, among others, net electric charge, net baryon number, and net lepton number. Yet, when we observe our universe today, it very clearly contains a baryon asymmetry, presumably created at early (pre-nucleosynthesis) times. Additionally, there may be a lepton asymmetry, as the number of charged leptons dramatically exceeds the number of charged anti-leptons (however, the neutrino/antineutrino statistics are virtually unknown). It is therefore reasonable to assume, since the universe

acquired a baryon and (possibly) a lepton asymmetry early on, it may have acquired a charge asymmetry as well.

This appendix, particularly section B.4, illustrates that an initial charge asymmetry cannot necessarily be constrained based upon measurements made today [128], at recombination [18], or even at nucleosynthesis [17]. Any charge asymmetry which is created before critical damping of equation (B–29) occurs will be exponentially driven away around $z \simeq 2.6 \times 10^{14}$, as determined in equation (B–30). This damping is sufficiently strong that it can remove a charge asymmetry of any magnitude, up to and even above the critical energy density of the universe.

Once any initial charge is wiped out, the universe continues to evolve, and the charge in it continues to evolve according to the dynamics in equation (B–26). The late-time solution to this (after critical damping but prior to recombination) is given by the expression below,

$$\delta_q = \frac{\sigma_T \, m_b}{3 \, \pi \, e^2} \left(\frac{\bar{\rho}_{\gamma,0}}{\bar{\rho}_{b,0}} \right) (\theta_\gamma - \theta_b). \tag{B–31}$$

This number is always small, so that $\delta_q \lesssim 10^{-40}$ at late times, which certainly satisfies all observed constraints.

It is worth noting that this analysis may be altered at sufficiently high energies, where Thomson scattering is a poor approximation of the actual electron-photon scattering. At energies of interest ($E \gtrsim 1$ GeV), non-relativistic scattering is not even a good approximation for proton-photon scattering. Above the Λ_{QCD} scale, in fact, it may not even make sense to discuss protons, as those particles will be dissociated into a quark-gluon plasma. A more sophisticated treatment may be needed to extract the exact behavioral details at these high energies.

The overall conclusion which can be drawn from this preliminary work, to be reinforced by a more rigorous calculation in the future, is that any net charge in the universe created above a temperature of $T \simeq 60$ GeV is driven away by cosmological dynamics. This indicates that a net charge of any magnitude could be generated at the

electroweak scale, at the time of Higgs symmetry breaking, at the time of supersymmetry breaking, at the end of inflation, or at the grand unification scale, and the universe would not be discernably different from a universe that was electrically neutral at all times.

REFERENCES

[1] E. Hawkins, S. Maddox, S. Cole, O. Lahav, D. S. Madgwick, P. Norberg, J. A. Peacock, I. K. Baldry, C. M. Baugh, J. Bland-Hawthorn, T. Bridges, R. Cannon, M. Colless, C. Collins, W. Couch, G. Dalton, R. De Propris, S. P. Driver, G. Efstathiou, R. S. Ellis, C. S. Frenk, K. Glazebrook, C. Jackson, B. Jones, I. Lewis, S. Lumsden, W. Percival, B. A. Peterson, W. Sutherland, and K. Taylor. The 2dF Galaxy Redshift Survey: Correlation Functions, Peculiar Velocities and the Matter Density of the Universe. *Monthly Notices of the Royal Astronomical Society*, 346:78–96, November 2003.

[2] E. F. Bunn and M. White. The 4 Year COBE Normalization and Large-Scale Structure. *Astrophysical Journal*, 480:6–+, May 1997.

[3] A. H. Guth. Inflationary Universe: A Possible Solution to the Horizon and Flatness Problems. *Physical Review D*, 23:347–356, January 1981.

[4] P. J. E. Peebles. *Principles of Physical Cosmology*. Princeton Series in Physics, Princeton, NJ: Princeton University Press, —c1993, 1993.

[5] C. L. Bennett, M. Halpern, G. Hinshaw, N. Jarosik, A. Kogut, M. Limon, S. S. Meyer, L. Page, D. N. Spergel, G. S. Tucker, E. Wollack, E. L. Wright, C. Barnes, M. R. Greason, R. S. Hill, E. Komatsu, M. R. Nolta, N. Odegard, H. V. Peiris, L. Verde, and J. L. Weiland. First-Year Wilkinson Microwave Anisotropy Probe (WMAP) Observations: Preliminary Maps and Basic Results. *Astrophysical Journal Supplement Series*, 148:1–27, September 2003.

[6] S. W. Hawking. The Development of Irregularities in a Single Bubble Inflationary Universe. *Physics Letters B*, 115:295–297, September 1982.

[7] A. A. Starobinsky. Dynamics of Phase Transition in the New Inflationary Universe Scenario and Generation of Perturbations. *Physics Letters B*, 117:175–178, November 1982.

[8] A. H. Guth and S.-Y. Pi. Fluctuations in the New Inflationary Universe. *Physical Review Letters*, 49:1110–1113, October 1982.

[9] J. M. Bardeen, P. J. Steinhardt, and M. S. Turner. Spontaneous Creation of Almost Scale-Free Density Perturbations in an Inflationary Universe. *Physical Review D*, 28:679–693, August 1983.

[10] A. A. Starobinskiĭ. Spectrum of Relict Gravitational Radiation and the Early State of the Universe. *Journal of Experimental and Theoretical Physics Letteres*, 30:682–+, December 1979.

[11] B. Allen. Stochastic Gravity-Wave Background in Inflationary-Universe Models. *Physical Review D*, 37:2078–2085, April 1988.

[12] M. Fukugita and P. J. E. Peebles. The Cosmic Energy Inventory. *Astrophysical Journal*, 616:643–668, December 2004.

[13] E. R. Siegel and J. N. Fry. A Thermal Graviton Background from Extra Dimensions [rapid communication]. *Physics Letters B*, 612:122–126, April 2005.

[14] J. M. Bardeen. Gauge-Invariant Cosmological Perturbations. *Physical Review D*, 22:1882–1905, October 1980.

[15] M. Dine and A. Kusenko. The origin of the matter-antimatter asymmetry. *Reviews of Modern Physics*, 76:1+–, 2004.

[16] G. Bertone, D. Hooper, and J. Silk. Particle dark matter: Evidence, Candidates and Constraints. *Physics Reports*, 405:279–390, 2004.

[17] E. Massó and F. Rota. Primordial Helium Production in a Charged Universe. *Physics Letters B*, 545:221–225, October 2002.

[18] C. Caprini and P. G. Ferreira. Constraints on the Electrical Charge Asymmetry of the Universe. *Journal of Cosmology and Astro-Particle Physics*, 2:6–+, February 2005.

[19] G. Steigman. Primordial Nucleosynthesis: Successes and Challenges. *International Journal of Modern Physics E*, 15:1–35, 2006.

[20] K. A. Olive and E. D. Skillman. A Realistic Determination of the Error on the Primordial Helium Abundance: Steps toward Nonparametric Nebular Helium Abundances. *Astrophysics Journal*, 617:29–49, December 2004.

[21] P. Meszaros. The Behaviour of Point Masses in an Expanding Cosmological Substratum. *Astronomy and Astrophysics*, 37:225–228, December 1974.

[22] C.-P. Ma and E. Bertschinger. Cosmological Perturbation Theory in the Synchronous and Conformal Newtonian Gauges. *Astrophysical Journal*, 455:7–+, December 1995.

[23] E. R. Siegel and J. N. Fry. Cosmological Structure Formation creates Large-Scale Magnetic Fields. *ArXiv.org:astro-ph/0604526*, 2006.

[24] P. J. E. Peebles. Recombination of the Primeval Plasma. *Astrophysical Journal*, 153:1–+, July 1968.

[25] J. N. Fry. Galaxy N-point Correlation Functions - Theoretical Amplitudes for Arbitrary N. *Astrophysics Journal Letters*, 277:L5–L8, February 1984.

[26] R. Schaeffer. Determination of the Galaxy N-point Correlation Function. *Astronomy and Astrophysics*, 134:L15+, May 1984.

[27] B. W. O'Shea, K. Nagamine, V. Springel, L. Hernquist, and M. L. Norman. Comparing AMR and SPH Cosmological Simulations. I. Dark Matter and Adiabatic Simulations. *Astrophysical Journal Supplement Series*, 160:1–27, September 2005.

[28] E. W. Kolb, S. Matarrese, A. Notari, and A. Riotto. Effect of Inhomogeneities on the Expansion Rate of the Universe. *Physical Review D*, 71(2):023524–+, January 2005.

[29] S. Rasanen. Constraints on Backreaction in a Dust Universe. *ArXiv Astrophysics e-prints*, April 2005.

[30] A. Notari. Late Time Failure of Friedmann Equation. *ArXiv Astrophysics e-prints*, March 2005.

[31] G. Geshnizjani, D. J. Chung, and N. Afshordi. Do Large-Scale Inhomogeneities Explain Away Dark Energy? *Physical Review D*, 72(2):023517–+, July 2005.

[32] É. É. Flanagan. Can Superhorizon Perturbations Drive the Acceleration of the Universe? *Physical Review D*, 71(10):103521–+, May 2005.

[33] C. M. Hirata and U. Seljak. Can Superhorizon Cosmological Perturbations Explain the Acceleration of the Universe? *Physical Review D*, 72(8):083501–+, October 2005.

[34] E. R. Siegel and J. N. Fry. The Effects of Inhomogeneities on Cosmic Expansion. *Astrophysical Journal Letters*, 628:L1–L4, July 2005.

[35] T. Abel, G. L. Bryan, and M. L. Norman. The Formation of the First Star in the Universe. *Science*, 295:93–98, January 2002.

[36] J. E. Gunn and B. A. Peterson. On the Density of Neutral Hydrogen in Intergalactic Space. *Astrophysical Journal*, 142:1633–1641, November 1965.

[37] S. P. Oh and S. R. Furlanetto. How Universal is the Gunn-Peterson Trough at z~6?: A Closer Look at the Quasar SDSS J1148+5251. *Astrophysical Journal Letters*, 620:L9–L12, February 2005.

[38] R. Cen. The universe was reionized twice. *Astrophysical Journal*, 591:12–37, 2003.

[39] R. A. Knop, G. Aldering, R. Amanullah, P. Astier, G. Blanc, M. S. Burns, A. Conley, S. E. Deustua, M. Doi, R. Ellis, S. Fabbro, G. Folatelli, A. S. Fruchter, G. Garavini, S. Garmond, K. Garton, R. Gibbons, G. Goldhaber, A. Goobar, D. E. Groom, D. Hardin, I. Hook, D. A. Howell, A. G. Kim, B. C. Lee, C. Lidman, J. Mendez, S. Nobili, P. E. Nugent, R. Pain, N. Panagia, C. R. Pennypacker, S. Perlmutter, R. Quimby, J. Raux, N. Regnault, P. Ruiz-Lapuente, G. Sainton, B. Schaefer, K. Schahmaneche, E. Smith, A. L. Spadafora, V. Stanishev, M. Sullivan, N. A. Walton, L. Wang, W. M. Wood-Vasey, and N. Yasuda. New Constraints on Ω_M, Ω_Λ, and w from an Independent Set of 11 High-Redshift Supernovae Observed with the Hubble Space Telescope. *Astrophysical Journal*, 598:102–137, November 2003.

[40] J. Melnick, R. Terlevich, and E. Terlevich. H II Galaxies as Deep Cosmological Probes. *Monthly Notices of the Royal Astronomical Society*, 311:629–635, January 2000.

[41] E. R. Siegel, R. Guzmán, J. P. Gallego, M. Orduña López, and P. Rodríguez Hidalgo. Towards a Precision Cosmology from Starburst Galaxies at z > 2. *Monthly Notices of the Royal Astronomical Society*, 356:1117–1122, January 2005.

[42] A. H. Guth and P. J. Steinhardt. The Inflationary Universe. *Scientific American*, 250:116–128, May 1984.

[43] C. L. Bennett, A. J. Banday, K. M. Gorski, G. Hinshaw, P. Jackson, P. Keegstra, A. Kogut, G. F. Smoot, D. T. Wilkinson, and E. L. Wright. Four-Year COBE DMR Cosmic Microwave Background Observations: Maps and Basic Results. *Astrophysical Journal Letters*, 464:L1+, June 1996.

[44] A. R. Liddle and D. H. Lyth. *Cosmological Inflation and Large-Scale Structure*. Cosmological Inflation and Large-Scale Structure, by Andrew R. Liddle and David H. Lyth, pp. 414. ISBN 052166022X. Cambridge, UK: Cambridge University Press, April 2000., April 2000.

[45] E. W. Kolb and M. S. Turner. *The Early Universe*. Frontiers in Physics, Reading, MA: Addison-Wesley, 1988, 1990, 1990.

[46] S. Sarkar. Big Bang Nucleosynthesis and Physics Beyond the Standard Model. *Reports of Progress in Physics*, 59:1493–1609, 1996.

[47] T. Kaluza. On the problem of unity in physics. *Sitzungsberichte der Preussischen Akademie der Wissenschaften. Physikalisch-Math*, 1921:966–972, 1921.

[48] O. Klein. Quantum theory and five-dimensional theory of relativity. *Zeitschrift f ur Physik*, 37:895–906, 1926.

[49] N. Arkani-Hamed, S. Dimopoulos, and G. Dvali. The Hierarchy Problem and New Dimensions at a Millimeter. *Physics Letters B*, 429:263–272, June 1998.

[50] N. Arkani-Hamed, S. Dimopoulos, and G. Dvali. Phenomenology, Astrophysics, and Cosmology of Theories with Submillimeter Dimensions and TeV Scale Quantum Gravity. *Physical Review D*, 59(8):086004–+, April 1999.

[51] L. Randall and R. Sundrum. Large Mass Hierarchy from a Small Extra Dimension. *Physical Review Letters*, 83:3370–3373, October 1999.

[52] L. Randall and R. Sundrum. An Alternative to Compactification. *Physical Review Letters*, 83:4690–4693, December 1999.

[53] Particle Data Group, S. Eidelman, K. G. Hayes, K. A. Olive, M. Aguilar-Benitez, C. Amsler, D. Asner, K. S. Babu, R. M. Barnett, J. Beringer, P. R. Burchat, C. D. Carone, S. Caso, G. Conforto, O. Dahl, G. D'Ambrosio, M. Doser, J. L.

Feng, T. Gherghetta, L. Gibbons, M. Goodman, C. Grab, D. E. Groom, A. Gurtu, K. Hagiwara, J. J. Hernández-Rey, K. Hikasa, K. Honscheid, H. Jawahery, C. Kolda, Y. Kwon, M. L. Mangano, A. V. Manohar, J. March-Russell, A. Masoni, R. Miquel, K. Mönig, H. Murayama, K. Nakamura, S. Navas, L. Pape, C. Patrignani, A. Piepke, G. Raffelt, M. Roos, M. Tanabashi, J. Terning, N. A. Törnqvist, T. G. Trippe, P. Vogel, C. G. Wohl, R. L. Workman, W.-M. Yao, P. A. Zyla, B. Armstrong, P. S. Gee, G. Harper, K. S. Lugovsky, S. B. Lugovsky, V. S. Lugovsky, A. Rom, M. Artuso, E. Barberio, M. Battaglia, H. Bichsel, O. Biebel, P. Bloch, R. N. Cahn, D. Casper, A. Cattai, R. S. Chivukula, G. Cowan, T. Damour, K. Desler, M. A. Dobbs, M. Drees, A. Edwards, D. A. Edwards, V. D. Elvira, J. Erler, V. V. Ezhela, W. Fetscher, B. D. Fields, B. Foster, D. Froidevaux, M. Fukugita, T. K. Gaisser, L. Garren, H.-J. Gerber, G. Gerbier, F. J. Gilman, H. E. Haber, C. Hagmann, J. Hewett, I. Hinchliffe, C. J. Hogan, G. Höhler, P. Igo-Kemenes, J. D. Jackson, K. F. Johnson, D. Karlen, B. Kayser, D. Kirkby, S. R. Klein, K. Kleinknecht, I. G. Knowles, P. Kreitz, Y. V. Kuyanov, O. Lahav, P. Langacker, A. Liddle, L. Littenberg, D. M. Manley, A. D. Martin, M. Narain, P. Nason, Y. Nir, J. A. Peacock, H. R. Quinn, S. Raby, B. N. Ratcliff, E. A. Razuvaev, B. Renk, G. Rolandi, M. T. Ronan, L. J. Rosenberg, C. T. Sachrajda, Y. Sakai, A. I. Sanda, S. Sarkar, M. Schmitt, O. Schneider, D. Scott, W. G. Seligman, M. H. Shaevitz, T. Sjöstrand, G. F. Smoot, S. Spanier, H. Spieler, N. J. C. Spooner, M. Srednicki, A. Stahl, T. Stanev, M. Suzuki, N. P. Tkachenko, G. H. Trilling, G. Valencia, K. van Bibber, M. G. Vincter, D. R. Ward, B. R. Webber, M. Whalley, L. Wolfenstein, J. Womersley, C. L. Woody, O. V. Zenin, and R.-Y. Zhu. Review of Particle Physics. *Physics Letters B*, 592:1–4, July 2004.

[54] G. F. Giudice, R. Rattazzi, and J. D. Wells. Quantum Gravity and Extra Dimensions at High-Energy Colliders. *Nuclear Physics B*, 544:3–38, April 1999.

[55] G. Mangano and P. D. Serpico. Neutrinos and Primordial Nucleosynthesis. *Nuclear Physics B Proceedings Supplements*, 145:351–354, August 2005.

[56] R. H. Cyburt. Primordial Nucleosynthesis for the New Cosmology: Determining Uncertainties and Examining Concordance. *Physical Review D*, 70(2):023505–+, July 2004.

[57] G. Frossati. Ultralow-Temperature Resonant Gravitational Wave Detectors, Present State and Future Prospects. *Advances in Space Research*, 32:1227–1232, October 2003.

[58] J. Weber. Detection and Generation of Gravitational Waves. *Physical Review*, 117:306–313, January 1960.

[59] K. S. Thorne. Gravitational-Wave Research: Current Status and Future Prospects. *Reviews of Modern Physics*, 52:285–299, April 1980.

[60] F. B. Estabrook and H. D. Wahlquist. Response of Doppler Spacecraft Tracking to Gravitational Radiation. *General Relativity and Gravitation*, 6:439–447, 1975.

[61] B. J. Carr. Cosmological Gravitational Waves - Their Origin and Consequences. *Astronomy and Astrophysics*, 89:6–21, September 1980.

[62] S. Hollands and R. M. Wald. Essay: An Alternative to Inflation. *General Relativity and Gravitation*, 34:2043–2055, December 2002.

[63] L. Kofman, A. Linde, and V. Mukhanov. Inflationary Theory and Alternative Cosmology. *Journal of High Energy Physics*, 10:57–+, October 2002.

[64] B. J. Carr. Some Cosmological Consequences of Primordial Black-Hole Evaporations. *Astrophysical Journal*, 206:8–25, May 1976.

[65] A. R. Liddle. How many Cosmological Parameters? *Monthly Notices of the Royal Astronomical Society*, 351:L49–L53, July 2004.

[66] P. A. M. Dirac. The Cosmological Constants. *Nature*, 139:323–+, 1937.

[67] G. Steigman. A Crucial Test of the Dirac Cosmologies. *Astrophysical Journal*, 221:407–411, April 1978.

[68] P. Sisterna and H. Vucetich. Time Variation of Fundamental Constants: Bounds from Geophysical and Astronomical Data. *Physical Review D*, 41:1034–1046, February 1990.

[69] L. Randall and S. Thomas. Solving the Cosmological Moduli Problem with Weak Scale Inflation. *Nuclear Physics B*, 449:229–247, February 1995.

[70] J. Ellis, G. B. Gelmini, J. L. Lopez, D. V. Nanopoulos, and S. Sarkar. Astrophysical Constraints on Massive Unstable Neutral Relic Particles. *Nuclear Physics B*, 373:399–437, April 1992.

[71] D. J. H. Chung, E. W. Kolb, A. Riotto, and I. I. Tkachev. Probing Planckian Physics: Resonant Production of Particles During Inflation and Features in the Primordial Power Spectrum. *Physical Review D*, 62(4):043508–+, August 2000.

[72] G. F. Giudice, E. W. Kolb, J. Lesgourgues, and A. Riotto. Transdimensional Physics and Inflation. *Physical Review D*, 66(8):083512–+, October 2002.

[73] A. Hebecker and J. March-Russell. Randall-Sundrum II Cosmology, AdS/CFT, and the Bulk Black Hole. *Nuclear Physics B*, 608:375–393, August 2001.

[74] A. Chodos and S. Detweiler. Where has the Fifth Dimension Gone? *Physical Review D*, 21:2167–2170, April 1980.

[75] L. M. Widrow. Origin of Galactic and Extragalactic Magnetic Fields. *Reviews of Modern Physics*, 74:775–823, 2002.

[76] A. A. Ruzmaikin, D. D. Sokolov, and A. M. Shukurov. *Magnetic Fields of Galaxies*. Moscow, Izdatel'stvo Nauka, 1988, 280 p. In Russian., 1988.

[77] A. J. Fitt and P. Alexander. Magnetic Fields in Late-Type Galaxies. *Monthly Notices of the Royal Astronomical Society*, 261:445–452, March 1993.

[78] U. Klein, R. Wielebinski, and H. W. Morsi. Radio Continuum Observations of M82. *Astronomy and Astrophysics*, 190:41–46, January 1988.

[79] D. Moss and A. Shukurov. Turbulence and Magnetic Fields in Elliptical Galaxies. *Monthly Notices of the Royal Astronomical Society*, 279:229–239, March 1996.

[80] P. P. Kronberg, J. J. Perry, and E. L. H. Zukowski. Discovery of Extended Faraday Rotation Compatible with Spiral Structure in an Intervening Galaxy at Z = 0.395 - New Observations of PKS 1229 - 021. *Astrophysical Journal*, 387:528–535, March 1992.

[81] R. M. Athreya, V. K. Kapahi, P. J. McCarthy, and W. van Breugel. Large Rotation Measures in Radio Galaxies at Z > 2. *Astronomy and Astrophysics*, 329:809–820, January 1998.

[82] G. B. Taylor, E. J. Barton, and J. Ge. Searching for Cluster Magnetic Fields in the Cooling Flows of 0745-191, A2029, and A4059. *Astronomical Journal*, 107:1942–1952, June 1994.

[83] K.-T. Kim, P. P. Kronberg, P. E. Dewdney, and T. L. Landecker. The Halo and Magnetic Field of the Coma Cluster of Galaxies. *Astrophysical Journal*, 355:29–37, May 1990.

[84] T. E. Clarke, P. P. Kronberg, and H. Böhringer. A New Radio-X-Ray Probe of Galaxy Cluster Magnetic Fields. *Astrophysical Journal Letters*, 547:L111–L114, February 2001.

[85] K.-T. Kim, P. P. Kronberg, G. Giovannini, and T. Venturi. Discovery of Intergalactic Radio Emission in the Coma-A1367 Supercluster. *Nature*, 341:720–723, October 1989.

[86] J. D. Barrow, P. G. Ferreira, and J. Silk. Constraints on a Primordial Magnetic Field. *Physical Review Letters*, 78:3610–3613, May 1997.

[87] B. Cheng, D. N. Schramm, and J. W. Truran. Constraints on the Strength of a Primordial Magnetic Field from Big Bang Nucleosynthesis. *Physical Review D*, 49:5006–5018, May 1994.

[88] J. P. Vallee. Observations of the Magnetic Fields Inside and Outside the Milky Way, Starting with Globules (~ 1 parsec), Filaments, Clouds, Superbubbles, Spiral Arms, Galaxies, Superclusters, and Ending with the Cosmological Universe's Background Surface (at ~ 8 Teraparsecs). *Fundamentals of Cosmic Physics*, 19:1–89, 1997.

[89] E. N. Parker. The Generation of Magnetic Fields in Astrophysical Bodies. II. The Galactic Field. *Astrophysical Journal*, 163:255–+, January 1971.

[90] S. I. Vainshtein and A. A. Ruzmaikin. Generation of the Large-Scale Galactic Magnetic Field. *Astronomicheskii Zhurnal*, 48:902–+, October 1971.

[91] S. I. Vainshtein and A. A. Ruzmaikin. Generation of the Large-Scale Galactic Magnetic Field. II. *Astronomicheskii Zhurnal*, 49:449–+, April 1972.

[92] H. Lesch and M. Chiba. Protogalactic Evolution and Magnetic Fields. *Astronomy and Astrophysics*, 297:305–+, May 1995.

[93] A. M. Howard and R. M. Kulsrud. The Evolution of a Primordial Galactic Magnetic Field. *Astrophysical Journal*, 483:648–+, July 1997.

[94] M. Steenbeck, F. Krause, and K. H. Rädler. A Calculation of the Mean Electromotive Force in an Electrically Conducting Fluid in Turbulent Motion Under the Influence of Coriolis Forces. *Zeitschrift Naturforschung Teil A*, 21:369–376, 1966.

[95] H. K. Moffatt. *Magnetic Field Generation in Electrically Conducting Fluids.* Cambridge, England, Cambridge University Press, 1978. 353 p., 1978.

[96] A. P. Kazantsev, A. A. Ruzmaikin, and D. D. Sokolov. Magnetic Field Transport by an Acoustic Turbulence-Type Flow. *Zhurnal Eksperimental noi i Teoreticheskoi Fiziki*, 88:487–494, February 1985.

[97] P. C. Tribble. Radio Haloes, Cluster Mergers, and Cooling Flows. *Monthly Notices of the Royal Astronomical Society*, 263:31–36, July 1993.

[98] I. B. Zeldovich and I. D. Novikov. *Relativistic Astrophysics. Volume 2 - The Structure and Evolution of the Universe /Revised and Enlarged Edition/.* Chicago, IL, University of Chicago Press, 1983, 751 p. Translation., 1983.

[99] C. J. Hogan. Magnetohydrodynamic Effects of a First-Order Cosmological Phase Transition. *Physical Review Letters*, 51:1488–1491, October 1983.

[100] J. M. Quashnock, A. Loeb, and D. N. Spergel. Magnetic Field Generation During the Cosmological QCD Phase Transition. *Astrophysical Journal Letters*, 344:L49–L51, September 1989.

[101] G. Baym, D. Bödeker, and L. McLerran. Magnetic Fields Produced by Phase Transition Bubbles in the Electroweak Phase Transition. *Physical Review D*, 53:662–667, January 1996.

[102] G. Sigl, A. V. Olinto, and K. Jedamzik. Primordial Magnetic Fields from Cosmological First Order Phase Transitions. *Physical Review D*, 55:4582–4590, April 1997.

[103] M. S. Turner and L. M. Widrow. Inflation-Produced, Large-Scale Magnetic Fields. *Physical Review D*, 37:2743–2754, May 1988.

[104] A. Ashoorioon and R. B. Mann. Generation of Cosmological Seed Magnetic Fields from Inflation with Cutoff. *Physical Review D*, 71(10):103509–+, May 2005.

[105] B. Ratra. Cosmological 'Seed' Magnetic Field from Inflation. *Astrophysical Journal Letters*, 391:L1–L4, May 1992.

[106] E. A. Calzetta, A. Kandus, and F. D. Mazzitelli. Primordial Magnetic Fields Induced by Cosmological Particle Creation. *Physical Review D*, 57:7139–7144, June 1998.

[107] A. Kandus, E. A. Calzetta, F. D. Mazzitelli, and C. E. M. Wagner. Cosmological Magnetic Fields from Gauge-Mediated Supersymmetry-Breaking Models. *Physics Letters B*, 472:287–294, January 2000.

[108] A.-C. Davis, K. Dimopoulos, T. Prokopec, and O. Törnkvist. Primordial Spectrum of Gauge Fields from Inflation. *Physics Letters B*, 501:165–172, March 2001.

[109] E. R. Harrison. Generation of Magnetic Fields in the Radiation Era. *Monthly Notices of the Royal Astronomical Society*, 147:279–+, 1970.

[110] E. R. Harrison. Origin of Magnetic Fields in the Early Universe. *Physical Review Letters*, 30:188–190, January 1973.

[111] L. Biermann. Uber den Ursprung der Magnetfelder auf Sternen und im Interstellaren Raum. *Zeitschrift fur Naturforschung*, 5A:65–71, 1950.

[112] R. E. Pudritz and J. Silk. The Origin of Magnetic Fields and Primordial Stars in Protogalaxies. *Astrophysical Journal*, 342:650–659, July 1989.

[113] K. Subramanian, D. Narasimha, and S. M. Chitre. Thermal Generation of Cosmological Seed Magnetic Fields in Ionization Fronts. *Monthly Notices of the Royal Astronomical Society*, 271:L15+, November 1994.

[114] R. M. Kulsrud, R. Cen, J. P. Ostriker, and D. Ryu. The Protogalactic Origin for Cosmic Magnetic Fields. *Astrophysical Journal*, 480:481–+, May 1997.

[115] N. Y. Gnedin, A. Ferrara, and E. G. Zweibel. Generation of the Primordial Magnetic Fields during Cosmological Reionization. *Astrophysical Journal*, 539:505–516, August 2000.

[116] S. I. Syrovatskii. Interstellar Gas Dynamics; Proceedings of the Sixth Symposium on Cosmical Gas Dynamics, Organized Jointly by the International Astronomical Union and the International Union of Theoretical and Applied Mechanics, Yalta, The Crimea, U.S.S.R., 8-18 September 1969. In H. J. Habing, editor, *IAU Symp. 39: Interstellar Gas Dynamics*, pages 192+–, 1970.

[117] F. Hoyle. Magnetic Fields and Highly Condensed Objects. *Nature*, 223:936+–, 1969.

[118] M. J. Rees. The Origin and Cosmogonic Implications of Seed Magnetic Fields. *Quarterly Journal of the Royal Astronomical Society*, 28:197–206, September 1987.

[119] S. Matarrese, S. Mollerach, A. Notari, and A. Riotto. Large-Scale Magnetic Fields from Density Perturbations. *Physical Review D*, 71(4):043502–+, February 2005.

[120] K. Takahashi, K. Ichiki, H. Ohno, and H. Hanayama. Magnetic Field Generation from Cosmological Perturbations. *Physical Review Letters*, 95(12):121301–+, September 2005.

[121] P. J. E. Peebles and J. T. Yu. Primeval Adiabatic Perturbation in an Expanding Universe. *Astrophysical Journal*, 162:815–+, December 1970.

[122] J. Silk and M. L. Wilson. Residual Fluctuations in the Matter and Radiation Distribution After the Decoupling Epoch. *Physica Scripta*, 21:708–713, 1980.

[123] M. L. Wilson and J. Silk. On the Anisotropy of the Cosmological Background Matter and Radiation Distribution. I - The Radiation Anisotropy in a Spatially Flat Universe. *Astrophysical Journal*, 243:14–25, January 1981.

[124] J. D. Jackson. *Classical Electrodynamics, 3rd Edition*. Classical Electrodynamics, 3rd Edition, by John David Jackson, pp. 832. ISBN 0-471-30932-X. Wiley-VCH , July 1998., July 1998.

[125] J. R. Bond and G. Efstathiou. Cosmic Background Radiation Anisotropies in Universes Dominated by Nonbaryonic Dark Matter. *Astrophysical Journal Letters*, 285:L45–L48, October 1984.

[126] J. R. Bond and G. Efstathiou. The Statistics of Cosmic Background Radiation Fluctuations. *Monthly Notices of the Royal Astronomical Society*, 226:655–687, June 1987.

[127] A. Kosowsky. Cosmic microwave background polarization. *Annals of Physics*, 246:49–85, 1996.

[128] S. Orito and M. Yoshimura. Can the Universe be Charged? *Physical Review Letters*, 54:2457–2460, June 1985.

[129] E. Bertschinger. Cosmics: Cosmological initial conditions and microwave anisotropy codes. *ArXiv Astrophysics e-prints*, June 1995.

[130] W. H. Press, S. A. Teukolsky, W. T. Vetterling, and B. P. Flannery. *Numerical Recipes in C. The Art of Scientific Computing*. Cambridge: University Press, —c1992, 2nd ed., 1992.

[131] A.-C. Davis, M. Lilley, and O. Törnkvist. Relaxing the Bounds on Primordial Magnetic Seed Fields. *Physical Review D*, 60(2):021301–+, July 1999.

[132] A. Lewis. CMB Anisotropies from Primordial Inhomogeneous Magnetic Fields. *Physical Review D*, 70(4):043011–+, August 2004.

[133] J. Delabrouille. Measuring CMB Polarisation with the Planck Mission. *Astrophysics and Space Science*, 290:87–103, March 2004.

[134] K. Ichiki, K. Takahashi, H. Ohno, H. Hanayama, and N. Sugiyama. Cosmological Magnetic Field: A Fossil of Density Perturbations in the Early Universe. *Science*, 311:827–829, February 2006.

[135] A. G. Riess. The Case for an Accelerating Universe from Supernovae. *Publications of the Astronomical Society of the Pacific*, 112:1284–1299, October 2000.

[136] P. J. Peebles and B. Ratra. The Cosmological Constant and Dark Energy. *Reviews of Modern Physics*, 75:559–606, April 2003.

[137] E. W. Kolb, S. Matarrese, A. Notari, and A. Riotto. Cosmological Influence of Super-Hubble Perturbations. *Modern Physics Letters A*, 20:2705–2710, 2005.

[138] E. W. Kolb, S. Matarrese, A. Notari, and A. Riotto. Primordial Inflation Explains why the Universe is Accelerating Today. *ArXiv High Energy Physics - Theory e-prints*, March 2005.

[139] E. Barausse, S. Matarrese, and A. Riotto. Effect of Inhomogeneities on the Luminosity Distance-Redshift Relation: Is Dark Energy Necessary in a Perturbed Universe? *Physical Review D*, 71(6):063537–+, March 2005.

[140] U. Seljak and L. Hui. Global Expansion in an Inhomogeneous Universe. In *ASP Conf. Ser. 88: Clusters, Lensing, and the Future of the Universe*, pages 267–+, 1996.

[141] P. J. E. Peebles. *The Large-Scale Structure of the Universe.* Research supported by the National Science Foundation. Princeton, N.J., Princeton University Press, 1980. 435 p., 1980.

[142] W. M. Irvine. Local Irregularities in a Universe Satisfying the Cosmological Principle. *Ph.D. Thesis*, 1961.

[143] D. Layzer. A Preface to Cosmogony. I. The Energy Equation and the Virial Theorem for Cosmic Distributions. *Astrophysical Journal*, 138:174–+, July 1963.

[144] J. M. Bardeen, J. R. Bond, N. Kaiser, and A. S. Szalay. The Statistics of Peaks of Gaussian Random Fields. *Astrophysical Journal*, 304:15–61, May 1986.

[145] J. A. Peacock and S. J. Dodds. Reconstructing the Linear Power Spectrum of Cosmological Mass Fluctuations. *Monthly Notices of the Royal Astronomical Society*, 267:1020–+, April 1994.

[146] J. A. Peacock and S. J. Dodds. Non-Linear Evolution of Cosmological Power Spectra. *Monthly Notices of the Royal Astronomical Society*, 280:L19–L26, June 1996.

[147] M. Davis and P. J. E. Peebles. On the Integration of the BBGKY Equations for the Development of Strongly Nonlinear Clustering in an Expanding Universe. *Astrophysical Journal Supplement Series*, 34:425–450, August 1977.

[148] N. A. Bahcall, F. Dong, P. Bode, R. Kim, J. Annis, T. A. McKay, S. Hansen, J. Schroeder, J. Gunn, J. P. Ostriker, M. Postman, R. C. Nichol, C. Miller, T. Goto, J. Brinkmann, G. R. Knapp, D. O. Lamb, D. P. Schneider, M. S. Vogeley, and D. G. York. The Cluster Mass Function from Early Sloan Digital Sky Survey Data: Cosmological Implications. *Astrophysical Journal*, 585:182–190, March 2003.

[149] L. Grego, J. E. Carlstrom, E. D. Reese, G. P. Holder, W. L. Holzapfel, M. K. Joy, J. J. Mohr, and S. Patel. Galaxy Cluster Gas Mass Fractions from Sunyaev-Zeldovich Effect Measurements: Constraints on Ω_M. *Astrophysical Journal*, 552:2–14, May 2001.

[150] H. Hoekstra, M. Franx, K. Kuijken, R. G. Carlberg, H. K. C. Yee, H. Lin, S. L. Morris, P. B. Hall, D. R. Patton, M. Sawicki, and G. D. Wirth. Weak-Lensing Study of Low-Mass Galaxy Groups: Implications for Ω_m. *Astrophysical Journal Letters*, 548:L5–L8, February 2001.

[151] S. Borgani, P. Rosati, P. Tozzi, S. A. Stanford, P. R. Eisenhardt, C. Lidman, B. Holden, R. Della Ceca, C. Norman, and G. Squires. Measuring Ω_m with the ROSAT Deep Cluster Survey. *Astrophysical Journal*, 561:13–21, November 2001.

[152] P. Schuecker, H. Böhringer, C. A. Collins, and L. Guzzo. The REFLEX Galaxy Cluster Survey. VII. Ω_m and σ_8 from Cluster Abundance and Large-Scale Clustering. *Astronomy and Astrophysics*, 398:867–877, February 2003.

[153] H. Feldman, R. Juszkiewicz, P. Ferreira, M. Davis, E. Gaztañaga, J. Fry, A. Jaffe, S. Chambers, L. da Costa, M. Bernardi, R. Giovanelli, M. Haynes, and G. Wegner. An Estimate of Ω_m without Conventional Priors. *Astrophysical Journal Letters*, 596:L131–L134, October 2003.

[154] J. Melnick, M. Moles, R. Terlevich, and J.-M. Garcia-Pelayo. Giant H II Regions as Distance Indicators. I - Relations Between Global Parameters for the Local Calibrators. *Monthly Notices of the Royal Astronomical Society*, 226:849–866, June 1987.

[155] J. Melnick, R. Terlevich, and M. Moles. Giant H II Regions as Distance Indicators. II - Application to H II Galaxies and the Value of the Hubble Constant. *Monthly Notices of the Royal Astronomical Society*, 235:297–313, November 1988.

[156] J. Melnick. Velocity Dispersions in Giant H II Regions II. Relations with the Absolute Luminosities of the Parent Galaxies. *Astronomy and Astrophysics*, 70:157–+, November 1978.

[157] R. Terlevich and J. Melnick. The Dynamics and Chemical Composition of Giant Extragalactic H II Regions. *Monthly Notices of the Royal Astronomical Society*, 195:839–851, June 1981.

[158] J. Melnick, R. Terlevich, and M. Moles. Giant HII regions as Distance Indicators. *Revista Mexicana de Astronomia y Astrofisica, vol. 14*, 14:158–164, May 1987.

[159] K. Hagiwara, K. Hikasa, K. Nakamura, M. Tanabashi, M. Aguilar-Benitez, C. Amsler, R. M. Barnett, P. R. Burchat, C. D. Carone, C. Caso, G. Conforto, O. Dahl, M. Doser, S. Eidelman, J. L. Feng, L. Gibbons, M. Goodman, C. Grab, D. E. Groom, A. Gurtu, K. G. Hayes, J. J. Herna'Ndez-Rey, K. Honscheid, C. Kolda, M. L. Mangano, D. M. Manley, A. V. Manohar, J. March-Russell, A. Masoni, R. Miquel, K. Mönig, H. Murayama, S. Navas, K. A. Olive, L. Pape, C. Patrignani, A. Piepke, M. Roos, J. Terning, N. A. Törnqvist, T. G. Trippe, P. Vogel, C. G. Wohl, R. L. Workman, W.-M. Yao, B. Armstrong, P. S. Gee, K. S. Lugovsky, S. B. Lugovsky, V. S. Lugovsky, M. Artuso, D. Asner, K. S. Babu, E. Barberio, M. Battaglia, H. Bichsel, O. Biebel, P. Bloch, R. N. Cahn, A. Cattai, R. S. Chivukula, R. D. Cousins, G. Cowan, T. Damour, K. Desler, R. J. Donahue, D. A. Edwards, V. D. Elvira, J. Erler, V. V. Ezhela, A. Fasso', W. Fetscher, B. D. Fields, B. Foster, D. Froidevaux, M. Fukugita, T. K. Gaisser, L. Garren, H.-J. Gerber, F. J. Gilman, H. E. Haber, C. Hagmann, J. Hewett, I. Hinchliffe, C. J. Hogan, G. Höhler, P. Igo-Kemenes, J. D. Jackson, K. F. Johnson, D. Karlen, B. Kayser, S. R. Klein, K. Kleinknecht, I. G. Knowles, P. Kreitz, Y. V. Kuyanov, R. Landua, P. Langacker, L. Littenberg, A. D. Martin, T. Nakada, M. Narain, P. Nason, J. A. Peacock, H. R. Quinn, S. Raby, G. Raffelt, E. A. Razuvaev, B. Renk, L. Rolandi, M. T. Ronan, L. J. Rosenberg, C. T. Sachrajda, A. I. Sanda, S. Sarkar, M. Schmitt, O. Schneider, D. Scott, W. G. Seligman, M. H. Shaevitz, T. Sjöstrand, G. F. Smoot, S. Spanier, H. Spieler, N. J. C. Spooner, M. Srednicki, A. Stahl, T. Stanev, M. Suzuki, N. P. Tkachenko, G. Valencia, K. van Bibber, M. G. Vincter, D. R. Ward, B. R. Webber, M. Whalley, L. Wolfenstein, J. Womersley, C. L. Woody, and O. V. Zenin. Review of Particle Properties. *Physical Review D*, 66(1):010001–+, July 2002.

[160] W. L. Freedman, B. F. Madore, B. K. Gibson, L. Ferrarese, D. D. Kelson, S. Sakai, J. R. Mould, R. C. Kennicutt, H. C. Ford, J. A. Graham, J. P. Huchra, S. M. G. Hughes, G. D. Illingworth, L. M. Macri, and P. B. Stetson. Final Results from the Hubble Space Telescope Key Project to Measure the Hubble Constant. *Astrophysical Journal*, 553:47–72, May 2001.

[161] M. Pettini, A. E. Shapley, C. C. Steidel, J.-G. Cuby, M. Dickinson, A. F. M. Moorwood, K. L. Adelberger, and M. Giavalisco. The Rest-Frame Optical Spectra of

Lyman Break Galaxies: Star Formation, Extinction, Abundances, and Kinematics. *Astrophysical Journal*, 554:981–1000, June 2001.

[162] D. K. Erb, A. E. Shapley, C. C. Steidel, M. Pettini, K. L. Adelberger, M. P. Hunt, A. F. M. Moorwood, and J.-G. Cuby. Hα Spectroscopy of Galaxies at z > 2: Kinematics and Star Formation. *Astrophysical Journal*, 591:101–118, July 2003.

[163] D. E. Osterbrock. *Astrophysics of Gaseous Nebulae and Active Galactic Nuclei*. Mill Valley, CA, University Science Books, 1989, 422 p., 1989.

[164] B. E. J. Pagel, M. G. Edmunds, D. E. Blackwell, M. S. Chun, and G. Smith. On the Composition of H II Regions in Southern Galaxies. I - NGC 300 and 1365. *Monthly Notices of the Royal Astronomical Society*, 189:95–113, October 1979.

[165] H. A. Kobulnicky and D. C. Koo. Near-Infrared Spectroscopy of Two Galaxies at z=2.3 and z=2.9: New Probes of Chemical and Dynamical Evolution at High Redshift. *Astrophysical Journal*, 545:712–727, December 2000.

[166] A. E. Shapley, D. K. Erb, M. Pettini, C. C. Steidel, and K. L. Adelberger. Evidence for Solar Metallicities in Massive Star-forming Galaxies at z >$\sim$ 2. *Astrophysical Journal*, 612:108–121, September 2004.

[167] K. D. Gordon, G. C. Clayton, K. A. Misselt, A. U. Landolt, and M. J. Wolff. A Quantitative Comparison of the Small Magellanic Cloud, Large Magellanic Cloud, and Milky Way Ultraviolet to Near-Infrared Extinction Curves. *Astrophysical Journal*, 594:279–293, September 2003.

[168] D. Calzetti, A. L. Kinney, and T. Storchi-Bergmann. Dust Extinction of the Stellar Continua in Starburst Galaxies: The Ultraviolet and Optical Extinction Law. *Astrophysical Journal*, 429:582–601, July 1994.

[169] D. Calzetti, L. Armus, R. C. Bohlin, A. L. Kinney, J. Koornneef, and T. Storchi-Bergmann. The Dust Content and Opacity of Actively Star-forming Galaxies. *Astrophysical Journal*, 533:682–695, April 2000.

[170] P. de Bernardis, P. A. R. Ade, J. J. Bock, J. R. Bond, J. Borrill, A. Boscaleri, K. Coble, B. P. Crill, G. De Gasperis, P. C. Farese, P. G. Ferreira, K. Ganga, M. Giacometti, E. Hivon, V. V. Hristov, A. Iacoangeli, A. H. Jaffe, A. E. Lange, L. Martinis, S. Masi, P. V. Mason, P. D. Mauskopf, A. Melchiorri, L. Miglio, T. Montroy, C. B. Netterfield, E. Pascale, F. Piacentini, D. Pogosyan, S. Prunet, S. Rao, G. Romeo, J. E. Ruhl, F. Scaramuzzi, D. Sforna, and N. Vittorio. A Flat Universe from High-Resolution Maps of the Cosmic Microwave Background Radiation. *Nature*, 404:955–959, April 2000.

[171] A. D. Linde. Chaotic Inflation. *Physics Letters B*, 129:177–181, September 1983.

[172] A. Albrecht and P. J. Steinhardt. Cosmology for Grand Unified Theories with Radiatively Induced Symmetry Breaking. *Physical Review Letters*, 48:1220–1223, April 1982.

[173] A. D. Linde. A New Inflationary Universe Scenario: A Possible Solution of the Horizon, Flatness, Homogeneity, Isotropy and Primordial Monopole Problems. *Physics Letters B*, 108:389–393, February 1982.

[174] U. Seljak and M. Zaldarriaga. A Line-of-Sight Integration Approach to Cosmic Microwave Background Anisotropies. *Astrophysics Journal*, 469:437–+, October 1996.

[175] K. Takahashi, K. Ichiki, H. Ohno, H. Hanayama, and N. Sugiyama. Generation of Magnetic Field from Cosmological Perturbations. *ArXiv Astrophysics e-prints*, January 2006.

[176] R. A. Lyttleton and H. Bondi. On the Physical Consequences of a General Excess of Charge. *Royal Society of London Proceedings Series A*, 252:313–333, September 1959.

[177] S. M. Carroll, W. H. Press, and E. L. Turner. The Cosmological Constant. *Annual Reviews of Astronomy and Astrophysics*, 30:499–542, 1992.

[178] M. Tegmark, M. Zaldarriaga, and A. J. Hamilton. Towards a Refined Cosmic Concordance Model: Joint 11-parameter Constraints from the Cosmic Microwave Background and Large-Scale Structure. *Physical Review D*, 63(4):043007–+, February 2001.

[179] G. H. Jacoby, D. Branch, R. Ciardullo, R. L. Davies, W. E. Harris, M. J. Pierce, C. J. Pritchet, J. L. Tonry, and D. L. Welch. A Critical Review of Selected Techniques for Measuring Extragalactic Distances. *Publications of the Astronomical Society of the Pacific*, 104:599–662, August 1992.

[180] B. E. Schaefer. The Hubble Diagram to z=6.3 with Swift Gamma Ray Bursts. *American Astronomical Society Meeting Abstracts*, 207:–+, December 2005.

[181] A. G. Riess, A. V. Filippenko, P. Challis, A. Clocchiatti, A. Diercks, P. M. Garnavich, R. L. Gilliland, C. J. Hogan, S. Jha, R. P. Kirshner, B. Leibundgut, M. M. Phillips, D. Reiss, B. P. Schmidt, R. A. Schommer, R. C. Smith, J. Spyromilio, C. Stubbs, N. B. Suntzeff, and J. Tonry. Observational Evidence from Supernovae for an Accelerating Universe and a Cosmological Constant. *Astronomical Journal*, 116:1009–1038, September 1998.

[182] S. Perlmutter, G. Aldering, G. Goldhaber, R. A. Knop, P. Nugent, P. G. Castro, S. Deustua, S. Fabbro, A. Goobar, D. E. Groom, I. M. Hook, A. G. Kim, M. Y. Kim, J. C. Lee, N. J. Nunes, R. Pain, C. R. Pennypacker, R. Quimby, C. Lidman, R. S. Ellis, M. Irwin, R. G. McMahon, P. Ruiz-Lapuente, N. Walton, B. Schaefer, B. J. Boyle, A. V. Filippenko, T. Matheson, A. S. Fruchter, N. Panagia, H. J. M.

Newberg, W. J. Couch, and The Supernova Cosmology Project. Measurements of Omega and Lambda from 42 High-Redshift Supernovae. *Astrophysical Journal*, 517:565–586, June 1999.

[183] L. Searle, W. L. W. Sargent, and W. G. Bagnuolo. The History of Star Formation and the Colors of Late-Type Galaxies. *Astrophysical Journal*, 179:427–438, January 1973.

[184] R. B. Tully and J. R. Fisher. A New Method of Determining Distances to Galaxies. *Astronomy and Astrophysics*, 54:661–673, February 1977.

[185] J. Gallego, J. Zamorano, M. Rego, O. Alonso, and A. G. Vitores. Observations of a Complete Sample of Hα Emission-Line Galaxies. Long-Slit Spectroscopy of Galaxies in UCM Lists 1 and 2. *Astronomy and Astrophysicss*, 120:323–356, December 1996.

[186] A. G. Vitores, J. Zamorano, M. Rego, O. Alonso, and J. Gallego. Photometric and Morphological Analysis of UCM Galaxies. I. Observations and Reductions. Morphological Classifications. *Astronomy and Astrophysicss*, 118:7–34, July 1996.

[187] R. Guzman, J. Gallego, D. C. Koo, A. C. Phillips, J. D. Lowenthal, S. M. Faber, G. D. Illingworth, and N. P. Vogt. The Nature of Compact Galaxies in the Hubble Deep Field. II. Spectroscopic Properties and Implications for the Evolution of the Star Formation Rate Density of the Universe. *Astrophysical Journal*, 489:559–+, November 1997.

[188] L. J. Kewley and M. A. Dopita. Using Strong Lines to Estimate Abundances in Extragalactic H II Regions and Starburst Galaxies. *Astrophysical Journal Supplement Series*, 142:35–52, September 2002.

[189] A. A. Penzias and R. W. Wilson. A Measurement of Excess Antenna Temperature at 4080 Mc/s. *Astrophysical Journal*, 142:419–421, July 1965.

[190] M. Marinelli and G. Morpurgo. The Electric Neutrality of Matter: A Summary. *Physics Letters B*, 137:439–442, April 1984.

[191] A. Dolgov and J. Silk. Electric Charge Asymmetry of the Universe and Magnetic Field Generation. *Physical Review D*, 47:3144–3150, April 1993.

[192] P. Langacker and S.-Y. Pi. Magnetic Monopoles in Grand Unified Theories. *Physical Review Letters*, 45:1–4, July 1980.

[193] A. Y. Ignatiev and G. C. Joshi. Possible Electric Charge Nonconservation and Dequantization in SU(2) × U(1) Models with Hard Symmetry Breaking. *Physics Letters B*, 381:216–220, February 1996.

[194] Y. Nambu. Concluding Remarks. *Physics Reports*, 104:237–258, February 1984.

[195] J. D. Bekenstein. Astronomical Consequences and Tests of Relativistic Theories of Variable Rest Masses. *Comments on Astrophysics*, 8:89–97, 1979.

[196] S. J. Landau, P. D. Sisterna, and H. Vucetich. Charge Conservation and Time-Varying Speed of Light. *Physical Review D*, 63(8):081303–+, April 2001.

[197] R. N. Mohapatra. Possible Nonconservation of Electric Charge. *Physical Review Letters*, 59:1510–1512, October 1987.

[198] S. Sengupta and P. B. Pal. Constraints on Cosmic Electric Charge Asymmetry and Neutrino Charge from the Microwave Background. *Physics Letters B*, 365:175–177, February 1996.

[199] M. S. Turner and J. N. Fry. Baryogenesis Without the Initial Presence of Superheavy Bosons. *Physical Review D*, 24:3341–3344, December 1981.

BIOGRAPHICAL SKETCH

Ethan Siegel was born on August 3rd, 1978, at Union Hospital in the Bronx, New York. He graduated from the Bronx High School of Science in 1996 and attended Northwestern University from 1996 to 2000, graduating with a triple degree in physics, classics, and the Integrated Science Program. He spent a year as a public school teacher at King/Drew Medical Magnet High School in Los Angeles, California, after which he moved to Florida to pursue a Ph.D. in astrophysics at the University of Florida. He has held a wide variety of jobs in the past, including employment as a day camp counsellor, a stockboy in a lingerie store on Broadway, a research employee for Fermilab and for NASA, a busboy in a kitchen in Rome, a private tutor, and a webpage designer. He currently resides in Madison, Wisconsin, with his roommate and two cats. He enjoys playing guitar, travelling, swing dancing, outdoor activities, and swilling alcohol in its many forms, as well as scaring children of all ages on Halloween.